Aus dem Interdisziplinärem Stoffwechsel-Centrum: Endokrinologie, Diabetes und Stoffwechsel, Kompetenzzentrum Seltene Stoffwechselerkrankungen
der Medizinischen Fakultät Charité – Universitätsmedizin Berlin

DISSERTATION

Improving Enzyme Replacement Therapy for Lysosomal Storage Diseases

zur Erlangung des akademischen Grades
doctor rerum medicinalium (Dr. rer. medic.)

vorgelegt der Medizinischen Fakultät
Charité – Universitätsmedizin Berlin

von

Nathalie Rigal
aus St-Cloud (Frankreich)

Datum der Promotion: 25.06.2017

Abstract

Lysosomal storage diseases (LSDs) are a group of rare, inherited metabolic disorders, whereby the deficiency of a single lysosomal enzyme leads to accumulation of metabolites in the lysosome cells. This in turn results in cellular dysfunction and clinical abnormalities such as enlarged organs, connective-tissue, ocular pathology and central nervous system dysfunction. To date, there is no cure for LSDs; enzyme replacement therapy (ERT) however can be used to treat several of these disorders. In such case, a recombinant enzyme is administered intravenously to patients and routed to the deficient cells via receptor mediated transport ways. Although ERT has proven to be successful in slowing down lysosomal storage and improving patient's quality of life, there are still a number of unmet needs. This includes A) the difficulties encountered during the production of the acid hydrolases, in particular the synthesis of mannose-6-phosphate (M6P), B) the loss of intravenously administered enzyme to the liver asialoglycoprotein receptor (ASGPR), C) the inability of ERT to cross the blood brain barrier. In an effort to address these numerous issues, an attempt was made to develop "tools" for the production of improved recombinant lysosomal enzymes. The initial focus was set upon modifying Glycotope's host cell line in order to increase M6P levels of the recombinant enzymes and thereby enhancing target-cell delivery. The resulting cell lines enabled production of recombinant α-Galactosidase A (GAL) enzymes exposing relative M6P levels close to 80 %, compared to the initial 40 % of the control enzyme. This increased M6P level in turn led to a 4-fold increase in receptor-mediated cellular uptake when tested *in vitro*. The second objective was the modification of the recombinant enzyme GAL itself. Emphasis was set upon addressing ASGPR-mediated product loss to the liver. A fusion enzyme was thereby generated exhibiting an up to 20-fold reduced affinity for the liver ASGPR when assessed *in vitro*. Furthermore, *in vivo* data generated during a mouse pharmacokinetic study, revealed that the liver uptake of the intravenously administered fusion enzyme was reduced by around 30 % compared to the reference enzyme. In addition, a 1.5-fold increase in kidney uptake was observed for the fusion enzyme. Finally, the transport of recombinant enzymes to the brain was investigated. To this end, several fusion enzyme formats were generated based on the so-called molecular Trojan-horse technique, whereby molecules are engineered to bind to transcytosis-triggering receptors (i.e. transferrin receptor (TFR)). Recombinant fusion products were successfully generated, purified and characterized *in vitro*, with at least one enzyme revealing bi-functionality. Indeed, the fusion product showed catalytic activity on one hand and TFR binding ability on the other, thus possibly enabling transcytosis across the BBB.

Keywords: Lysosomal storage disease, enzyme replacement therapy, recombinant protein expression, fusion protein, mannose-6-phosphate, asialoglycoprotein receptor, blood-brain barrier.

Zusammenfassung

Lysosomale Speicherkrankheiten (LSK) bilden eine Gruppe von seltenen genetisch bedingten und vererbbaren Stoffwechselerkrankungen. Allen Erkrankungen ist gemeinsam, dass ein lysosomales Enzym in der Funktionalität eingeschränkt ist oder komplett fehlt. Stoffwechselprodukte reichern sich zunächst in den Lysosomen verschiedener Zellen an und gelangen ab einer bestimmten Konzentration in den extrazellulären Raum. Dies führt zu gesundheitlichen Störungen und Symptomen, die mit Veränderungen des Zellstoffwechsels verbunden sind und im weiteren Verlauf zum Zelltod führen. Je nach Art der Erkrankung kommt es zu Schädigungen des Nervensystems, der Knochen, Muskeln, Nieren und Milz, des Herzens und weiterer Organe. Seit ca. 10 Jahren stehen Enzymersatztherapien (ERT) zur Verfügung. Hierbei wird das betroffene Enzym mittels rekombinanter Proteintechnik hergestellt und dem Patienten durch regelmäßige Infusionen verabreicht. Obwohl die derzeit eingesetzte ERT in der Lage ist, einen Teil der fehlende Enzymaktivität in verschiedenen Zellen auszugleichen, hat sich gezeigt, dass die Herausforderung darin besteht, alle betroffenen Zellen bzw. Gewebe spezifisch und effizient zu erreichen. Des Weiteren stellt auch die Herstellung der rekombinanten Enzyme oft eine Herausforderung dar, insbesondere die schwer steuerbare Synthese von Mannose-6-Phosphat (M6P). Letztens liegt die größte Herausforderung darin, dass viele der LSK neurologische Störungen verursachen, die bis heute nicht durch ERT behandelt werden können. Der Grund dafür ist die Blut-Hirn-Schranke (BHS), deren Überwindung für größere Moleküle schwierig ist. Zur Optimierung aktueller ERT wurde im Rahmen der vorliegenden Arbeit die Leerzelllinie der Firma Glycotope modifiziert, um die Synthese von M6P zu verbessern. Die resultierende Zelllinie ermöglichte die rekombinante Expression von α-Galactosidase A (GAL) Molekülen, die einen bis zu 2-fach höheren M6P Anteil zeigten. In *in vitro* Experimente konnte nachgewiesen werden, dass die Aufnahme der hoch phosphorylierten GAL-Enzyme in Zielzellen verbessert war. Darüber hinaus wurde das Enzym GAL mittels „Protein-engineering“ so verändert, dass die hohen Verluste, die aufgrund der Aktivierung des Asialoglycoprotein-Rezeptors (ASGPR) in der Leber auftreten, verringert werden konnten. Das resultierende Fusionsenzym wies *in vitro* eine bis zu 20-fach reduzierte Bindung an den ASGPR auf. Zusätzlich konnte *in vivo* in Mäusen gezeigten werden, dass bis zu 30 % weniger Fusionsenzym in die Leber gelangte. Zuletzt wurde im Rahmen der vorliegenden Arbeit ein Ansatz initiiert, der den Transport von rekombinanten Enzymen durch die BHS ermöglichen sollte. Die Moleküle, die im Rahmen dieses Experimentes erzeugt wurden, beruhen auf dem Prinzip der „Trojan-horse technology“, wobei ein rekombinantes Protein mittels „Protein-engineering“ so modifizier wird, dass es an einen Transzytose-Rezeptor bindet und so durch die BHS geschleust werden kann (z.B. Transferrinrezeptor).

Mehrere Fusionsenzym-Varianten wurden rekombinant hergestellt, aufgereinigt und *in vitro* getestet. Es konnte gezeigt werden, dass mindestens ein Fusionsenzym an den Transferrinrezeptor bindet und somit möglicherweise durch rezeptorvermittelte Transzytose die BHS durchqueren könnte.

Schlagwörter: Lysosomale Speicherkrankheiten, Enzymersatztherapien, Rekombinante Proteinexpression, Fusionsproteine, Mannose-6-phosphate, Asialoglycoproteinrezeptor, Blut-Hirn-Schranke.

Table of contents

1 Introduction

Lysosomes are spherical organelles functioning as the digestive system of the cell. First defined in 1955 by De Duve, these membrane-enclosed vesicles are responsible for the degradation of a variety of molecules including proteins, nucleic acids, carbohydrates, lipids, and cellular debris. These molecules are either taken up from outside by endocytosis and phagocytosis or secreted from within the cell by autophagy (De Duve 2005). Inside the lysosome, enzymes are responsible for the catabolism of the different polymers. To function efficiently, these acid hydrolases require a pH of 5.0, maintained in the lysosome by membrane-bound ATP-dependent proton pumps (Cooper 2000). Malfunction of lysosomal enzymes and consequently of the lysosomes leads to severe metabolic disorders called lysosomal storage diseases (LSDs), a group of rare, genetically inherited diseases. These malfunctions are often the direct result of mutations in the acid hydrolase gene which can either alter enzyme synthesis (unstable or inactive enzyme is produced) or even prevent it altogether. The severity of LSDs, which determines the time of onset and the pace of the disease, depends in part on the residual enzyme activity. Fifteen to twenty percent of normal enzyme activity is usually enough to carry out cellular function (Leinekugel *et al.* 1992). Consequently, heterozygote carriers of LSDs whose enzyme activity is 50 % of normal are clinically unaffected. Symptoms develop when residual enzyme activity falls below a threshold of 15 % to 20 %. In addition, LSDs show allelic variation, i.e., different mutations of the same gene occur. Mutations that leave no residual enzyme activity cause severe, early-onset illness. Milder mutations cause insidious, late- or adult-onset illness. However there is no close phenotype/genotype relation. The standard treatment for the majority of these disorders involves correction of the deficit by repeated injections of a recombinant lysosomal enzyme preparation. This treatment is known as enzyme replacement therapy (ERT).

1.1 Lysosomal enzymes

The catabolic pathway of the lysosome comprises a scaffold of interconnected enzymatic reactions. Over fifty different acid hydrolases are found within the lysosome, each one being responsible for a specific catabolic reaction. The degradation of sphingolipids is at the heart of lysosomal catabolism as illustrated in Figure 1. The acid hydrolases are not produced in the lysosome, but in other sub-cellular compartments including the endoplasmic reticulum (ER) and

the Golgi apparatus. Following their successful synthesis within these organelles (see 1.1.1), the enzymes are routed to the lysosome via endocytic vesicles which are known as endosomes (see 1.1.3).

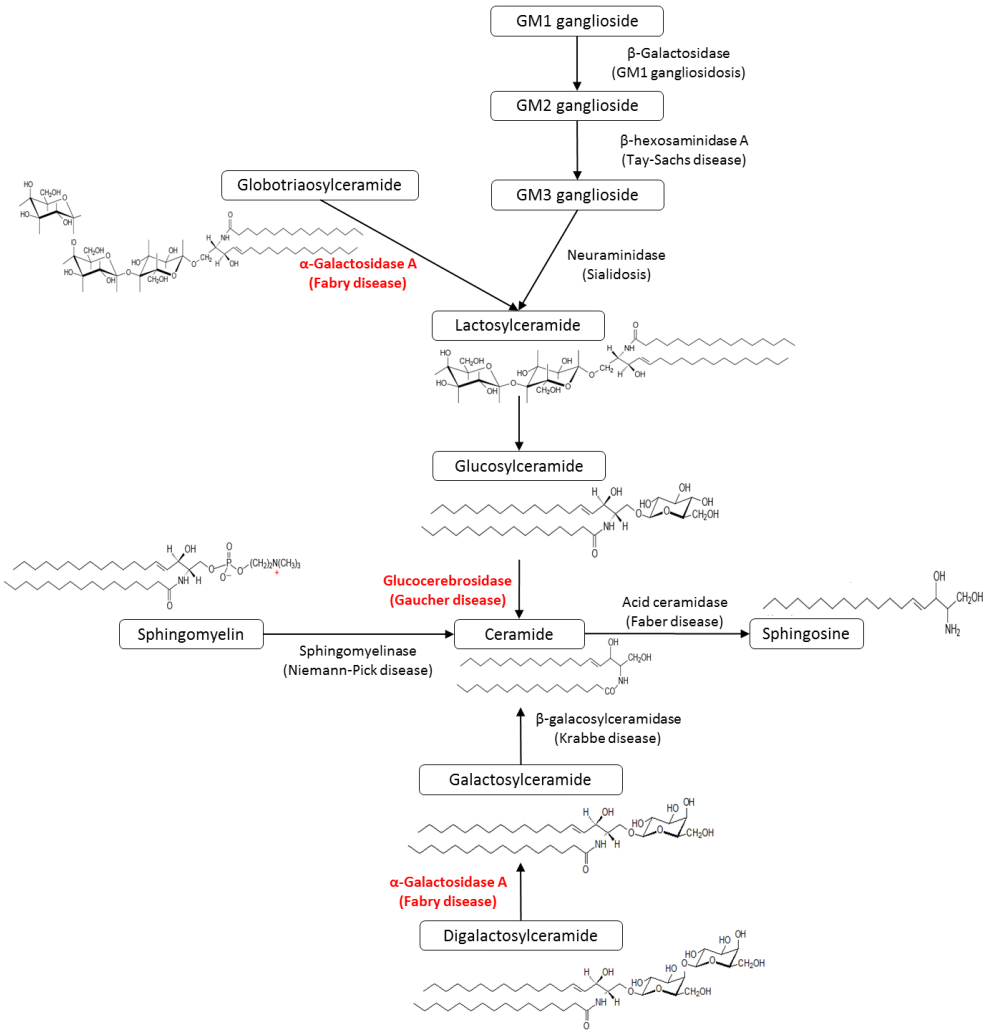

Figure 1 Metabolic pathways of various forms of sphingolipids.

1.1.1 Synthesis of lysosomal enzymes

The synthesis of lysosomal enzymes starts in the cell nucleus, where chromosomal DNA is transcribed into messenger RNA (mRNA) which is in turn used as a synthesis-template in the endoplasmic reticulum (ER). Just like over 50 % of human proteins, lysosomal enzymes are glycoproteins. This means that following initial synthesis in the ER, the enzymes undergo a series of post-translational modifications whereby carbohydrate moieties are enzymatically attached to the polypeptide backbone. This process is known as glycosylation (Kornfeld R. and Kornfeld S. 1985). Lysosomal hydrolases are exclusively N-glycosylated, i.e., the glycans are attached by an N-glycosidic bond to accessible asparagine (Asn) residues found in an

Asn-X-Serine or Asn-X-Threonine sequon, where X can be any amino acid. The glycosylation process is initiated in the ER, where a precursor glycan composed of 14 sugars is attached to the growing nascent polypeptide chain. Following this step, the oligosaccharide portion is modified by a series of glycosidases and glycosyltransferases (Figure 2a). The first structures resulting from this processing are high-mannose-type carbohydrates. Further modifications in the Golgi lead to the generation of complex and hybrid-type oligosaccharides. The different carbohydrate moieties are depicted in Figure 2b.

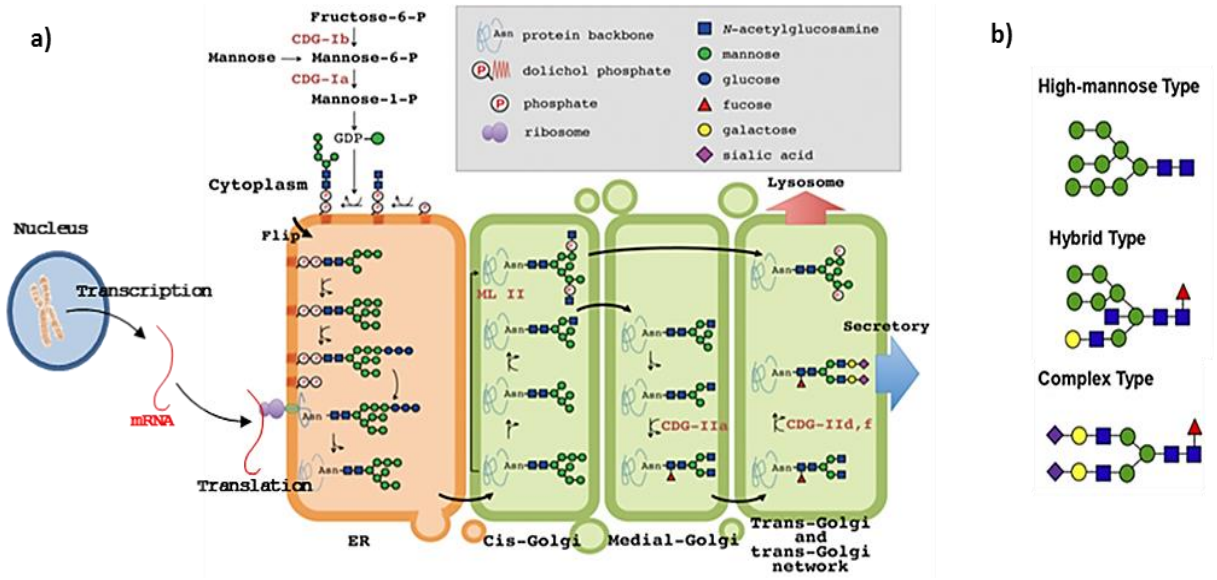

Figure 2 Synthesis of lysosomal enzymes a) Synthesis and maturation of N-glycosylation (adapted from Nakayama *et al.* 2013) b) The different types of N-glycan moieties.

For a given glycoprotein, a variety of so called glyco-isoforms are generated due to heterogeneity in N-glycosylation site occupation and composition (Varki and Kornfeld 2009). Glycosylation has a significant impact on physicochemical properties of lysosomal enzymes such as solubility, charge, size, folding and stability. This is fundamental for the biological properties of acid hydrolases and in particular for the activity, circulation half-life, receptor interaction and trafficking (Van Beers and Bardor 2012).

1.1.2 Maturation of lysosomal enzymes: synthesis of the mannose-6-phosphate marker

Following the initiation of the protein synthesis and glycosylation in the ER, the lysosomal enzyme precursors move to the Golgi apparatus (cis- then trans-Golgi), where the newly attached N-glycan undergoes further maturation (e.g. sialylation, fucosylation and phosphorylation). This is the point

at which the hydrolases receive their unique and very important trafficking marker in the form of mannose-6-phophate residues (M6P). Mannose-6-phosphate is the recognition marker which enables segregation of the newly synthesized lysosomal enzymes from the secretory route and vesicular delivery of the enzymes to the lysosome (Sly W. and Fischer H. 1982). The initial step of lysosomal enzyme phosphorylation occurs in the cis-Golgi. There, as pictured in Figure 3, the N-acetylglucosamine-1-phosphotransferase, attaches N-acetylglucosamine-1-phos-phate (GlcNAc-1-P) to the C-6 position of mannose residues present in high-mannose glycans (Reitman and Kornfeld 1981). Later, in the *trans*-Golgi, the α-N-acetylglucosaminyl-1-phosphodiester glycosidase removes the N-Acetylglucosamine (GlcNAc) moiety, thereby uncovering the M6P residues (Varki and Kornfeld 2009).

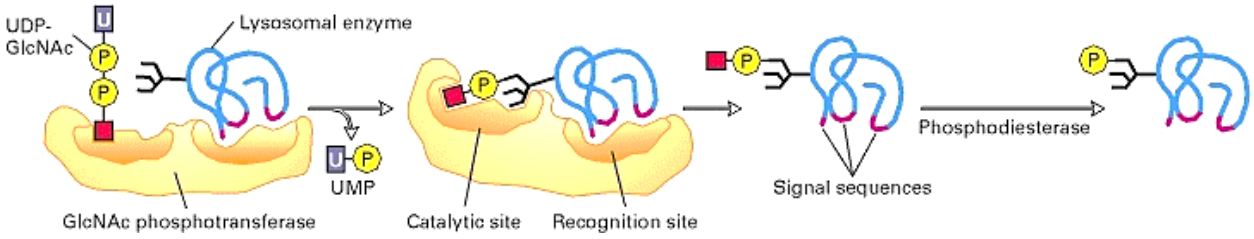

Figure 3 Phosphorylation of mannose residues present on lysosomal enzyme N-glycan (from Lodish *et al.* 2000).

Hydrolases lacking M6P will not be routed to the lysosome but rather secreted. This is the case in Mucolipidosis II disease (i-cell disease) for example, where the phosphotransferase enzyme is deficient. Consequently, the lysosomal enzymes cannot be phosphorylated and hypersecretion of the hydrolases occurs, leaving substrate to accumulation in the lysosomes (Braulke *et al.* 2013). Nonetheless, it has been reported that despite the presence of a M6P marker, 5 to 10% of correctly synthesized lysosomal enzymes are mistrafficked and escape the cell via the secretory pathway (Kornfeld 1987).

Just like the process of N-glycosylation, phosphorylation of lysosomal enzymes is a highly variable process yielding heterogeneous phosphorylated glycan. Indeed, significant variance is observed in the type and size of N-glycans that are phosphorylated (i.e. high-mannose or hybrid-type), in the residues generated (M6P or M6P-GlcNAc), in the number of mannose residues that are actually phosphorylated (maximum of 2 per glycan "tree") and in their location on the glycan structure (Varki and Kornfeld 1980, Bohnsack *et al.* 2009). This can strongly influence the enzyme's affinity with regards to its trafficking receptor (Figure 4). Indeed, phosphorylated high-mannose glycans have a higher binding affinity than phosphorylated

hybrid-type glycans. Furthermore, a glycan "tree" baring two phosphates (bis-M6P) has the highest binding affinity of all structures.

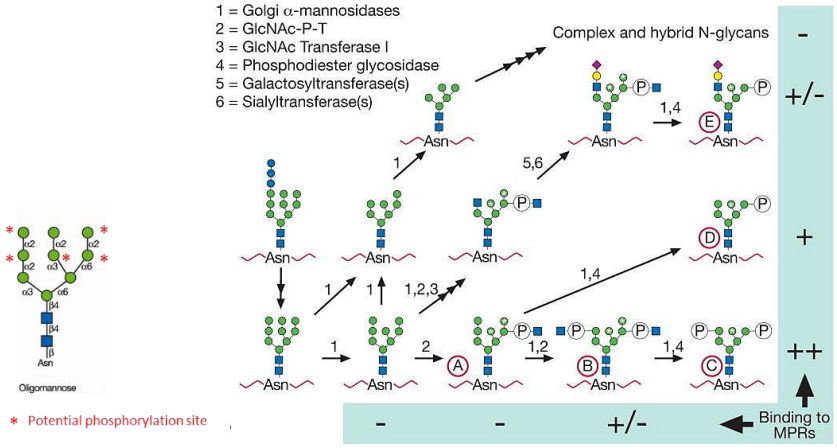

Figure 4 Possible phosphorylation sites on N-Glycan and relative affinity for the mannose 6-phosphate receptors (MPRs). The affinities for the MPRs are indicated as follows: [++] strong; [+] moderate; [+/−] weak; [−] no binding (adapted from Varki *et al.* 2009).

1.1.3 Lysosomal enzyme trafficking: delivery to the lysosomes

Once phosphorylated, acid hydrolases are recognized by the mannose-6-phosphate receptors (MPRs) in the *trans*-Golgi network and enclosed within clathrin-coated vesicles (Kaplan *et al.* 1977). Following the removal of the clathrin coat, these transport vesicles fuse with late endosomes and the gradually decreasing pH causes the hydrolases to dissociate from the MPR. As the pH further decreases, the MPRs are recycled to the Golgi apparatus and the late endosomes containing the active acid hydrolases merge into lysosomes (Figure 5a). Mannose-6-phosphate receptors (MPRs) are membrane-bound p–type lectins. Two types of MPRs exist, the larger 300kDa cation-independent receptor (CI-MPR) and the smaller 46kDa homodimeric cation-dependent receptor (CD-MPR) (Munier *et al.* 1996) (Figure 5b). Both receptors are involved in the intracellular transport of newly synthesized lysosomal proteins. Despite extensive investigation, some aspects, such as the relative roles and specialized functions of each MPR in protein targeting or even the question why two receptors are present, remain unresolved. However, what is known so far is that the CI-MPR is more efficient than the CD-MPR with regard to M6P-trafficking, in part due to its higher and broader affinity range for the various phosphorylated structures (Song *et al.* 2009). Moreover, although both receptors are able to cycle to the plasma membrane, only the CI-MPR is capable of endocytosing extracellular glycoproteins. This plays an essential role for example in the recapture of the 5 to 10% mistrafficked lysosomal hydrolases

(see above), but even more so when considering enzyme replacement therapy (ERT) and cell surface uptake of the exogenous recombinant enzymes (see 1.3). Interestingly, the CD-MPR on the other hand has been suggested as being responsible for the 5 to 10 % mistrafficking of correctly synthesized lysosomal enzymes (Chao *et al.* 1990).

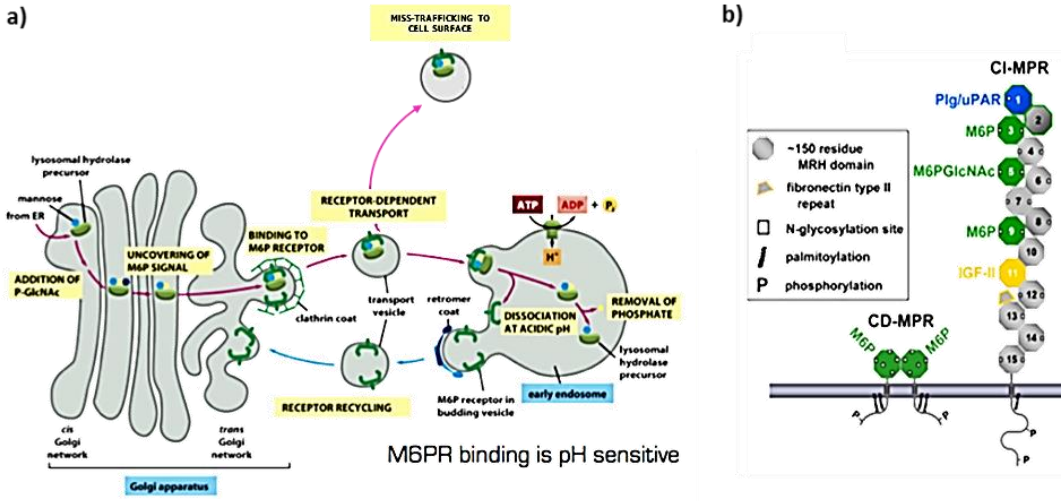

Figure 5 Mannose-6-phosphate receptor (MPR) mediated trafficking a) Subcellular trafficking pathways of lysosomal enzymes b) Structure of the two MPRs (adapted from Varki *et al.* 2009).

Although mannose-6-phosphate receptors (MPRs) play a major role in the intracellular trafficking of lysosomal enzymes, alternative targeting routes have also been described recently. Among them are lysosomal integral membrane protein LIMP-2 and sortilin (Coutinho *et al.* 2012). LIMP-2 was shown to be implicated in the delivery of acid β-glucosidase to the lysosomes, one of the acid hydrolases known to be synthesized without M6P. Sortilin, a multifunctional receptor capable of binding several different ligands (e.g. neurotensin, receptor-associated protein (RAP)) is also thought to be involved in the targeting of several proteins to the lysosome, including sphingolipid activator proteins (prosaposin and GM2 activator protein), acid sphingomyelinase or cathepsins D and H. However, these alternative mechanisms only play a secondary role and the correct synthesis and presence of M6P remains fundamental for almost all lysosomal enzymes.

1.1.4 Therapeutic relevance of glycosylation and lysosomal enzymes

As described earlier, glycosylation plays a major role in glycoprotein folding, stability, trafficking as well as functionality. This is not only true for naturally occurring lysosomal enzymes, illustrated by M6P dependent trafficking (see 1.1.2) or glycosylation-related misfolding and activity loss (Berg-Fussman *et al.* 1993, Wang *et al.* 2011), but also especially when considering their

recombinant counterparts and their use for enzyme replacement therapy (ERT) (see 1.3). In such case, pharmacokinetics (i.e. serum half-life) and pharmacodynamics (i.e. cellular distribution) of the recombinant glycoprotein become key features and these can directly be affected by glycosylation. For example, large amounts of sialic acid can increase the circulation half-life of an enzyme, while on the other hand exposure of terminal galactose and mannose residues can drastically decrease it (Walsh and Jefferis 2006). Thus glycosylation naturally influences therapeutic efficacy of recombinant lysosomal enzymes.

The glycan composition of a protein can also impact drug tolerability due to the influence of certain glycan moieties on immunogenicity (Lis and Sharon 1993, Imperiali and O'Connor 1999). Indeed, some glycan "motifs" considered foreign or non-human (Figure 6) may induce immune responses following administration of the drug substance. One such example is N-glycolylneuraminic acid (Neu5Gc), a glycan "motif" which can be produced by the Chinese hamster ovary (CHO) cell. Indeed, Neu5Gc results from an enzyme which is highly expressed and active in most mammals but not in humans (Hossler *et al.* 2009). Therefore, Neu5Gc-carrying proteins would automatically be registered as "foreign" by the human immune system.

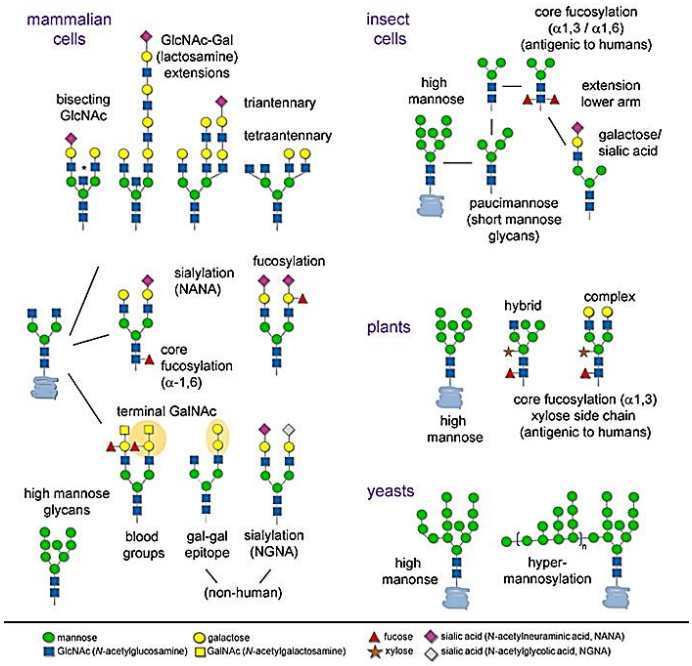

Figure 6 Species-specific glycosylation patterns (from Varki *et al.* 2009).

In addition to infusion reactions or inflammations, immune responses can manifest themselves in the form of inhibitory anti-drug antibodies (ADAs). Such antibodies interfere with or neutralize the effect of the administered drug, leading to an inefficient treatment (De Groot and Scott 2007). In the case of lysosomal storage disease (LSD) for example, neutralizing ADAs were reported for

enzyme replacement therapy (ERT) preparations used to treat Fabry disease, namely agalsidase beta (Fabrazyme®) and agalsidase alpha (Replagal®). Indeed, following clinical trials, antibodies to recombinant GAL were detected in 3 of 14 patients treated with 0.2 mg/kg Replagal® versus 24 of 29 patients treated with 1.0 mg/kg Fabrazyme® (Linthorst *et al.* 2004). One explanation for the differences in ADA levels observed could be the use of different production methods to generate the ERT preparations. Indeed as shown in Table 1, the choice of host cell can directly influence recombinant protein glycosylation; as agalsidase alpha is produced in human cells, this could explain the lower ADA levels found when compared to agalsidase beta which is a product derived from Chinese hamster ovary cell (CHO).

Table 1 "Non-human sugars" found when comparing various production host-cells.

Host system	Similarity to human glycans	"Non-human sugars" produced
CHO	High	Trace amount of α-GAL, Neu5Gc
NS0/SP2/0	High	Small amount of α-GAL, Neu5Gc
Yeast	Low	High-mannose
Plant	Low	Bisecting β1,2 xylose, α1,3 fucose
Transgenic animals	Low	High-mannose, Neu5Gc

1.2 Lysosomal enzyme deficiencies

If the synthesis of a lysosomal enzyme is altered, thereby leading to inactive or missing enzymes (no synthesis), lysosomal storage diseases (LSDs) can arise. Lysosomal storage diseases are a group of rare inherited metabolic disorders characterized by the dysfunction of a given lysosomal enzyme (Scriver *et al.* 2001). This results in progressive intra-lysosomal accumulation of undigested macromolecules, such as glycogen, sphingolipids, mucopolysaccharides and glycoproteins. As lysosomes are present in every cell type (except red blood-cells), different organs and systems may be affected simultaneously. If left untreated, LSDs lead to cellular dysfunction and arising clinical abnormalities including enlarged organs (organomegaly), connective tissue and ocular pathology, as well as central nervous system (CNS) dysfunction. Depending on the type of mutation and therefore the degree of the enzyme malfunction, individuals can experience moderate to severe physical impairments and, in the worst case, death at an early age. Since the identification of the first lysosomal disease namely Morbus Pompe (Hers 1963), over 40 different disorders have been described. Classification of LSDs is based on the enzyme defect in the degradation pathway and the type of substrate accumulation

(Reuser *et al.* 1994, Wilcox 2004, Vellodi 2005). Sphingolipidoses for example, are one class of LSDs specifically affecting the sphingolipid metabolism of the lysosome (Table 2).

Table 2 Lysosomal storage diseases of the Sphingolipidoses class.

Disease	Enzyme deficiency	Storage product
Fabry disease	α-Galactosidase	Globotriaosylceramide (Gb3)/ Digalactosaylceramide
Farber disease (lipogranulomatosis)	Ceramidase	Ceramide
Gaucher disease	Glucocerebrosidase	Glucosylceramide
GM1 gangliosidosis	β-Galactosidase	GM1 ganglioside /Galactosyloligosacharides /Keratin sulphate
Tay-Sachs disease	α-Subunit of β-hexosaminidase	GM2 ganglioside/asialo-GM2
Sandhoff disease	β-Subunit of β-hexosaminidase	GM2 ganglioside/Asialo-GM2/Globoside
Globoid cell leukodystrophy (Krabbe disease)	Galactosylceramidase	Galactosylceramide, Galactosylsphingosine
Metachromatic leukodystrophy	Arylsulfatase A	Sulfatides
Niemann-Pick A and B	Sphingomyelinase	Sphingomyelin

Other classes of LSDs include the glycogen storage diseases or the mucopolysaccharidoses. In the case of Sphingolipidoses, the CNS is primarily affected and to a variable degree visceral organs. Clinical features vary in subtypes but neurodegeneration is a common sign. This class includes Morbus Gaucher (see 1.2.1) and Morbus Fabry (see 1.2.2).

1.2.1 Acid β-glucosidase deficiency: Morbus Gaucher

Morbus Gaucher is an autosomal recessive inherited disorder and the most frequent lysosomal storage disease (LSD) (incidence of 1:50 000 live births for type I). It is caused by intra-lysosomal deficiency of the enzyme acid β-glucosidase (glucosylceramidase (GBA) EC 3.2.1.45) normally responsible for degradation of glucosylceramides (Brady *et al.* 1966). Accumulation of these glucocerebrosides occurs almost exclusively in cells of the mononuclear phagocyte system and are referred to as Gaucher cells. Gaucher cells are glycosphingolipid-engorged macrophages which displace normal cells in visceral organs and the bone marrow. This process induces chronic inflammation stimulating other inflammatory cells, which is subsequently believed to lead to clinical abnormalities of the liver and spleen (hepato- and splenomegaly), low blood platelets, skeletal disorders and bone lesions (osteoporosis).

Gaucher disease can be divided into several subtypes based on presence, onset and severity of neurological involvement:

- type I: non-neuronopathic form
- type II: acute neuronopathic form
- type III sub-acute neuronopathic form

Enzyme replacement therapy has become the standard treatment for type I Gaucher disorders as well as for the treatment of visceral symptoms found in type III patients (sees 1.3.2). In types II and III Gaucher disease, however, the brain and peripheral nervous system are severely affected, making treatment difficult (see 1.3.4).

1.2.2 Acid α-galactosidase deficiency: Morbus Fabry

Morbus Fabry is an X-linked inherited lysosomal storage disorder characterized by the accumulation of globotriaosylceramide Gb3 in various tissues (Sweeley and Klionsky 1963). This is the result of α-galactosidase A (GAL, EC 3.2.1.22) deficiency, a lysosomal enzyme normally responsible for the catabolism of these sphingolipids (Brady *et al.* 1967). Intra-lysosomal accumulation of Gb3 occurs mainly in the endothelial, perithelial, and smooth muscle cells of blood vessels but also in many other different cell types of the heart, kidneys, eyes, and peripheral nervous system (Zarate and Hopkin 2008). For this reason, Morbus Fabry is often referred to as a multi-system disease. Due to the X-linked inheritance of the disease, differences in clinical manifestations are observed in males and females. Typical hemizygous male patients have no detectable GAL activity and onset occurs during childhood and adolescence (Desnick *et al.* 1995*)*. Clinical features include neuropathic pain and angiokeratoma, development of proteinuria, left ventricular hypertrophy and arrhythmias (Germain 2010). Death usually results from renal failure or stroke. Atypical males with residual GAL activity may be asymptomatic or develop a mild, late onset form of the disease primarily limited to cardiac manifestations. Enzyme replacement therapy has been available for treatment of Fabry Disease since 2001 (see 1.3.3). Early treatment is recommended in order to avoid irreversible damage resulting of Gb3 accumulation.

1.3 Treating lysosomal enzyme deficiencies

Over the past decade, several therapy options have been developed to treat patients affected by lysosomal storage diseases (Table 3).

Table 3 Therapeutic strategies for lysosomal storage diseases (adapted from Bruni *et al.* 2007).

Therapeutic Strategy	Rationale	Significant clinical/experimental experience	Eligibility
Bone Marrow Transplantation (BMT)	Replacement of the deficient enzyme activity by intravenous infusion of hematopoietic progenitor cells	• MPS I (Hurler Syndrome) • MPS II (Hunter Syndrome) • MPS III (Sanfilippo Syndrome) • MPS IV (Morquio Syndrome) • MPS VI (Maroteaux-Larry Syndrome) • Gaucher Disease • Metachromatic Leukodystrophy (MLD)	1. Transplantation occurs early (under 3 years) 2. IQ above 70 3. Transplantation occurs in the setting of appropriate neuropsychiatric follow-up assessment and support 4. A suitable donor is available
ERT	Replacement of the deficient enzyme activity by intravenous infusion of exogenous enzyme able to reach intracellular target	• Gaucher Disease Type 1 and 3 • Fabry Disease • MPS I (Hurler, Hurler/Scheie Syndrome) • MPS II (Hunter Syndrome) • MPS VI (Maroteaux-Larry Syndrome) • Pompe Disease	ERT is advisable only in forms of LSDs without mental retardation, since the exogenous enzyme does not cross the hemato-encephalic barrier
Substrate Reduction Therapy (SRT)	Reduction of the formation of lysosomal substance down to a rate at which the residual enzyme activity can catabolize stored and incoming lysosomal substance	• Gaucher Disease Type 1 • Tay-Sachs Disease • Sandhoff Disease • GM1 gangliosidosis • Niemann-Pick Disease Type C	SRT can be used only in presence of residual activity
Chemical Chaperon Therapy (CCT)	Binding to stabilize the misfolded enzymes, thus increasing their folding and trafficking and improving their residual activity	• Gaucher Disease • Fabry Disease • GM1 gangliosidosis • Pompe Disease	CCT relies on endogenous activity of variant enzyme. It cannot be used for genotypes that do not produce a protein product.

These therapies include chaperone therapy, where small molecules are generated to help stabilize the patients' deficient enzyme and restore sufficient catalytic activity; substrate reduction therapy

(SRT), where the formation of the storage product is hindered via substrate depletion; hematopoietic stem cells transplantation (HSCT), which, however, remains a very invasive procedure. The most promising results to date have been achieved with enzyme replacement therapy (ERT), the first treatment ever developed for lysosomal storage disorders (LSDs). However, altogether none of the treatments have proven to be sufficient. Recently, attempts to combine the therapies were made (i.e. ERT + chaperones) in order to provide a more effective and broad treatment. Nonetheless, major improvements for the individual treatment options are necessary in order to address all medical needs related to the very complex LSDs.

1.3.1 Enzyme replacement therapy

Enzyme replacement therapy (ERT) is a treatment for lysosomal storage diseases (LSDs), whereby a recombinant version of the deficient enzyme is given intravenously to patients at regular intervals (e.g. bi-weekly). Once in the blood, the enzyme is transported to various cells via receptor-mediated endocytosis and delivered to the lysosomes. The concept for ERT first arose in the 1960s when De Duve observed the endocytic delivery mechanism of extracellular substances to lysosomes, via phagosomes. "*This* [discovery] *obviously opens up many possibilities for interaction, including replacement therapy"* (De Duve 1964, De Duve and Wattiaux 1966). However, it wasn't till later that this rationale could really be implemented, once the cause behind LSDs was better understood (i.e. a single enzyme defect as the root cause), the exact mechanism of endocytic delivery was revealed (i.e. discovery of carbohydrate receptors) and a sustainable enzyme source became available (i.e. recombinant expression technology). Indeed, during the late 1960s, various experiments allowed to really understand that the existence of so called "corrective factors" (later identified as lysosomal enzymes) enabled cross-correction of lysosomal disorder in a co-culture model (Fratantoni *et al.* 1968). These observations were further developed when the first form of ERT was implemented in a patient-derived Fabry fibroblast, using plant-derived enzyme (Dawson *et al.* 1973). Dawson concluded that *"it may be possible to replace the specific missing lysosomal hydrolase in various sphingolipidoses and other storage diseases. Although we do not propose to effect enzyme replacement therapy in vivo with a plant enzyme, such studies in tissue culture are valid, and eventually human α-galactosidase, of comparable activity and purity, will become available*". In combination with the later discovery of cell surface carbohydrate receptors (Ashwell *et al.* 1974), it became clear that lysosomal enzymes could be brought to diseased cells "from outside", that the enzymes carried specific carbohydrate moieties enabling specific cellular uptake via carbohydrate-receptor mediated endocytosis and that the enzymes

would subsequently be delivered to the lysosome thus correcting the defect (Hickman *et al.* 1974, Stahl *et al.* 1976). By the end of the seventies, the lysosomal recognition marker mannose-6-phosphate was identified (Kaplan *et al.* 1977, Sly *et al.* 1978) and the development of the first Food and Drug Administration (FDA) approved ERT could begin.

1.3.2 Enzyme replacement therapy for Gaucher disease: engineering of recombinant β-Glucosidase

Morbus Gaucher was the first lysosomal storage disease (LSD) treated with enzyme replacement therapy (ERT). Cells affected by the sphingolipid storage, are predominantly of macrophage phenotype (Boven *et al.* 2004). This means that the endocytic receptor of interest in this case is the mannose receptor, as it is highly expressed at the surface of these cell types (Stahl *et al.* 1976). In the early 1970s, Brady and his team showed that single intravenous injections of human glucocerebrosidase, purified from healthy plasma tissues, could be beneficial for treatment of Gaucher disease (Brady *et al.* 1974). However this native form of the enzyme gave limited results, due in part to the fact that it was unable to reach all the affected cells and in particular the liver macrophages (Kupffer cells). It became clear that the enzyme needed remodeling in order to increase its tissue specificity (Furbish *et al.* 1981). The carbohydrate chains were sequentially trimmed *in-vitro* using sialidase, galactosidase and N-acetylglucosaminidase enzymes, thereby exposing the so called core mannose residues (Figure 7a). This enabled specific targeting of the enzyme to the macrophages. The modified enzyme proved remarkably effective (Barton *et al.* 1991) and was approved in 1991 by the Food and Drug Administration (FDA) under the name of Ceredase®. (Alglucerase, Genzyme Corporation). This was the first commercially available ERT for the treatment of Gaucher type I. Ceredase® has since been replaced by a recombinant form of the human enzyme and is known as Cerezyme® (Imiglucerase, Genzyme Corporation) (Grabowski *et al.* 1995). Cerezyme® is produced using Chinese hamster ovarian (CHO) cells, a mammalian cell line of choice due to its rapid growth and high protein yields. In order to achieve a comparable efficacy to its predecessor Ceredase®, Cerezyme® is also modified post production in order to expose the valuable α-mannosyl residues of its carbohydrate side chains (Friedman *et al.* 1999). In recent years, two more ERT products became available for the treatment of M. Gaucher: Velaglucerase alpha (VPRIV®, Shire HGT) produced in a human cell line and Taliglucerase alpha (ELELYSO®, Protalix Biotherapeutics) produced in carrot cells. Just like Cerezyme®, both products rely on the mannose-receptor-mediated targeting of affected cells and are thus engineered accordingly (Figure 7b and c).

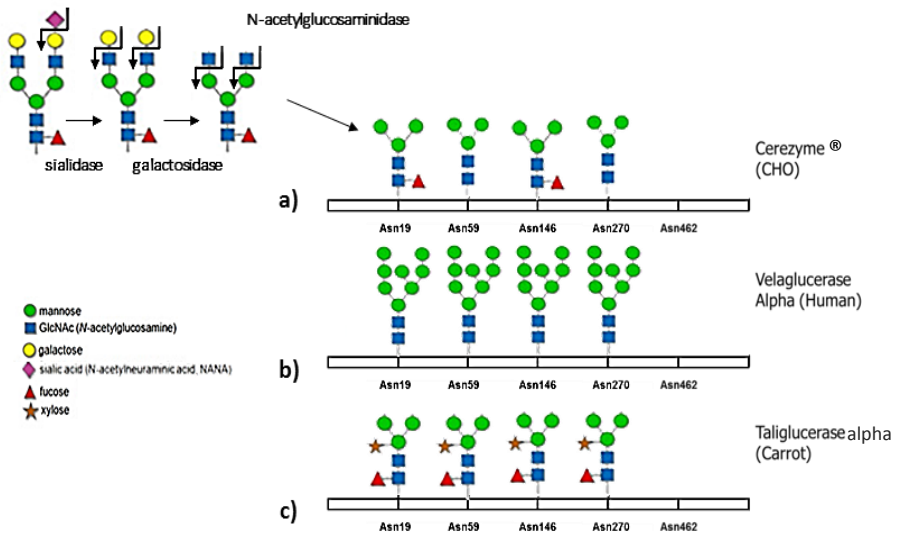

Figure 7 Mannose-terminated-β-glucosidases for ERT a) Cerezyme®, modified by sequential deglycosylation b) Velaglucerase alpha (VPRIV ®), produced in presence of Kifunensine I an inhibitor of the mannosidase I enzyme c) Taliglucerase alpha (ELELYSO®), produced in plant cells specially engineered to produce core mannose structures.

Enzyme replacement therapy is to date the standard of care for M. Gaucher patients of the type I and can be an option for Type III patients. However, the treatment only addresses visceral features as the access to the central nervous system of patients and thereby treatment of the neuronopathic aspect remains impossible (see 1.3.4.2). This unfortunately leaves Type II patients without a treatment option.

1.3.3 Enzyme replacement therapy for Fabry disease: engineering recombinant α-Galactosidase A

Morbus Fabry is the second lysosomal storage disease (LSD) for which enzyme replacement therapy (ERT) was developed in 2001. However, unlike in Morbus Gaucher, where affected cells are predominantly of the same phenotype, thus enabling “easy” targeting of a single receptor in order to reach them all, Fabry disease is a uniquely complex disease affecting a variety of cell types (multisystem disorder). Therefore, it was necessary to identify a receptor expressed on all or most of the affected cell types and at sufficient levels. At first this proved challenging, thus increasing the level of difficulty for the development of a targeted recombinant enzyme. Fortunately, increased interest given to lectin receptors and their function (Ashwell and Morrel 1974) led to the identification of mannose-6-phosphate receptors (MRPs) (Kaplan *et al.* 1977) and opened up new possibilities for ERT. Indeed, MPRs are ubiquitously expressed in the human body (Funk *et al.* 1992), making them an ideal target for ERT for Morbus

Fabry. However, identification of the mannose-6-phosphate (M6P) mediated sorting mechanism was not sufficient; it was not until recombinant protein expression technology became available that a successful therapy could be developed. Indeed, unlike tissue-isolated β-glucosidase (GBA) which in part already carried the "useful" targeting N-glycan (high-mannose), α-galactosidase A (GAL) isolated from human tissues (i.e. placenta, plasma, liver etc.) mostly lacked the required M6P glycan. This was the result of the enzymes being routed to the lysosome where removal of the M6P marker by specific hydrolases occurs. Consequently, tissue-extracted enzyme, which is to a large part composed of processed enzymes, was not an efficient solution (Desnick *et al.* 1979, Bishop *et al.* 1981). However, development of recombinant expression technology changed this. Recombinant product is engineered to be secreted by the host cell, i.e., in most cases the recombinant enzymes carry the indispensable M6P moieties. Thus a large amount of phosphorylated α-galactosidase A enzyme becomes available (Ioannou *et al.* 1992). In 2001, the FDA approved Fabrazyme®, a recombinant GAL produced in CHO cells that is 85 % phosphorylated. A few years later, a second ERT product called Replagal® became available. This recombinant GAL produced in human cells has 60 % phosphorylated N-glycan but is nonetheless efficiently taken up by target cells.

1.3.4 Limitations of enzyme replacement therapy

The theory behind enzyme replacement therapy (ERT) is in essence a simple one. A recombinant form of the deficient enzyme is produced and given to patients intravenously. Once in the blood circulation, the recombinant enzyme is recognized by selected cell surface carbohydrate receptors, internalized and transported to the lysosome. However the reality is somewhat different. Recognition and delivery of the recombinant substances is not as specific as it could and should be, leaving some organs or tissues less "corrected" than others. One reason for this is the challenge which glycan synthesis can represent during recombinant production processes and the resulting glycan heterogeneity (see 1.1.1 and 1.3.4.1). Another problem is that not all patients are eligible for treatment with ERT, in particular patients with neuropathic disorders (i.e. Type II and III Gaucher disease) which to date remain untreatable using ERT due to the problems posed by the blood-brain barrier (BBB) (see 1.3.4.2). Furthermore, there are problems with gauging efficacy of a treatment in these highly variable disorders, in particular for Morbus Fabry. Indeed, compared with other LSDs, the evaluation of the response to ERT in Fabry disease is complicated by the fact that, for example, no obvious morphological changes occur in response to ERT. In Gaucher disease, for example, the characteristic organomegaly is substantially

reduced with ERT. In Fabry disease, much of the critical organ pathology often remains subclinical until the late stages of the disease (Mehta *et al.* 2010). Finally, the therapies are expensive, limiting access to patients in those countries that are able to afford expensive health care (Wraith 2006).

1.3.4.1 Glycosylation related mistargeting to the liver

The uptake of circulating proteins by the liver can be divided into two pathways: the uptake by Kupffer cells mediated by the mannose receptor (MR) and the uptake by hepatocytes mediated by the asialoglycoptrotein receptor (ASGPR), the latter being the predominant uptake route. As mentioned earlier, in the case of enzyme replacement therapy (ERT), the preferred way of harboring recombinant enzymes to diseased cells is via targeting of selected carbohydrate receptors such as MR or mannose-6-phosphate receptor (MPR). The recombinant enzymes must therefore carry selected glycan structures (i.e. mannose for β-glucocerebrosidase (GBA); mannose-6-phosphate (M6P) for α-galactosidase A (GAL)). However, as mentioned before, this is extremely difficult to control due to the heterogeneity of carbohydrate processing (see 1.1.1). In the case of M6P for example, problems can arise in the first step of the phosphorylation process and the transfer of GlcNAc-P becomes a bottleneck in most cells. As a result, processing of the enzyme can be incomplete. This can be further aggravated when recombinant over-expression is performed as even more recombinant product needs to be processed. Consequently, carbohydrate processing of the recombinant forms is typically incomplete, resulting in a mixture of N-glycans: M6P, non-M6P, high-mannose, complex type etc. The less M6P is present, the less product will be delivered to the cells. In addition, of the M6P moieties that are actually present at the end of the synthesis, only selected ones are relevant. For example, bis-M6P N-glycans (two M6P residues on the same N-glycan) will be bound with high affinity by the MPR, whereas mono-M6P N-glycans (1 M6P residue on an N-glycan) will be bound with a moderate affinity, i.e., enzyme targeting to the receptor will strongly vary (see 1.1.2). Furthermore, non-phosphorylated mannose can be recognized by the mannose receptor of the liver cells leading to product loss (Zhang *et al.* 2011). To complicate matters further, dead or damaged cells release enzymes such as phosphatases into the culture medium which may remove phosphate groups. The resulting dephosphorylated mannose structures can also lead to a therapeutic protein mistargeting to the mannose receptor of the liver macrophages.

Another example of glycosylation-related mistargeting when considering ERT, is the uptake of enzymes by the liver asialoglycoprotein receptor (ASGPR) via terminal galactose (tGal) or galactosamine (tGalNAc) moieties. The mixture of glycan resulting from the highly variable

glycosylation process means that sialylation may not be sufficient. And, if consequently tGal or tGalNAc sugars are present, therapeutic protein will be lost to liver hepatocytes via the ASGPR. In current therapies, over 50 % of the injected dose (ID) of recombinant enzyme is lost to the liver. Not only does this mean that most of the enzyme is lost to hepatocyte cells which do not necessarily require it, but in addition, circulation life is reduced possibly resulting in suboptimal biodistribution as the enzyme does not have enough time to reach certain tissues. These limitations, which also apply to a number of other therapeutic proteins, have led to the development and implementation of half-life extension strategies (Kontermann 2011). They not only target a reduced ASGPR binding (i.e. increasing degree of sialic acid) but generally also tackle all the routes responsible for premature therapeutic protein clearing (Figure 8). The resulting modified recombinant molecules are often referred to as long-acting. Such techniques have also been used for recombinant lysosomal enzymes, predominantly in the form of a fusion protein (i.e. PEG polymer conjugation or Fc fusion).

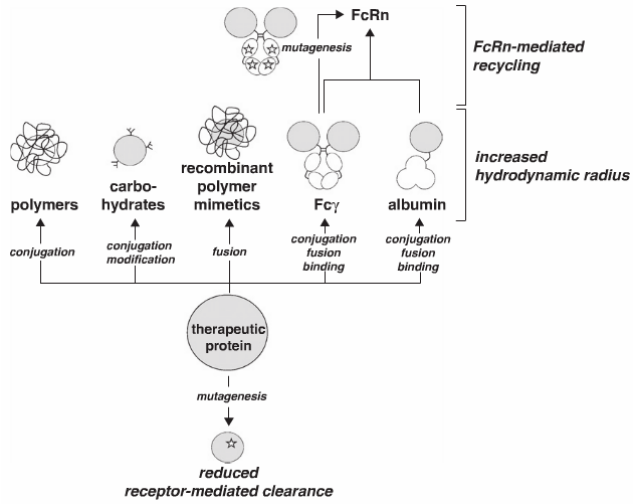

Figure 8 Half-life extension strategies, including hydrodynamic volume increase, FcRn-mediated recycling and stability modulation of protein-receptor complexes in the sorting endosome (from Kontermann 2011).

1.3.4.2 The unreachable CNS

The biggest weakness of enzyme replacement therapies (ERTs) to date resides in their inability to treat the central nervous system (CNS). This is because the recombinant enzymes are too large to overcome the blood brain barrier (BBB) which separates the brain parenchyma from blood circulation. As most disorders comprise severe CNS complications, this means ERT can't treat neurological LSDs or at least not efficiently enough. The BBB is a physical barrier that restricts the entry of substances circulating in the blood into the brain. This filter-like structure, designed

to protect the brain from dangerous particles, is a sophisticated layer of cells comprising endothelial cells, basal lamina, astrocytes and pericytes (Figure 9).

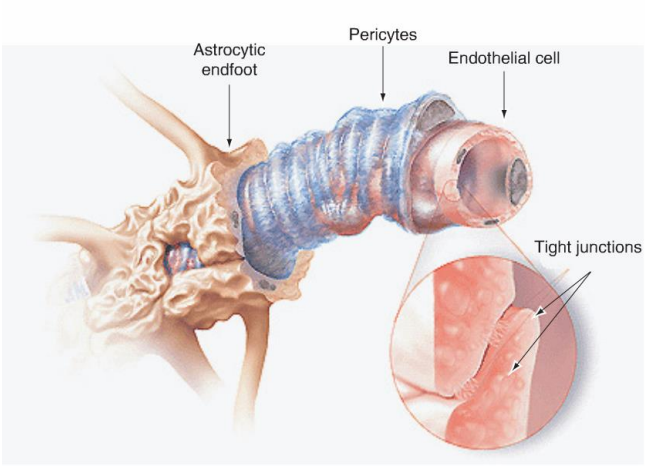

Figure 9 Schematic representation of a cerebral capillary: surrounding pericytes and astrocytic end feet project on to the endothelial cells of the cerebral capillaries, induce and maintain the blood–brain barrier (Gaillard *et al.* 2005).

The endothelial cells are closely connected to each other by tight junctions and adherence junctions. They enable diffusion and active transport of selected molecules but are impermeable to most other molecules, especially those larger than 400Da (Abbott et al. 2010). This applies to every recombinant lysosomal enzyme.

In recent years, efforts have been made to address this major flaw but no product has yet reached approval stage. Intrathecal ERT is one example of circumventing the BBB (Calias *et al.* 2014). The cerebral spinal fluid (CSF) naturally circulates between the spinal column and the brain. The enzyme is shuttled to the spinal fluid by a catheter. In order to minimize the chances of infection or injury due to repeated spinal puncture, a small port is generally implanted in the abdomen of patients just under the skin. While this method has shown promising results in clinical phases I and II, it remains highly invasive. Moreover following administration, the therapeutic product accesses the venous circulation but still has to pass the brain-CSF barrier by diffusion. This mechanism, however, grants limited access to the parenchyma and remains localized (Gaillard *et al.* 2005, Aird 1984). A more promising approach lies within the so called “molecular Trojan-horse technology” (Pardridge 2006). As mentioned earlier, the BBB is impenetrable to large molecules including recombinant enzymes. However, some large molecules such as transferrin and insulin for example are still able to penetrate the brain parenchyma despite their size. This is the result of specific transport mechanisms at the apical side of the brain endothelial cells (Figure 10).

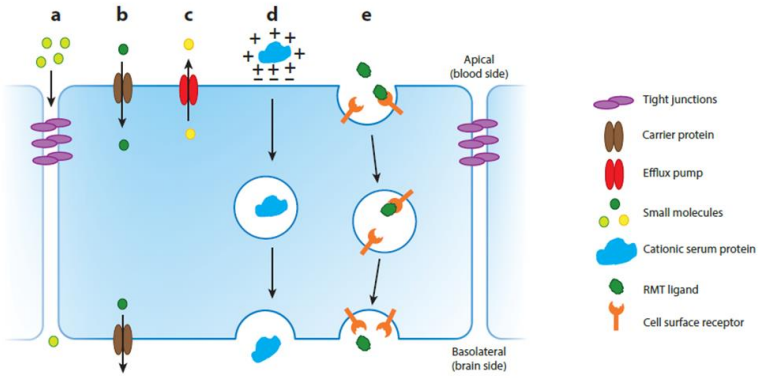

Figure 10 Endogenous blood-brain barrier (BBB) transport routes a) Paracellular diffusion of hydrophilic molecules b) Carrier-mediated transport c) Drug efflux pumps d) Adsorptive-mediated transport e) receptor-mediated transport (RMT) (adapted from Lajoie and Shusta 2015).

Amongst these transport mechanisms, the process known as receptor-mediated transcytosis (RMT) is of particular interest. Given receptors recognize specific ligands, bind and endocytose them prior to transporting them from one side to the other. Molecular Trojan horse technology takes advantage of these mechanisms by re-engineering the drug of interest so that it is recognized by these receptors. In this case, either the ligand, a portion of the ligand (peptide) or a mimetic antibody directed against the chosen ligand-receptor is coupled to the therapeutic protein (Pardridge and Boado 2012). The resulting fusion protein ideally retains the therapeutic protein functionality and in addition, due to the attached "ligand domain", can be recognized and transported across the BBB by the specific receptor. To date, several recombinant lysosomal enzymes have been modified in this manner in order to bind to the human insulin receptor for example. *In vitro* and in particular *in vivo* data have shown the ability of these molecules to be safely transported into the brain in unprecedented amounts (Boado *et al.* 2013).

1.4 Aim of the study

The aim of this project was to address some of the weaknesses or inadequacies that persist in enzyme replacement therapy (ERT). Availability, targeting and distribution of the recombinant enzymes are essential for an efficient ERT. For most lysosomal storage diseases (LSDs), this implies controlled presence of important carbohydrate structures, prolonged circulation half-life and reduced liver uptake, all directly related to good tissue availability and biodistribution.

A critical quality attribute of almost all ERTs is the presence of mannose-6-phosphate (M6P) residues among the N-glycans of the recombinant therapeutic protein. Increasing the levels of M6P on ERTs has been observed to promote uptake and subsequently the activity of treatments for lysosomal storage diseases both *in vitro* and *in vivo* (Zhu *et al.* 2004, Zhu *et al.* 2005). For this reason, work was undertaken to A) engineer a more appropriate production host cell line, with the ability to robustly deliver recombinant enzymes demonstrating high levels of M6P, B) address the issues related to the high liver uptake of the recombinant enzymes used in ERT, due to the asialoglycoprotein receptor (ASGPR) of the hepatocyte cells. Engineering work was therefore initiated in order to "redesign" the recombinant lysosomal enzyme so as to avoid ASGPR recognition. Finally, C) experiments regarding the "ERT/blood-brain barrier (BBB) problematic" were also undertaken. The strategy relied on the "molecular Trojan-horse technology" whereby recombinant proteins are reengineered to enable receptor-mediated transcytosis (RMT). The aim here was to generate an active recombinant fusion enzyme capable of "transcytosing" through brain endothelial cells.

2 Materials and Methods

2.1 Cell culture

Recombinant protein expression was performed in Glycotope's human host cell line H9D8 (deposited under DSM ACC 2806 at the "DSMZ-Deutsche Sammlung von Mikroorganismen und Zellkulturen GmbH" in Braunschweig in Germany). H9D8 is derived from human myeloid leukemia cells and is part of the GlycoExpress (GEX™) platform technology. The GEX™ platform enables the glyco-optimization of a variety of fully human glycosylated biopharmaceuticals by using a toolbox of glyco-engineered proprietary human cell lines that allow for optimization of a series of different determining sugars such as sialic acid (Goletz *et al.* 2008, Patent N° WO2008028686 A2). The H9D8 cell line was fully sequenced by next generation sequencing and is DHFR positive (dhfr+) (see 2.3).

H9D8 cultures were maintained at 37°C, 8 % CO_2 and 95 % humidity in GTM 8.1 medium (Biochrom AG, Germany) supplemented with lipids and 1xHT supplements (from 50X Gibco™ HT stock, 41065-012, Life Technologies now ThermoFisher Scientific). Subculturing occurred every two to three days. Transfected H9D8 cells were cultured in the same manner with the exception of 1x HT supplements which were replaced with selection agent methotrexate (MTX) (M8407, Sigma Aldrich, Germany).

T47D (HTB-133™, ATCC®, Germany) cells and NIH/3T3 mouse fibroblast cells (CR-1658, ATCC®, Germany) were maintained at 37°C, 5 % CO_2 and 95 % humidity in Dubelcco's Modified Eagle Medium (DMEM, 11960-044, ThermoFisher Scientific) supplemented with 5 % foetal bovine serum (FBS, S0115, Biochrom AG, Germany) and 2 mM L-Glutamine (from 200 nM Gibco® stock solution, 25030, Life technologies, now ThermoFisher Scientific). Subculturing occurred every two to three days.

2.2 Molecular biology

Genes encoding the designed fusion proteins were generated and ordered. These genes (or inserts) were then incorporated into Glycotope's proprietary expression vectors (GT expression vector) in order to enable stable transfection of cells and recombinant protein expression. A schematic

overview, illustrating the different molecular steps involved in the generation of the inserts and their incorporation into expression vectors are shown in Figure 11 and detailed hereinafter.

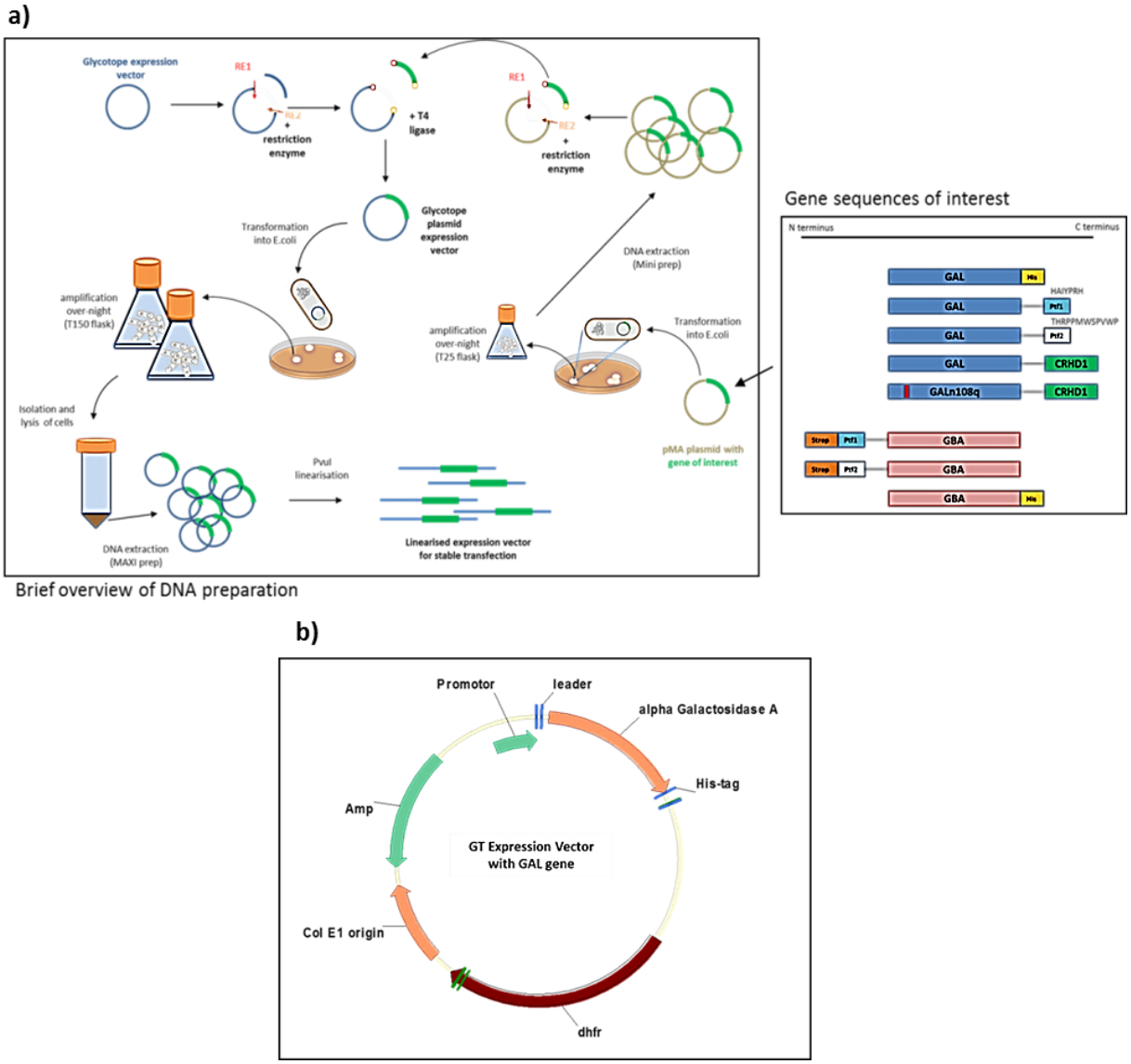

Figure 11 a) Schematic of various genes encoding recombinant enzymes and preparation of the Glycotope expression vector (GT expression vector) for stable transfections b) Example of a finalized GT expression vector map (non-linearized), including the promotor and leader sequences, the gene of interest (in this case GAL-His) and the dhfr gene for the cell selection. Amp refers to the ampicillin resistance.

In total, eight constructs were generated using these methods. Four of these were based on the gene sequence of the lysosomal enzyme α Galactosidase A (GAL), with either a His tag (GAL His), transferrin receptor binding peptides (GAL-Ptf1 or GAL-Ptf2) or the carbohydrate recognition domain H1 (CRDH1) of the human ASGPR (GAL-CRDH1). In addition, a GAL CRDH1 construct lacking one glycosylation site (Asn108) was generated (GALn108q CRDH1). Finally, three additional constructs were generated based on lysosomal enzyme β glucosidase (GBA) with

either a His Tag (GBA-His) or transferrin receptor binding peptides in combination with a streptavidin tag (Strep-Ptf1-GBA or Strep-Ptf2-GBA). Both the His- and Strep-tags were introduced to facilitate recombinant protein purification via affinity chromatography (see 2.6).

2.2.1 Bacterial transformation and small-scale amplification of recombinant DNA

All cDNA sequences were synthesized by GeneArt (Life Technologies, now ThermoFisher Scientific) and usually delivered in GeneArt's pMA or pMK_RQ plasmid vectors. Upon delivery, plasmid DNA was transformed into chemically competent *E.coli* cells (NEB 5-alpha Competent *E.coli* strain, C2987, New England Biolabs) by heat shock technique according to the suppliers' instructions. Briefly, between 1 and 5 µl plasmid DNA (1 pg to 100 ng) was added to one vial of cells (50 µl) and incubated on ice for 30 min. Following this, a 30-second heat shock at 42°C was performed after which cells were laid on ice again (5 min). Cells were then re-suspended in 950 µl of pre-heated "Super-Optimal broth with Catabolite repression outgrowth medium" (S.O.C medium, B9020S, New England Biolabs) and agitated at 37°C for 60 min. Following this incubation period, 50-100 µl of cell mix was plated onto an agar selection plate for colony formation over-night at 37°C. Only bacteria having transiently integrated the DNA of interest survive, due to the antibiotic resistance present on the plasmid/expression vector (i.e. AMP = ampicillin resistance).

The resulting cDNA-carrying colonies were amplified overnight in 10 mL of LB medium, 37°C in order to generate larger amounts of cDNA. On the following day, cells were pelleted and plasmid DNA extracted using a QIAprep Spin Miniprep kit (27104, Qiagen, Germany) according to the suppliers' instructions.

2.2.2 Restriction digests of pMA_cDNA and GT expression vector

Following plasmid DNA amplification (2.2.1), the genes of interest were "cut out" of the GeneArt delivery vectors by restrictive enzyme digestion (Fast Digest restriction enzymes, New England Biolabs). In parallel, the GT expression vector, into which the gene encoding DNA of interest was to be inserted, was treated with the same restriction enzymes in order to generate matching ends. The restrictive digests were set up and performed as advised by the supplier: components and respective amounts used in the different digestion mixes are listed in Table 4. For the GT expression vector, an additional dephosphorylation step was performed following its linearization by restrictive enzymes in order to prevent "blunt end" assembly-reforming

plasmid DNA. To this end, 4 µl of Fast AP enzyme (FastAP Thermosensitive Alkaline Phosphatase, EF0651, ThermoFisher Scientific) was added to the GT expression vector digest mix and incubated for 10 min at 37°C.

Table 4 Setup for restriction enzyme digest of vector DNA and insert DNA.

Components	Vector digest mix	*Insert* digest mix
DNA	8 µg	4 µg
10 × Fast Digest Puffer	8 µl	4 µl
Enzyme 1 (10 U/µl)	1 µl	0,5 µl
Enzyme 2 (10 U/µl)	1 µl	0,5 µl
Millipore-H_2O	Fill to 80 µl	Fill to 40 µl

2.2.3 Gel agarose analysis and DNA extraction

The evaluation of the restrictive digests performed earlier (see 2.2.2), followed by DNA isolation were performed by gel agarose electrophoresis. To this end, digestion mixes were loaded onto a 0.8 % agarose gel and run in 1x Tris-acetate-EDTA (TAE) buffer (161-0743, Bio-Rad, Germany) for 120 to 150 min at 70 Volts per centimeter. Following this, the gel was stained in GelRed™ (41003, Biotrend, Germany) 0,1M Sodium-salt (NaCl, 3957.2, Carl Roth, Germany) solution for 10 to 20 min before visualization of the different DNA bands under UV light. Identification of cDNA (inserts) and linearized GT expression vector was then performed prior to excision (Figure 12).

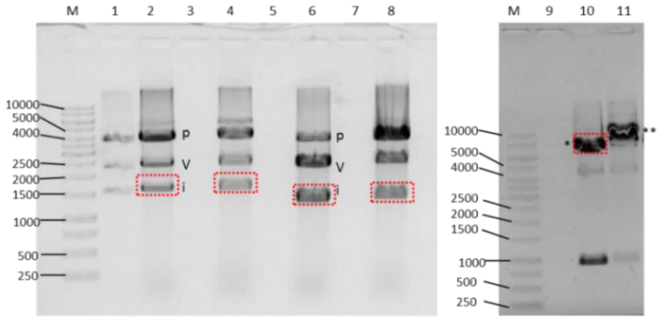

Figure 12 Example of agarose gel electrophoresis analysis of restriction digests. M: 1kb marker, lanes 1,3,5,7 and 9 are empty, lanes 2 and 4: pMA_GBA HindIII/XbaI digest, lanes 6 and 8: pMK_RQ_GAL HindIII/XbaI digest, lanes 10 and 11: GT expression vector HindIII/XbaI digest. The respective bands are p: undigested plasmid, v: linearized vector (empty), i: insert or cDNA (GBA of GAL), * linearized GT vector (empty), ** undigested GT vector. Excised bands are labelled with a red dotted line.

Following identification of the various DNA bands, molecules of interest (linear GT expression vector (*) and GeneArt produced cDNA inserts (i)) were excised from gel using a scalpel and loaded into 2mL Eppendorf tubes for further processing. The isolation of the DNA from the excised agarose pieces was then performed using a NucleoSpin® Gel and PCR clean-up kit (740609, Macherey-Nagel, Germany) according to the suppliers' instructions.

2.2.4 Ligation of the recombinant expression vector

Next, the isolated cDNA molecules were ligated into the linearized and dephosphorylated GT expression vector isolated previously (see 2.2.3), in order to generate the final expression vector. To this end, the two DNA "pieces" were co-incubated with T4 DNA ligase (Rapid DNA Ligation Kit,11635379001, Roche) and incubated overnight in a thermocycler (TPersonal Thermocycler, Biometra, Analytic Jena) using the predefined ligation program. The detailed composition of the reaction mix is shown in Table 5 below.

Table 5 Ligation reaction mix composition.

Components	Amount
„empty" GT vector	50 ng
insert (ng)	$\frac{5 \times 50 \times \text{bp insert}}{\text{bp vector}}$
T4 DNA ligase	1 µl
T4 DNA ligase buffer (5X)	4 µl
Sterile H_2O	Fill to 20 µl

2.2.5 Large-scale DNA amplification and purification

The newly generated expression vectors were next amplified. To this end, following its overnight incubation, the ligation mix (2.2.4) was transformed into chemically competent E.coli cells, as described previously (2.2.1) with the difference that the entire 20 µl ligation mix was added to the cells. The successfully transformed bacterial colonies were then amplified overnight in 250 cm^2 shake-flasks (Corning, Germany) in order to generate large amounts of the final expression vector. On the following day, cells were pelleted and plasmid DNA extracted using an EndoFree Plasmid Maxi Kit (12362, Qiagen), according to suppliers' instructions.

2.2.6 Linearization and final purification of the expression vectors

In order to be able to use the newly generated expression vectors for stable transfection of expression host cell line H9D8, the plasmid vectors must first be linearized. Indeed, the goal of a stable transfection is to integrate the gene of interest into the host's genome. This is better achieved with a linear DNA molecule as opposed to a circular DNA molecule (plasmid). To this end, 100 µg of the purified plasmid expression vector was incubated with 5µl PvuI restriction enzyme (ER0622, ThermoFisher Scientific) and 20 µl of a 10x restriction buffer and filled to 200 µl final volume with H_2O. The reaction mix was left to incubate overnight at 37°C.

Following PvuI linearization, DNA extraction was performed by phenol/chloroform precipitation. Briefly, 200 µl of roti-phenol/chloroform (A156, Carl-Roth) solution was added to the linearized expression vector and the mix vortexed and spun down for 10 min at 6000 rpm. The upper phase was carefully transferred into a fresh 1.5 mL Eppendorf tube before repeating the roti-phenol/chloroform step. Then, 200 µl of tri-chloromethane/chloroform (7331.1, Carl Roth) solution was added, the mix vortexed and centrifuged 1min at 13000 rpm. The upper phase was then transferred into a peqGold Phase Trap A tube (30-0015A, Peqlab, VWR) and the tri-chloromethane/chloroform step repeated. The resulting upper phase was then transferred into a sterile Safe-lock tube (Eppendorf) and 20 µl of a 3 M sodium acetate solution added as well as 200 µl ethanol. The mix was then vortexed, revealing a DNA precipitation. The DNA was pelleted by 10min centrifugation at 13000 rpm and washed with 100 µl of 70 % ethanol (9065.5, Carl Roth). The pellet was then air-dried and finally resuspended in endotoxin-free sterile water.

2.3 Stable transfection of cells for recombinant protein expression

In order to produce the aforementioned constructs, stable transfections of Glycotope's H9D8 cells were performed using the appropriate expression vector. This was done by cell electroporation according to the manufacturers' protocol, using a *Cell Line Nucleofector*® Kit *V* (VACA-1001, Amaxa Biosystems, Lonza). Briefly, $2x10^6$ viable cells were spun down for 5 min at 1200 rpm. The cell pellet was then re-suspended in 100 µl NFS Mix (100 µl Supplement I + 450 µl Nucleofector Solution V) before adding 9 µg of linearized DNA (prepared above). The cell mix was then transferred to a cuvette for electroporation. Following electroporation, 500 µl of pre-warmed GTM 8.1 medium was carefully added to the cells before

transferring them to a 6-well plate (TPP) and incubating them at 37°C, 5 % CO_2 and 90 % humidity.

Once the cells have been transfected, selection of those having successfully integrated the recombinant DNA into their genome needs to occur. To this end, the GT expression vector (Figure 11b) carries a selection marker enabling such a step, namely the dihydrofolate reductase gene (DHFR). The DHFR enzyme catalyzes the conversion of folate to tetrahydrofolate, a precursor necessary for the *de novo* synthesis of purines, pyrimidines and glycine. Substances such as methotrexate (MTX) inhibit the DHFR enzyme and this leads to cell-death as a result of nucleotide depravation. However, the DHFR enzyme used by Glycotope carries a mutation making it is less sensitive to MTX and thereby conferring a substantial drug resistance to only those cells having integrated the GT expression vector (McIvor R. S. and Simonsen C., 1990). Therefore, 48hrs post electroporation, methotrexate (MTX) was added to the culture medium (final concentration of 25 nM) to initiate the selection phase. At this stage, cultures are referred to as pool cultures. In addition, following the "elimination" of non-transfected cells, a gradual increase of the MTX concentration in the medium leads to preferential survival of cells presenting numerous copies of the DHFR gene and therefore of the GT expression vector. This is referred to as the amplification phase. Following several amplification rounds with increasing MTX concentration (up to 400 nM), single-cell cloning was performed in order to isolate high-producing clones from within the pools (see 2.4).

Stably transfected H9D8 cells were routinely cultured as described in paragraph 2.1, however without the addition of HT supplements. Instead, the required MTX concentration (depending on the amplification level) was added. During supernatant production (culture scale-up), stably transfected cells were cultivated in MTX-free medium from the point the culture volume reached 50mL.

2.4 Single-cell cloning

Following stable cell transfection, pool cultures can be screened in order to isolate higher producing single cells. The isolated cells are then left to multiply and later become the production clones. This selection step ensures a more robust and reproducible production process. In general, for a given recombinant product, 3 to 4 production clones are retained at the end of a cell cloning procedure.

Two methods exist: serial dilution of cells and isolation using a semi-solid cloning matrix (Figure 13).

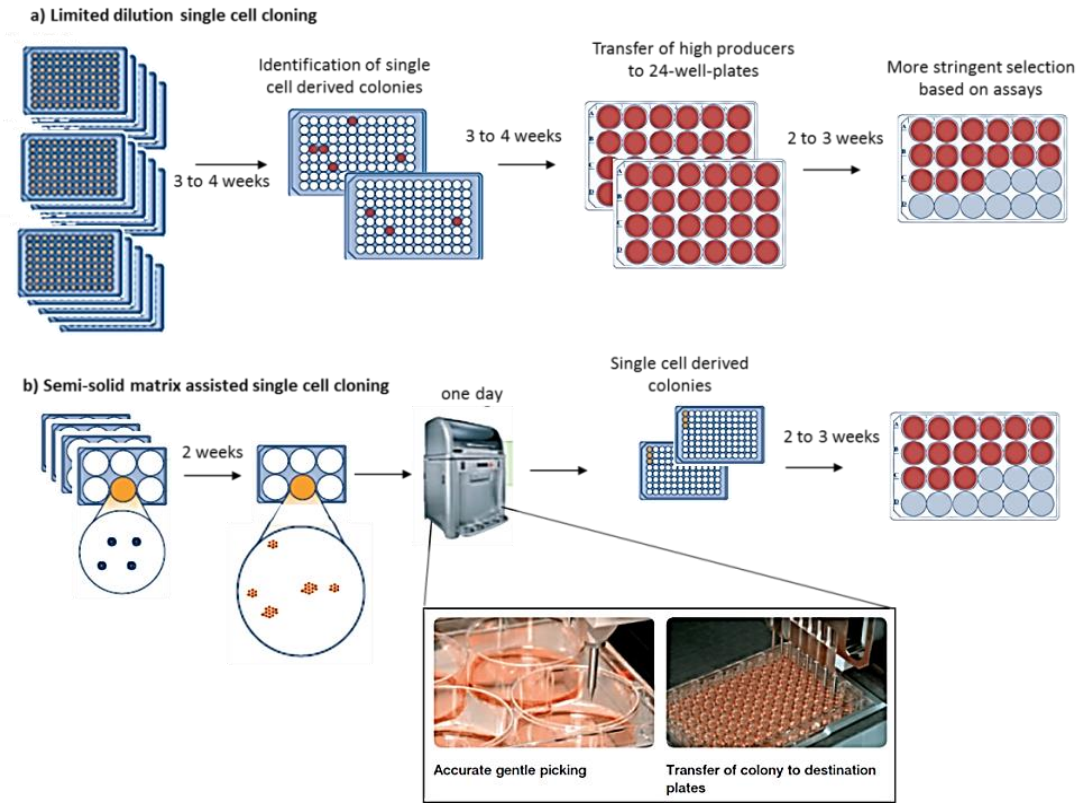

Figure 13 First steps of two cell line development techniques a) limited dilution (see2.4.1) b) clone matrix (see 2.4.2).

2.4.1 Generation of production clones by limited dilution

In this method, the pool of transfected cells was diluted down stepwise in GTM 8.1 medium, so to obtain 1 living cell per 200 µl (5 cells.mL^{-1}). The diluted cell suspension was then aliquoted into 96-well plates (TPP) with 200 µl per well. Plates were then incubated at 37°C, 8 % CO_2 and 95 % humidity. On a weekly basis, plates were screened microscopically in order to identify the wells containing only one cell or single-cell-derived colonies. These selected single cells were then

left to multiply for several weeks until they reached sufficient confluency (>30 %) for upscale into 24-well plates. This is referred to as the amplification step. Amplification was repeated until the single-cell-derived colonies reach T25 culture-flask (TPP) scale. In between amplification rounds, clones were assessed for product yield in order to selectively keep and amplify clones with a high productivity.

2.4.2 Generation of production clones using clone-matrix

In this method, single cells were not isolated in 96-well plates but on a semi-solid clone-matrix. This enables a better segregation of the cells and resulting colonies. To this end, 50 mL of 2x concentrated GTM medium (Biochrom AG.) was mixed together with 40 mL of Clone Matrix concentrate (K85000, Molecular Devices) for semi-solid medium and topped up to a final volume of 100 mL using water (H_2O ultra-pure, 10977-035, Gibco®, Life Technologies). An appropriate volume of pool culture was then gently added to the freshly prepared semi-solid medium so to have between 100 and 1000 living cells per mL of matrix. The semi-solid cell mixture was then transferred to 6-well plates (CELLSTAR, Greiner) at 2 mL per well, taking care not to create any air bubbles. Plates were incubated at 37°C, 8 % CO_2 and 95 % humidity for a period of 10 to 14 days. Following this incubation period, when enough colonies were observed in the single wells, isolation was performed using a ClonePix system (Molecular Devices). This device recognizes distinct single cell colonies and "picks" them, with the help of small metal pins, in order to transfer them into 96-well plates pre-filled with GTM 8.1 (200 µl/well). From this point on, the same amplification and productivity assessment steps as described previously (2.4.1) are put in place in order to obtain selected high producing clone cultures in 25 cm² T-flasks (TPP).

2.5 Re-engineering of Glycotope's H9D8 host cell line

2.5.1 Mutation of H9D8 cell line

This method was adapted from Marnell's publication (Marnell et al. 1984) and an overview of the selection procedure is presented in Figure 14. Briefly, H9D8 cells ($1x10^6$ cells in GTM 8.1 supplemented with lipids and 1xHT) were treated with 100 µg/mL ethylmethanesulfonate (EMS, M0880, Sigma Aldrich) for 3 hrs at 37°C, 8 %CO_2 and 95 % humidity. Following this incubation, EMS-containing medium was removed by centrifugation (5 min, 1200 rpm) and cells were washed with phosphate buffer saline (1x PBS, Dubelcco PBS, L1825, Biochrom AG). The pelleted cells were then resuspended in

supplemented GTM 8.1 culture medium and left to incubate at 37°C, 8 %CO2 and 95 % humidity for a period of 3 to 4 weeks or until their viability had reached over 75-80 %. At this point, the culture temperature was increased to 40°C for a period of 24 hrs. A "toxin cocktail", containing 1 µg/mL Exotoxin A (ExA, P0184, Sigma Aldrich) and 33 ng/mL Diphtheria toxin (DT, D0564, Sigma Aldrich), was then added to the cells and left to co-incubate for another 24 hrs. Following this, cells were extensively washed in order to remove all traces of toxins. After resuspension in supplemented GTM 8.1 culture medium, cells were maintained for a period of 4-weeks, until viability returned above 80 %. At this point, single cell cloning was performed using the semi-solid cloning-matrix method (see 2.4.2). The selected single cell clones were then screened for reduced acidic vesicle content using a flow cytometry (FACS) based assay described below (2.5.2).

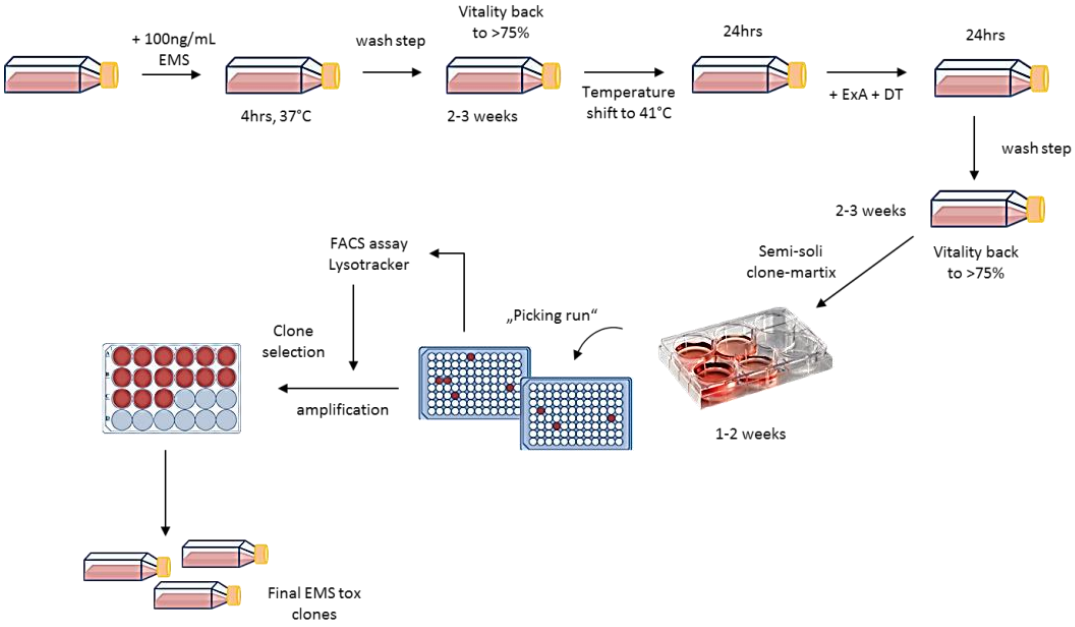

Figure 14 Generation of EMS tox H9D8 cell line for improved mannose-6 phosphorylation.

2.5.2 Acidic vesicle quantification using flow cytometry

Acidic vesicle quantification was performed using LysoTracker® Green DND (L7526, Life Science Technologies) in a flow cytometry assay (FACs). Lysotracker® dye consists of a fluorophore linked to a weak base, the latter enabling the dye to selectively accumulate in cellular compartments with low internal pH such as lysosomes. For this purpose, EMS tox H9D8 clones were seeded in a 96-well plate (round-bottom well, TPP) at a viable cell concentration of $2x10^5$ cells.mL^{-1} (200 µl/well) and incubated for 24 hrs at 37°C, 8 % CO_2 and 95 % humidity.

The temperature was then increased to 40°C ("permissive" temperature) in order to "activate" the mutation. On the following day, cells were spun down and re-suspended in culture medium supplemented with LysoTracker® dye (50 nM final concentration) and co-incubated for 60 min at 37°C, 8 % CO_2 and 95 % humidity. Cells were then washed twice and re-suspended in 100 µl 1x PBS prior to FACs analysis. Two controls were run in parallel: one containing normal H9D8 cells (negative control) and another containing H9D8 cells treated with Bafilomycin (Bafilomycin A1 from *Streptomyces griseus*, B1793, Sigma Aldrich) (positive control). Indeed, Bafilomycin inhibits ATP-dependent proton pumps normally involved in vesicle acidification and thereby mimics a deficiency in endosomal acidification.

2.6 Recombinant protein purification

This section describes the different purification techniques used to isolate the various recombinant lysosomal enzymes generated during this project.

2.6.1 Poly-histidine-Tag affinity chromatography

A self-packed nickel-nitrilotriacetic acid (NINTA) column (cOmplete™ resin, Cat. 5893682001, Roche) was equilibrated in "buffer A" composed of 50 mM Tris-HCl pH 7.0 (Tris-HCl, 9090.3, Carl Roth), 300 mM NaCl and 50 mM Imidazole-HCl (I3386, Sigma). Following this, the culture supernatant was loaded onto the column and after completion, a washed step using buffer A was performed to return the absorbance levels to a baseline value. The recombinant protein of interest was then eluted from the column using "buffer B" composed of 50 mM Tris-HCl pH 7.0, 300 mM NaCl and 500 mM Imidazole-HCl.

This method was used for the purification of both GAL-His and GBA-His proteins.

2.6.2 Streptavidin affinity chromatography

Strep-Tactin® superflow column (2-1207-001, iba-lifescience) was equilibrated in "buffer C" composed of 50 mM sodium phosphate buffer pH 7.0 (71504, Sigma Aldrich) and 300 mM NaCl. After loading culture supernatant onto the column, a wash step was performed using buffer C, until the absorbance signal returned to baseline. Recombinant protein was eluted from the column using "buffer D" composed of 50 mM Sodium-phosphate buffer pH 6.5, 300 mM NaCl and 2,5 mM d-desthiobiotin (D-1411, Sigma Aldrich).

This method was used for the purification of both Strep-Ptf1-GBA and Strep-Ptf2-GBA proteins.

2.6.3 Galactose affinity chromatography

Galactose affinity chromatography was used in two different ways depending on the protein of interest that needed to be extracted. The galactose-coupled resin used for this purpose was prepared as described in the literature (Inhibashi et al. 1994). Briefly, sepharose 4B resin (GE Healthcare) was washed with water and then equilibrated in a carbonate buffer pH 10 (A135.1, Carl Roth), before being activated for 2 hrs using divinylsulfone (Cat. 821215, Merck-Millipore). Following its activation, sepharose resin was incubated overnight in carbonate buffer pH 8.0 containing D-galactose (G0750, Sigma Aldrich). The galactose-coupled sepharose (GAL-sepharose) was washed, then "deactivated" by 3hrs incubation in carbonate buffer pH 9.0 containing 0.002 volumes of beta-mercaptoethanol (4227.3, Carl Roth). Finally the GAL-sepharose was packed into a column cartridge and washed extensively with a 10 mM Hepes pH 7.4 (Hepes, HN78.3, Carl Roth), 30 mM $CaCl_2$ (CN93.2, Carl Roth) buffer.

- Purification of CRDH1 fusion proteins

Prior to purification, the culture supernatant pH was adjusted to 7.0 and supplemented with 50 mM $CaCl_2$. The supernatant was then loaded onto a GAL-sepharose column (see above) pre-equilibrated in 10 mM Hepes pH 7.4, 30 mM $CaCl_2$ buffer. Following this, a wash step using 10 mM Hepes pH 7.4, 30 mM $CaCl_2$ buffer was performed, followed by the elution step using a 10 mM Hepes pH 7.4, 2 mM Ethylenediaminetetraacetic acid (EDTA, 8040.2, Carl Roth) buffer.

This method was used for the purification of GAL-CRDH1 and GALn108q-CRDH1 and CRDH1 proteins.

- Purification of GAL construct without a tag

This method was adapted from Yasuda and colleagues (Yasuda et al. 2004). Briefly, the cell culture supernatant pH was adjusted to 4.5 using citrate-phosphate pH 4.5 buffer (Carl Roth), then filtered using 0.22 µm bottle-top filters (TPP). Supernatant was then loaded onto a GAL-sepharose column equilibrated in a 25 mM citrate-phosphate pH 4.5, 100 mM NaCl buffer. Following a wash step with 25 mM citrate-phosphate pH 4.5, 100 mM NaCl buffer, recombinant protein was eluted by running a one-step gradient of 25 mM citrate-phosphate pH 6.0, 100 mM NaCl, 100 mM D-galactose buffer.

This method was used for the purification of both GAL-Ptf1 and GAL-Ptf2 proteins.

2.6.4 Size exclusion chromatography

Size exclusion chromatography (SEC) was performed in some cases to increase sample purity but also to determine aggregate and fragment levels. For this purpose, a Superdex 200 10/300 GL SEC column (17-5175-01, GE Healthcare) was equilibrated in 10 mM Hepes pH 7.0, 150 mM NaCl buffer. A sample of interest was then injected at the recommended flow rate of 0.5 mL/min and the monomer peak collected for further use.

2.7 Enzyme activity assays

The α-galactosidase A (GAL) activity in cell lysates or medium was determined using synthetic substrates para-nitrophenyl-α-(D)-galactopyranoside (pNP-GAL, N0877, Sigma Aldrich) or 4-methylumbelliferyl-α-(D)-galactopyranoside (4MU-GAL, M7633, Sigma Aldrich). Briefly, a substrate solution was prepared containing either 10 mM pNP-GAL or 5mM 4MU-GAL dissolved in 10 mM sodium acetate pH 4,6 buffer (Cat. 1062640050, Merck KGaA). The reaction mixtures, consisting of 50 µl sample and 50 µl substrate solution, were incubated in a black 96-well plate (OptiPlate, Perkin Elmer) at 37 °C for a given period. The reaction was terminated by addition of 100 µl of a 0.1 M Glycin (3908.3, Carl Roth)/Sodium hydroxide (NaOH, 319481, Fluka) pH 10 buffer. Absorbance (OD415nm for pNP-GAL) or fluorescence (ex 350 nm/em 418 nm, for 4MU-GAL) was then measured using an Enspire® 2300 plate reader (Enspire® Multimode plate reader, Perkin Elmer).

The acid β-glucosidase (GBA) activity in cell lysates or medium was determined using synthetic substrates para-nitrophenyl-β-(D)-glucopyranoside (pNP-G, N7006, Sigma Aldrich)) or 4-methylumbelliferyl-β-(D)-glucopyranoside (4MU-G, M3633, Sigma Aldrich). Briefly, a substrate solution was prepared containing either 10 mM pNP-G or 5 mM 4MU-G dissolved in 50 mM sodium phosphate pH 5.0, 5 mM sodium taurocholate (T4009, Sigma Aldrich), 0,15 % triton X-100 (X-100, Sigma Aldrich) buffer. The reaction mixtures, consisting of 50 µl sample and 50 µl substrate solution were incubated in a black 96-well plate (OptiPlate, Perkin Elmer) at 37°C for a given period. The reaction was terminated by adding 100 µl of 0.1 M Glycin/NaOH pH 10 buffer. Absorbance (OD 415 nm for pNP substrate) or fluorescence (ex 350 nm/em 418 nm for 4MU substrate) was then measured using an Enspire® 2300 plate reader (Enspire® Multimode plate reader, Perkin Elmer).

2.8 Mannose-6-phosphate and N-glycan analysis

Analysis of N-glycans comprising mannose-6-phosphate was performed by capillary electrophoresis (CE) coupled to laser-induced fluorescence (LIF) detection, in short CE-LIF (Figure 15). In this method, an electric field is generated inside the capillary mounted between two electrolyte-filled vials: an anode (+) and a cathode (-). This enables the electrophoretic migration of molecules along the electroosmotic gradient and separation depending on the charge and size of these molecules. The molecules are usually labelled prior to injection on CE-LIF so as to enable their detection when reaching the other end of the capillary. The resulting collection of signals or peaks is called electropherogram. Because carbohydrate structures differ in size and charge, entities such as sialic acid or phosphorylated mannose can be isolated and analyzed using this technique.

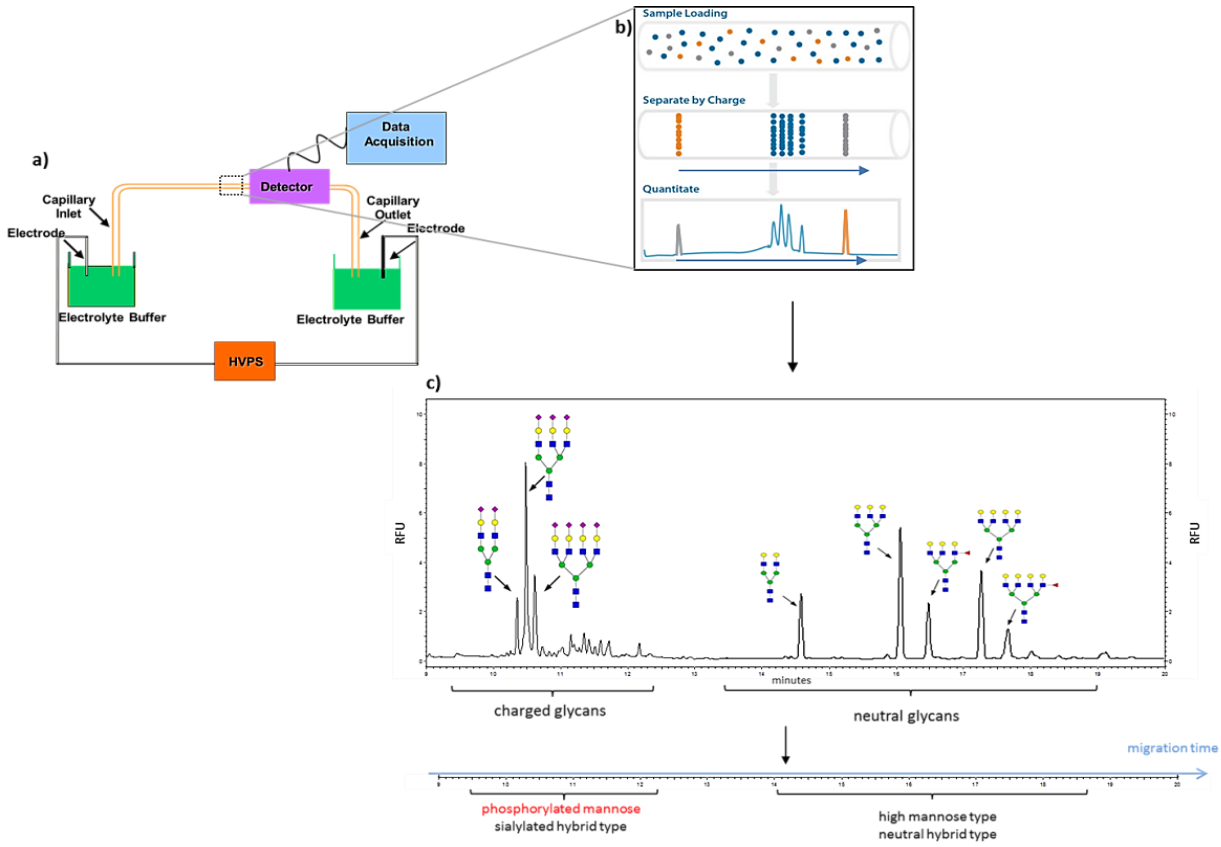

Figure 15 Principle of capillary electrophoresis coupled to laser-induced fluorescence (CE-LIF) a) CE-LIF assembly b) capillary-based separation and migration of molecules c) summary of N-glycan migration profile based on charge and type.

2.8.1 Enzymatic N-glycan release and labelling

The N-glycans were enzymatically removed from GAL-His or GAL-CRDH1 proteins using endoglycosidase H (EndoH, P0702S, New England Biolabs). This enzyme specifically releases high-mannose and hybrid-type N-glycans which are of particular interest for phosphorylation analysis. The highly specific release of these N-glycans results in a less complicated electropherograms facilitating unambiguous structure annotation.

The released N-glycans were then fluorescently labelled with 8-aminopyrene-1,3,6-trisulphonic acid (APTS, GS24-APTS labelling kit, Prozyme) by incubation at 50°C for 60 min. The one-pot reaction includes a reductant (sodium cyanoborohydrate) for stabilization of the intermediate labelling product (Schiff base) to result in an amine bond. Following this, the labelled N-glycans were purified by means of solid phase extraction (SPE) in order to remove labelling reagent excess. As a control, APTS labelled N-glycans were treated with alkaline phosphatase to remove any phosphate moieties. This results in a peak shift within the electropherogram specifically indicating phosphorylated high-mannose- and hybrid-type N-glycans.

For UltraPerformance Liquid Chromatography (UPLC®) analysis, N-glycans were enzymatically removed using PNGase F (GlycoWorks Rapid PNGase F and Buffer, Cat. 186007990, Waters). In this case all types of N-glycans are released. The released glycans were then fluorescently labelled with 2-aminobenzamide (2-AB), using the 2-AB Glycan Labeling Kit (Ludger, cat. no. LT-KAB-A2) and Ludger Clean S Glycan Cleanup Cartridges (Ludger, cat no. LC-S-A6) according to the manufacturer's instructions.

2.8.2 Capillary electrophoresis-laser induced fluorescent profiling of N-glycans

Capillary electrophoresis separations of APTS labelled N-glycans were performed on a Beckman PA800 Plus Pharmaceutical Analysis System equipped with a 3 mW 488 nm solid state laser and a 520 nm band-pass filter for laser induced fluorescence detection under the control of 32 Karat software, version 9.0 (Beckman Coulter, Brea, CA, USA). Separations were preformed using N-CHO neutral coated capillaries (360 μm O.D., 50 μm I.D.). The total capillary length was 60 cm with an effective separation length of 50 cm from the injection to the detector (BEC PN 477601, Beckman Coulter). For all experiments, a commercially available carbohydrate separation buffer was used (Beckman Coulter). The separation temperature was 25°C and the

applied potential was 30 kV, (500 V/cm reverse polarity). Prior to use, the capillary was conditioned by subsequent rinsing with water and carbohydrate separation buffer for 10 min at 30psi. The capillary was rinsed with carbohydrate separation buffer for 5 min at 30 psi between injections. Maltose (M9171, Sigma Aldrich) was used as internal standard in order to normalize migration time variations in between runs and to control labelling efficiency. Samples were injected hydrodynamically at 0.5 psi for 30 s with a water dip after each step of the injection sequence. The data collection rate of the instrument was 4 Hz. Migration times were converted to relative migration times using the maltose internal standard to compensate slight variations of the migration time from run to run. Phosphorylated and non-phosphorylated high-mannose-type N-glycans were assigned by comparison of relative migration times to references. Two references were used: the first being APTS labelled N-glycans of RNAse B (P7817S, New England Biolabs) which exclusively comprises high-mannose N-glycans, the second being N-glycans of GAL enzyme after treatment with alkaline phosphatase which results in a shift of phosphorylated N-glycan peaks.

The relative molar amount of phosphorylation was calculated from the total peak area of all phosphorylated high-mannose and hybrid-type N-glycans versus the total peak area of high-mannose and hybrid-type N-glycans (with or without phosphorylation).

2.8.3 N-glycan profiling using UltraPerformance Liquid Chromatography (UPLC®)

The 2-AB labelled N-Glycan samples prepared earlier (2.8.1) were dissolved with a 100 mM ammonium formate acetonitrile solution (40/60% (v/v)) and subsequently injected on an ACQUITY UPLC® Glycan BEH Amide Column, 130Å, 1.7µm, 2.1mm x 150mm (Waters, cat. no. 186004741; Milford, USA) using an Acquity UPLC® (Waters) instrument coupled to a fluorescence detector (FLR). A linear gradient of 100 mM aqueous ammonium formate buffer, pH 4.5 (mobile phase A) and acetonitrile (mobile phase B) was used for glycan separation. The flow rate was 0.5 mL/min. Glycan structures for each detected peak were identified using the GlycoBase 3.0 database (Waters).

2.9 3T3 mouse fibroblast uptake assay

The cellular uptake of GAL-His variants was investigated in NIH/3T3 mouse fibroblast cells (refer to 2.1). Cells were seeded in T-flasks (TPP) and grown to confluency in DMEM medium

supplemented with 5% heat-inactivated FBS and 2 mM L-glutamine. One day prior to sample addition, cells were transferred into 6-well plates (TPP) at a density of $2x10^5$ cells.mL^{-1}. Various amounts of enzymes were then added to the cells on the following day and left to incubate at 37°C for 24 hrs. The medium was then carefully removed, the cells washed four times with ice-cold 1x PBS, including one acid wash step in between washes with ice cold 0.2 M glycin/HCl buffer. Finally, cells were detached using Accutase (L11-007, GE Helathcare), then lysed by adding 150 µl per well of 10 mM sodium-acetate pH 5.0, 0.15 % Triton X-100 buffer (5 min, 4°C). Cell lysates were then subjected to three freeze/thaw cycles (-80°C/37°C) before centrifugation at 12,000 rpm for 10 min in 1,5 mL Eppendorf tubes (Eppendorf, Germany) to remove cell debris. The intracellular activity was measured using synthetic substrate 4MU-GAL as described previously in paragraph 2.7. Protein concentrations were determined by the bicinchoninic acid method (Micro BCA™ Protein Assay Kit, 23235, ThermoFisher Scientific) following the manufacturers' protocol. The intracellular activity of GAL-His variants was expressed as milliunits per mg total protein in lysate ($mU.mg^{-1}$), one unit being defined as the amount of enzyme required to release 1 µmol substrate per min.

2.10 CRDH1 receptor ELISA

To assess binding affinity of the asialoglycoprotein receptor (ASGPR) to the recombinant enzymes, a receptor-based enzyme-linked immunosorbent assay (receptor ELISA) was developed. To this end, the truncated carbohydrate recognition domain of the human ASGPR, namely CRDH1, was produced in-house and used in various assays.

A nunc MaxiSorp® flat-bottom 96-well plate (44-2404-21, Affymetrix eBioscience) was coated with 200 ng CRDH1 per well, in 1x TBS buffer (from 10x Roti® Stock, 1060.1, Carl Roth, Germany) and left overnight at 4°C. Following 3 wash steps using 10 mM Hepes pH 7.0, 150 mM NaCl, 10 mM CaCl2 buffer, the plate was "blocked" for 1 hr at room temperature by addition of 200 µl per well of wash buffer supplemented with 2 % bovine serum albumin (BSA, 8076.3, Carl Roth). Following another three wash cycles, 50 µl of each sample was added to each receptor-coated well and left to incubate for 2 hrs at room temperature. The plates were once again thoroughly washed before adding 50 µl per well of a diluted (1:5000) mouse monoclonal anti-GAL antibody (12078-MM07, Sino Biologicals) and incubating for 1 hr at room temperature. Finally, following three wash steps, horseradish peroxidase (HRP) coupled goat anti-mouse-IgG detection antibody (115-035-068, Jackson ImmunoResearch Laboratories Inc.) was added at 50 µl

per well (diluted 1:5000 in wash buffer) and left to incubate for 1 hr at room temperature. Colorimetric detection occurred by using 1-Step™ NBT/BCIP Substrate Solution (34042, ThermoFisher Scientific). Reaction was stopped after 10 to 15 min by addition of 50 µl per well of 1 N sulfuric acid (H2SO4, 4623.1, Carl Roth) and absorbance in wells was measured (OD 450 nm) using an Enspire® 2300 plate reader (Enspire® Multimode plate reader, Perkin Elmer).

2.11 Surface Plasmon Resonance (Biacore)

Binding affinity to the asialoglycoprotein receptor (ASGPR) was also assessed by surface plasmon resonance (SPR) technique using a Biacore™ 3000 system (GE Healthcare, Germany). Purified CRDH1 protein was immobilized onto a CM5 sensor chip (BR-1005-30, GE Healthcare) using standard amine coupling technique. Briefly, chip surface was "activated" by injecting 60 µl of ethyl(dimethylaminopropyl) carbodiimide/N-Hydroxysuccinimide (EDC/NHS) mix then coated by injection of a 12 µg/mL solution of purified CRDH1 in 10 mM sodium-acetate pH 5.0 buffer. Inactivation of the chip surface was then fulfilled by injection of 70 µl of ethanolamine (E0135, Sigma Aldrich). Running buffer during all steps was composed of 10 mM Hepes pH 7.2 solution containing 20 mM $CaCl_2$ and 0,005 % tween-20 (9127,2, Carl Roth).

For binding kinetics, serial dilutions of recombinant protein samples were prepared in running buffer. Binding was determined following a 5 min injection at a flow rate of 50 $\mu l.min^{-1}$. Regeneration of the chip surface was performed by 15 µl injections of a 5 mM EDTA solution followed by 10 µl injections of a 10 mM Hydrochloric acid solution. A second chip, namely the C1 sensor chip (BR-1005-35, GE Healthcare) was also tested. This chip has a matrix-free carboxymethylated dextran surface which reduces background noise resulting from unspecific interactions that could occur between the matrix and the lectins.

2.12 Transferrin receptor-mediated cell-binding assay

To assess binding properties of various recombinant proteins (GAL-Ptf1, GAL-Ptf2, Strep-Ptf1-GBA and Strep-Ptf2-GBA) to transferrin receptor TFR, T47D cells were used. Indeed, like most myeloid cells, T47D highly express TFR at their cell surface, as they require high levels of iron due to their rapid proliferation.

In a 96-well plate (TPP), a total of $1x10^5$ cells per well were set up. After a wash step using 1x PBS, cell pellets were resuspended in 1xPBS containing 5 % FBS and cooled down at 4°C for 20 min. Recombinant enzyme samples were then added to the cold cells and left to incubate at 4°C for 2 hrs. Following two wash steps using ice-cold 1x PBS, cells were then incubated with the diluted (1:1000) primary antibody at 4°C for 1 hr (either rabbit polyclonal anti-GBA antibody [ab118304, Abcam] or rabbit polyclonal anti-GAL antibody [ab70520, Abcam]). Again, cells were washed twice with ice-cold PBS prior to the final 20 minute incubation period with a diluted (1:200) Dylight-488 conjugated goat anti-rabbit IgG (H+L) detection antibody (111-485-144, Jackson ImmunoResearch Laboratories). Following two wash steps, cells were re-suspended in 100 µl of 1x PBS before being analyzed in the flow cytometer (BD FACS Canto™ II, BD Science).

For inhibition studies, prior to co-incubation with the samples, cells were additionally incubated 3 hrs at 4°C in the presence of the inhibitor (Ptf1 or Ptf2 peptides). Enzyme was then added directly to well for co-incubation with the inhibitor.

2.13 Animal study

To assess serum half-life and biodistribution of GAL enzymes, a mouse pharmacokinetic study (PK) was performed. Treatment and handling of the animals was performed by EPO (Berlin, Germany). Groups comprising three animals each were injected intravenously with 5mg per kilogram body-weight of recombinant enzyme preparation (GAL-His, GAL-CRDH1 or GALn108qCRDH1). Blood samples were taken at different times (tail vain) and serum stored at −20°C until enzyme activity assessment at a later time. Plots of recombinant biological activity over time were constructed for each animal and initial as well as terminal half-lives ($t_{1/2}$), were calculated from these plots as described by Shargel (Shargel *et al.* 2005).

In addition, at a given time following intravenous administration, mice were euthanized and the livers, hearts and kidneys removed and stored at -20°C. The tissues were homogenized in ice-cold 27 mM citric-acid buffer, pH4,6 with 46 mM sodium-phosphate and 0,15 % triton X-100 using a gentle MACS dissociator (Miltenyibiotec). Then, the homogenates were subjected to freeze/thaw cycles (-80°C/room temperature) three times and finally centrifuged for 30 min at 12,000 rpm. Supernatant was collected and recombinant enzyme activity determined.

2.14 Statistics

Results are presented as mean ± SEM when adequate. Data was analyzed statistically using the GraphPad Prism 5 software (GraphPad Software, La Jolla California USA, www.graphpad.com). The Student's t-test was applied for comparison between individual pairs of means. Three or more groups were analyzed using one-way ANOVA. Differences with a p-value of $p < 0.05$ were considered as being significant.

3 Results

3.1 Production of highly phosphorylated recombinant lysosomal enzymes

The first objective of this project was to reengineer Glycotope's host cell line H9D8 in order to obtain an improved host with respect to the production of recombinant lysosomal enzymes. The focus here was on the phosphorylation of the recombinant enzymes during expression in order to obtain a robust production process for highly phosphorylated molecules which are more likely to reach target cells. Indeed, unmodified host cell line H9D8 on average phosphorylates 45 ± 3 % of α-Galactosidase A's carbohydrate structures leaving room for improvement.

The experimental work performed in this section was based on previous findings (Marnell *et al.* 1984), a CHO cell mutant (G.7.1) being generated with a heat sensitive defect in endosomal acidification. The resulting defect, a "deactivated" proton pump, led to increased secretion of phosphorylated lysosomal enzymes, as these could not be delivered anymore to the lysosomes via the acidic vesicle trafficking route.

3.1.1 Generation of H9D8 mutants (EMS Tox H9D8)

The modification of host cell line H9D8 was performed by introducing a point mutation using chemical reagent ethylmethanesulfonate (EMS). Following mutagen treatment, surviving cells were screened using a "toxin cocktail" selection (see 2.5.1). This produced a total of 576 single cell colonies possibly bearing the intended mutation. The toxins used require acidic vesicle trafficking in order to become lethal, therefore preferably leaving possible endosomal acidification mutant cells alive (see 4.1.1). Once the selected cells had sufficiently proliferated, flow cytometry-based screening for acidic vesicle (AV) content of each isolated single cell derived colony was performed. A sample diagram is presented in Figure 16a. The mean relative fluorescence units (RFU), measured for each colony, were normalized against the mean RFU value of the internal control H9D8. The resulting relative value is defined as "percent acidity" (% acidity) and better indicates if a clone has a normal or a lower level of acidic vesicles, normal being a value of 100 % set by untreated H9D8 cells. The resulting diagram is shown in Figure 16b. The results revealed variations in the relative acidity levels when looking at the different single cell-derived colonies. Whereas some clones remained close to H9D8 control, with acidic vesicle levels above 80 %, several single cell-derived mutant colonies had a significantly lower acidic vesicle level,

with the relative acidity level ranging between 40 and 70%. Moreover, these low acidic vesicle levels were comparable to Bafilomycin-induced control measured at a relative acidity level of 50 to 60 %.

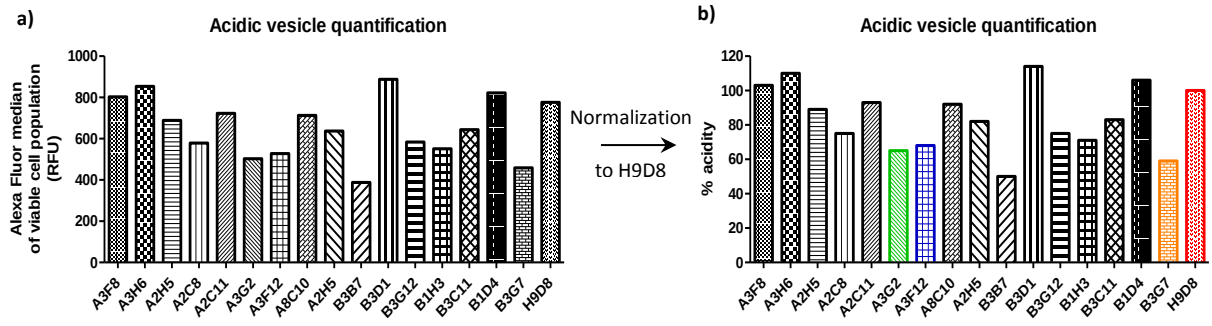

Figure 16 Flow cytometry-based acidic vesicle quantification of EMS tox H9D8 clones. Cells were incubated with Lysotracker® Green Dye prior to relative fluorescent intensity being measured in FACS instrument a) Example of a screening round (raw data, n=1) b) normalization of relative fluorescence units (RFU) to H9D8 in order to express the "% acidity" of each clone.

Following seven screening rounds, this selection procedure resulted in the identification of 42 single cell colonies (out of 576) with significantly reduced acidic vesicle levels (<70 % acidity). These clones were amplified further and repeat screening rounds at a later stage were performed. Repeat screening made it possible to select three mutated H9D8 clones with robust low acidic vesicle levels. These selected candidates were kept as the potential new production host cell lines and defined as EMS tox A3F12, A3G2, and B3G7. The summary data for the 6-well plate selection stage of these final clones is presented in Figure 17.

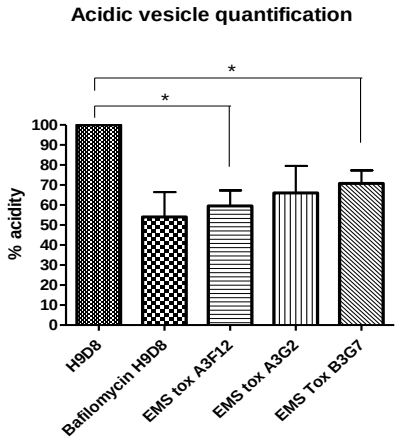

Figure 17 Summary of the flow cytometry based acidic vesicle quantification rounds for the selected EMS tox H9D8 clones. The mean relative acidity to normal H9D8 cells is plotted for each clone (±SEM, n=3), (*) indicates a significantly reduced acidity (Student's t-test, $p<0.05$).

The diagram shows that during the 6-well plate screening rounds, all three mutant clones reproducibly achieved reduced relative acidity values ranging between 55 and 70 % acidity.

In summary, the combined treatment of host cell line H9D8 with EMS and DT/ExA toxin cocktail made it possible to isolate of three mutated H9D8 clones namely, EMS tox A3F12, A3G2, and B3G7. These clones repeatedly exhibited significantly reduced acidic vesicle content compared to untreated H9D8 host cells when assessed in a Lysotracker® Green-based flow cytometry assay. The next step consisted in testing the new clones with regard to recombinant production of lysosomal enzyme GAL in order to see if these metabolic changes translated into modified enzyme phosphorylation.

3.1.2 Recombinant expression of GAL-His in new EMS Tox H9D8 mutants

The newly generated mutant clones A3F12, A3G2 and B3G7 were stably transfected with recombinant human GAL-His expression vector (see 2.2). The originating transfection pools were amplified up to 100 or 200 nM MTX, thereby achieving a sufficient product concentration of around 0.5 to 1 µg recombinant GAL per milliliter culture medium. Scale-up to spinner flasks (0.25 to 1 L) was then performed and cells were left to grow for 5 to 7 days (small-scale batch production). On day 2 of the spinner culture, the temperature was increased to 40°C ("permissive" temperature) in order to activate the "phosphorylation mutation". The resulting supernatants were purified over a Ni-NTA affinity chromatography column, yielding between 0.5 to 1 mg recombinant GAL-His per liter of culture supernatant. Initial characterization of the purified enzymes was performed by SDS-PAGE and activity analysis, in order to assess structural and functional integrity of the new enzymes. Gel electrophoresis (Figure 18) revealed no structural disparities between the different samples, with all GAL-His enzymes migrating to an apparent molecular weight of around 48 kDa. This was comparable to the reference product, GAL-His derived from H9D8.

With regards to enzyme activity, the kinetic profiles (Figure 19) also confirmed sample comparability on a functional level. The curves were fitted using the Michealis-Menten model. The resulting catalytic parameter revealed similar specific activities (less than 2 % variance), maximum velocities Vmax (less than 1.5 % variance) and K_M (less than 2 % variance) for all the enzymes.

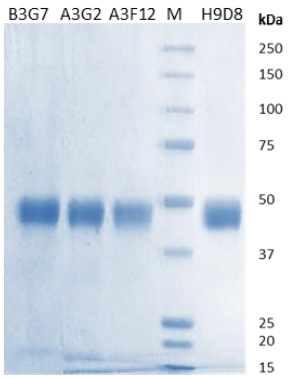

Figure 18 SDS-PAGE analysis (10 % gel, coomassie blue staining) of NiNTA-purified GAL-His protein expressed in either one of the three EMS Tox H9D8 clones (B3G7, A3G2 or A3F12) or in H9D8 cell (M indicates the protein marker).

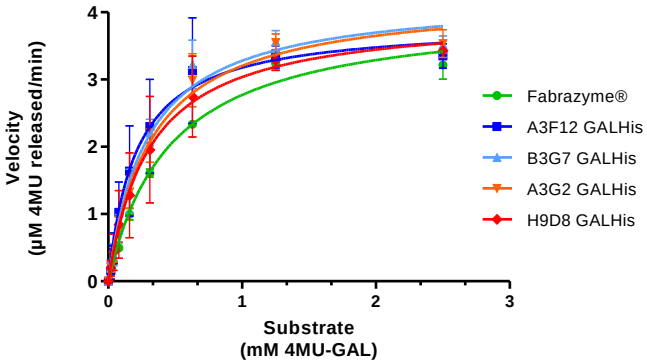

Sample	V_{max} (µM 4MU released/min)	K_M (mM)	Specific activity (mmol 4MU released/min/mg of enzyme)
GAL-His from A3F12	3.92	0.29	3.15
GAL-His from A3G2	4.23	0.32	3.64
GAL-His from B3G7	4.23	0.29	3.68
GAL-His from H9D8	4.16	0.41	3.27
Fabrazyme®	4.16	0.50	3.24

Figure 19 Kinetic profiles for mutant-derived GAL-His (±SEM, n=3); enzyme samples (12 ng/well) were incubated with varying 4MU-GAL substrate concentrations (0 to 2.5 mM/well) and left to incubate for 60 min at 37°C. Reaction was then stopped and substrate hydrolysis measured (µM 4MU released/min). The curves were fitted in GraphPad Prism based on the Michaelis-Menten kinetic model. Resulting catalytic parameters are listed in the table below (V_{max}-maximal velocity; K_M-Michealis constant).

Following this initial evaluation, further characterization of the enzymes was undertaken with regard to glycosylation, phosphomannosyl levels and cellular functionality. In order to determine the relative mannose-6-phosphate (M6P) content of recombinant GAL-His enzymes derived from each EMS tox H9D8 clone, glycan analysis by CE-LIF was established. This was first done using Fabrazyme®. Briefly, enzymatic treatment by Endo H enabled the selective release of

oligomannose and hybrid-type structures from protein backbone. The detached carbohydrates were then purified and labelled with APTS prior to being loaded onto the capillary (see 2.8). The resulting electropherogram is presented in Figure 20a. Differences in electrophoretic mobility allow for distinct separation of the various carbohydrates according to size and charge. First of all, four oligomer structures were identified, namely pentamannose (GlcNAc-Man5 or M5), hexamannose (GlcNAc-Man6 or M6), heptamannose (GlcNAc-Man7 or M7) and octamannose (GlcNAc-Man8 or M8), with migration times (t_m) of around 7.3 min, 7.8 min, 8.3 min and 8.7 min, respectively. Due to the fact that phosphorylated mannose structures are negatively charged, they are expected to have an increased electrophoretic mobility in comparison to the oligomannose structures. In other words, phosphorylated mannose structures are expected to be found to the left of the M5 peak. Indeed, this was the case for Fabrazyme® sample, with peaks observed at earlier migration times ranging between 5.8 min to 7.0 min. These signals were additionally confirmed as being phosphorylated N-glycan, by running a control sample: alkaline phosphatase-treated Fabrazyme®. The corresponding electropherogram, presented in Figure 20b, clearly shows disappearance of the peaks normally detected between 5.8 min and 7 min. Furthermore, signal intensities of oligomannose entities (M5, M6, M7 and M8) significantly increased as a result of the additional dephosphorylated oligomannose moieties.

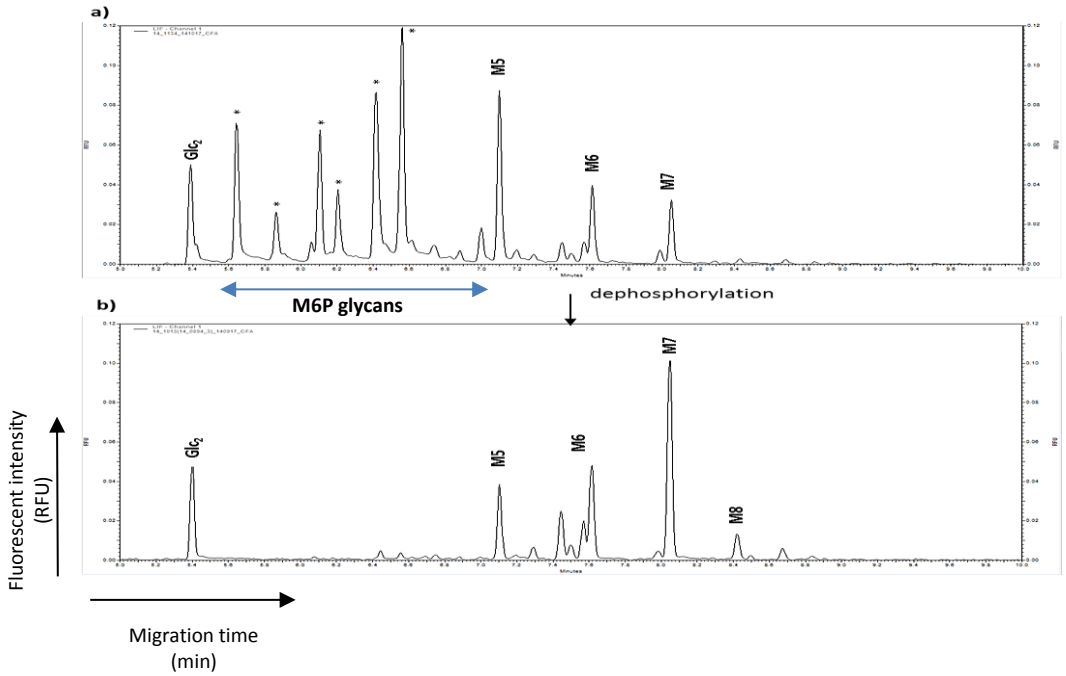

Figure 20 CE-LIF electropherogram a) Hybrid and mannose-type glycans, originating from Fabrazyme®, were APTS labelled and analyzed by CE-LIF. b) Phosphomannosyl entities were confirmed by treatment of the sample with alkaline phosphatase. Phosphorylated mannose structures are marked with an asterisk (*); Glc_2 indicates the maltose standard; M5, M6, M7 and M8 indicate penta-, hexa, hepta- and octamannose structures.

Following the correct annotation of the various signals detected, a relative quantification of the different entities was performed. By adding up the peak areas corresponding to the phosphorylated carbohydrates and then normalizing this value to the remaining structures, a relative degree of phosphorylation was determined. An absolute quantification was however not possible. This methodology was then applied to all GAL-His samples (Figure 21).

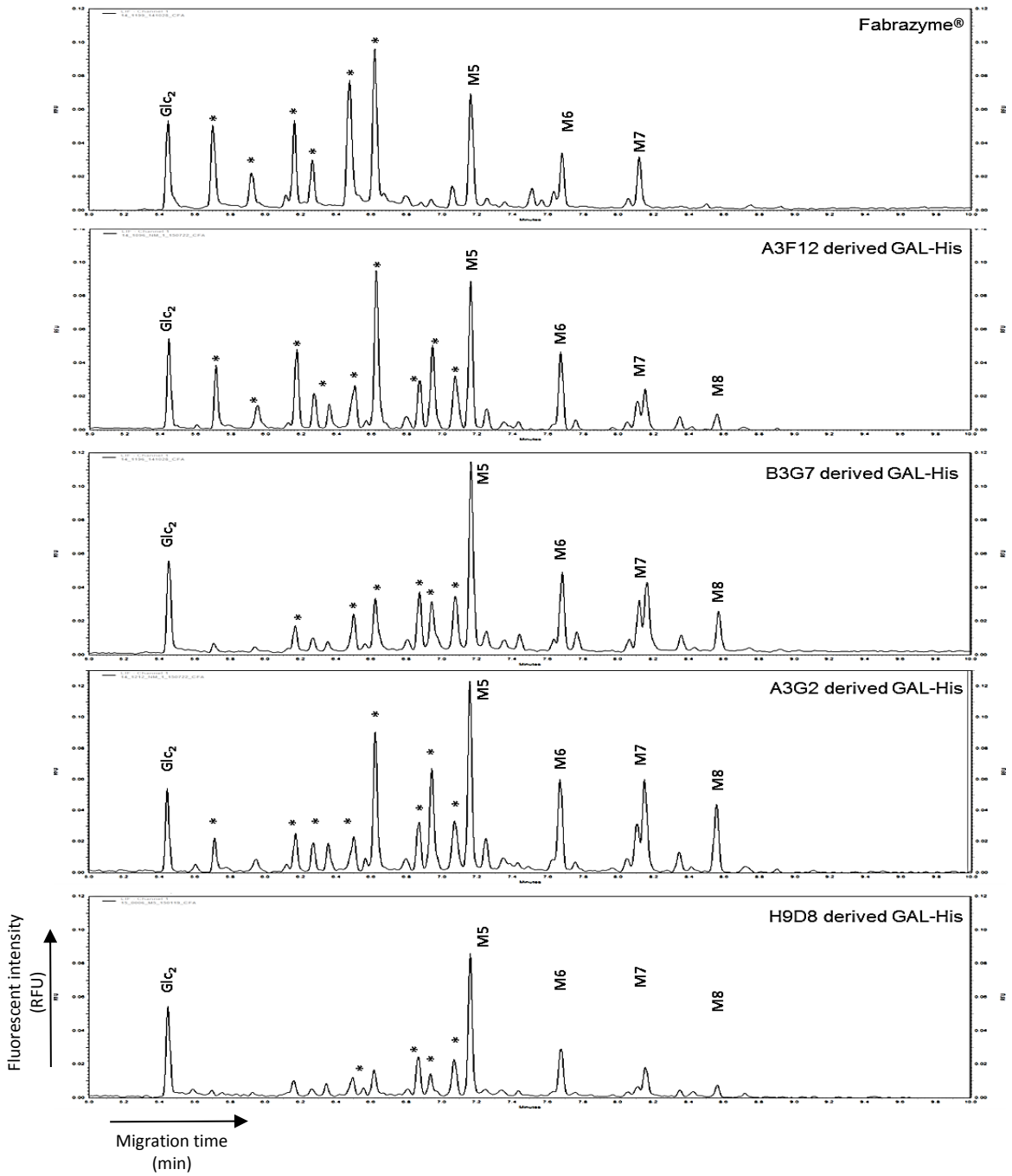

Figure 21 N-Glycan electropherograms of various GAL samples. Analysis of the hybrid and mannose-type glycans, derived from various GAL-His samples, was performed by CE-LIF, as described in Materials and Methods. Phosphorylated mannose structures are marked with an asterisk (*); Glc_2 indicates the maltose standard; M5, M6, M7 and M8 indicate penta-, hexa, hepta- and octamannose structures.

Looking at the electropherograms generated from the mutant derived GAL-His glycans, differences can be immediately observed. This was particularly true when looking at the phosphorylated mannose signals detected between 5.8min and 7min which clearly revealed that not all mutants had an increased phosphorylation. Indeed, when comparing GAL-His derived from EMS Tox B3G7 mutant and normal H9D8 cells, the data revealed relative phosphorylation degrees of 50 ± 4 % and 45 ± 3 %, respectively. For GAL-His derived from either EMS tox A3G2 or A3F12 however, electropherograms were somewhat different with regards to phosphorylated mannose peaks. Indeed, in the migration window between 5.8 min and 7min, a clear increase in the number of peaks as well as their intensities could be observed, correlating with an overall increase in the degree of phosphorylation. Relative quantification revealed an M6P level of around 79 ± 4 % for A3F12 derived product, a value significantly higher than that of H9D8 derived GAL-His. Furthermore, this value is very comparable to Fabrazyme® which showed relative M6P levels of 76 ± 2 %. Finally, for A3G2 the relative level of phosphorylation was somewhat lower than A3F12 with a value of 59 ± 2 %. This however still represents an increase by 14 % of glycan phosphorylation when compared to H9D8 cells.

In addition to the CE-LIF data, N-glycan profiling of the different samples was performed by UltraPerformance Liquid Chromatography (UPLC®) (see 2.8.3). This analysis helps to better understand which glycan structures are present on each of the GAL variants. In a similar manner to CE-LIF, a chromatogram is generated following injection of a 2-AB labelled glycan sample. Each signal (or peak) corresponds to a type of N-glycan present in the sample. Indeed, the mobility of the labelled glycans varies according to size and charge and therefore according to the type of oligosaccharide. Cross-referencing of the retention times with an oligosaccharide data base (i.e. GlycoBase 3.0 database, Waters) allows to identify the type of oligosaccharide "responsible" for the peak. An exemplary annotated chromatogram is present in Figure 22. Finally, by integrating each individual peak area, relative amounts of oligosaccharide forms can then be determined. In this case, the focus was upon hybrid and high-mannose-type glycans, as only these structures can be phosphorylated (see 1.1.2). The corresponding numerical values resulting from the peak integration are presented in Table 6.

The data revealed a 2-fold increase in oligomannose levels for all the mutant derived products, pushing this glycoform to a relative level ranging between 12 % and 15 % compared to the 7 % in "normal" H9D8-GAL. However, the levels achieved by the mutant cells were inferior to that of approved drug Fabrazyme® (29 %). The UPLC® analysis also revealed differences in hybrid-type structures. Indeed, A3G2 and B3G7 derived product showed hybrid-type glycan levels of around

16% and 17% respectively, values comparable to that of H9D8-GAL (12 %). In contrast, A3F12 derived product showed a 2-fold lower amount of hybrid-type glycan with a level of 6 %, a value comparable to Fabrazyme® which bears 8 % of the hybrid glycoform. When looking at the overall relative amounts of glycans which are "eligible" for M6P (i.e. hybrid+high-mannose), B3G7 derived product was highest with 32 % "M6P eligible" structures, followed by A3G2-GAL at 29 % and finally H9D8-GAL and A3F12-GAL at 19 and 18 %, respectively. However, these values were inferior to those measured for Fabrazyme® (37 % "M6P eligible" structures).

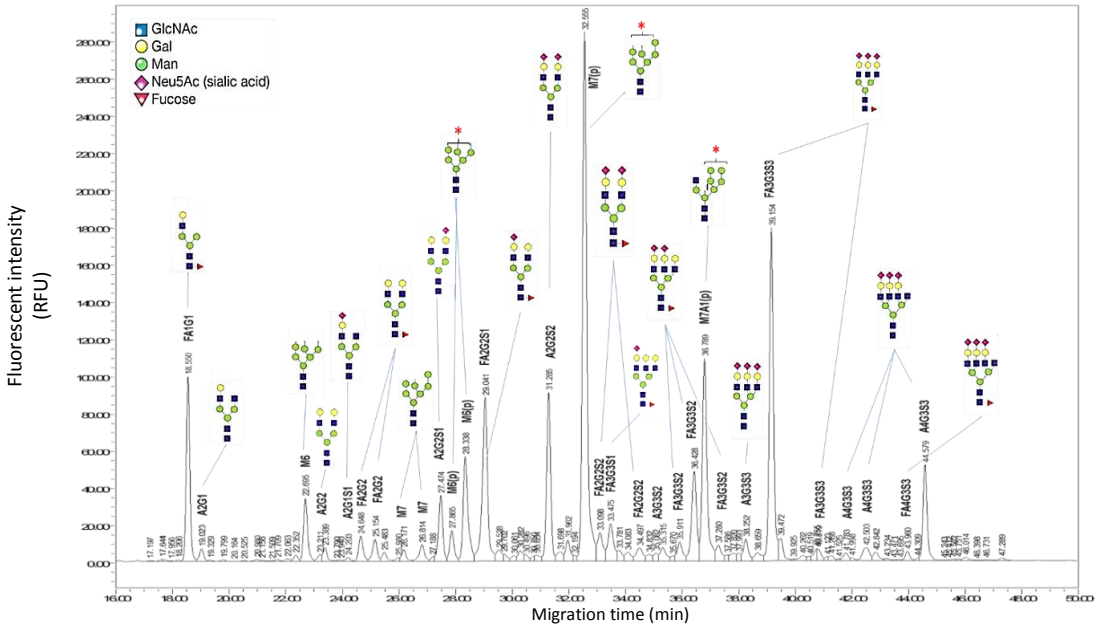

Figure 22 Annotated N-glycan profile of Fabrazyme®, generated by UPLC® coupled to a fluorescent detector. For each annotation (i.e. A2G2S2), an exemplary N-glycan isomer is shown. Phosphorylated N-glycans are marked with a red star (*). Neu5Ac (S) = sialic acid; Man (M) = mannose; Gal (G) = galactose; GlcNAc (G) = N-Acetylglucosamine.

Table 6 Oligosaccharide analysis of 2-AB labelled N-glycan by UltraPerformance Liquid Chromatography (UPLC®, n=1). The numerical values from de CE-LIF analysis (P45-46) were also added for a better overview (±SEM, n=3).

Oligosaccharide Type	Relative molar amount of glycoform (%)				
	Fabrazyme®	GAL-His from H9D8	GAL-His from ems tox A3G2	GAL-His from ems tox A3F12*	GAL-His from ems tox B3G7
Hybrid	8	12	16	6	17
High-mannose	29	7	13	12	15
"M6P eligible" structures (hybrid+high-mannose)	37 (8+29)	19 (12+7)	29 (16+13)	18 (6+12)	32 (17+15)
Phosphorylated (CE-LIF data)	76 ± 2%	45 ± 3%	59 ± 2%	79 ± 4%	50 ± 4%

*measured using UPLC® coupled to mass spectrometry (UPLC®-MS) resulting in a higher resolution.

3.1.3 Functional characterization of EMS Tox H9D8 derived product

Functional characterization of the mutant cell derived GAL-His enzymes, was performed by assessing receptor mediated internalization into mouse fibroblasts. The emphasis here was on whether variations would be seen as a result of the different phosphorylation degrees observed earlier (3.1.2). To this end, NIH-3T3 mouse fibroblast cells were used, as they not only express cell surface mannose-6-phosphate (M6P) receptor (MPR) but are also relatively comparable to target cells such as Fabry fibroblasts. Cells were seeded in 24-well plates and co-incubated for 24 hours with varying enzyme concentrations (0.5 and 30 µg/mL). Following this, cells were washed and lysed in order to quantify accumulated GAL activity. The resulting internalization rates, presented in Figure 23, are expressed as substrate hydrolysis per milligram of protein (in lysate) per hour (µmol 4MU released.mg lysate^{-1}.h^{-1}). In addition, binding characteristics were calculated using GraphPad Prism software by fitting the data with a one-site binding hyperbola model.

The results of the uptake assay showed a clear improvement in internalization of the mutant cell derived product. Whereas GALHis-H9D8 reached maximal levels of around 7 µmol 4MU released.mg lysate^{-1}.h^{-1}, GAL-His derived from A3F12, B3G7 and A3G2 mutants reached maximal levels of 14, 21 and 30 µmol 4MU released.mg lysate^{-1}.h^{-1}, respectively. The mutants achieved maximal internalization levels comparable to those of the commercial controls Farbazyme® and Replagal® evaluated at about 25 µmol 4MU released.mg lysate^{-1}.h^{-1}. It is important to note the differences in the initial uptake rate (between 0 and 10 µg/mL), which directly correlates with the respective enzyme affinities for the mannose-6-phosphate receptor (MPR). In this case, A3F12 mutant derived enzyme showed the highest affinity (143nM) and binding potential (0.14) of the three mutants, values which were 7-fold better than the H9D8 derived product. By contrast, A3G2 derived product, which achieved the highest overall uptake, showed a 3-fold reduced affinity (430nM) when compared to A3F12 product, but with a similar binding potential (0.12). Finally, B3G7 mutant derived enzyme exhibited the lowest binding affinity of all (1867nM) and an almost 3-fold lower binding potential (0.045) than A3F12 derived product.

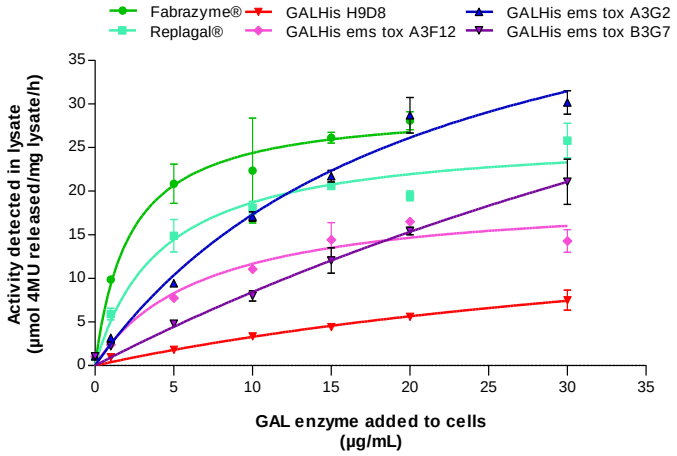

	Fabrazyme®	Replagal®	H9D8	A3F12	A3G2	B3G7
B_{max} (µmol 4MU released. mg lysate^{-1}.h^{-1})	29.7	26.6	20	19.7	53.1	84
k_d (nM)	46	83	1061	143	430	1867
BP (B_{max}/k_d)	0.61	0.32	0.019	0.14	0.12	0.045

Figure 23 Internalization profiles of the mutant derived GAL-His enzymes. The 3T3 mouse fibroblasts seeded in a 24-well plate were co-incubated with concentration series (0 to 30µg/mL) of the various enzymes (n=2), for a period of 24 hours. Following this, cells were collected, washed and lysed. The lysates were analyzed for α-galactosidase A (GAL) activity levels (4MU assay) and for protein content (BCA). The resulting internalization profiles were fitted in GraphPad Prism based on a one-site binding model and the resulting parameters listed in the table below (B_{max}-maximal binding; k_d-binding constant; BP-binding potential).

To summarize, host cell H9D8 was modified following chemical treatment and clones were generated exhibiting a reduced amount of acidic vesicles. Upon transfection with human α-Galactosidase A (GAL) expression vector, these same mutants produced recombinant enzymes bearing increased levels of oligomannose carbohydrates when compared to H9D8 derived product, as well as increased relative phosphorylation. Furthermore, in comparison to H9D8 derived GAL-His, all the mutant-cell-derived GAL-His enzymes were internalized to a higher extent by mouse fibroblast cells. The highest uptake observed reached an up to 4-fold higher level than H9D8 derived GAL-His and was comparable to commercially available substances.

3.2 Re-engineering recombinant lysosomal enzymes GAL-His in order to reduce mistargeting to liver asialoglycoprotein receptor

As mentioned before, enzyme replacement therapy (ERT) is related to a high loss of therapeutic agent to the patient's liver, mostly resulting from the asialoglycoprotein receptor (ASGPR) of the hepatocytes. This not only leads to increased therapeutic cost but above all to an unfavorable drug distribution. One way of reducing ASGPR binding can be by increasing the sialic acid content of a recombinant product (Kontermann 2011). This however, requires either specific modification of the production host cell itself or post-production modification of the recombinant protein, the latter being costly. In both cases, robustness and efficiency of these procedures is questionable, which is why in this project a new approach was tested. Indeed, the recombinant enzymes were modified directly on a molecular level in order to generate so-called fusion enzymes with reduced ASGPR binding affinity.

3.2.1 Molecular re-engineering of GAL-His encoding DNA

As mentioned previously, the asialoglycoprotein receptor (ASGPR) is a hetero-oligomeric complex comprising two polypeptide subtypes H1 and H2. Each subunit is composed of a transmembrane domain, a polypeptide stalk bearing several N-linked oligosaccharides and finally a C-type lectin domain capable of binding galactose moieties in a calcium dependent manner (Figure 24a). While the native ASGPR always contains both H1 and H2 subtypes, H1 has been described as being the major requirement for binding and subsequent receptor-mediated endocytosis of proteins (Bider *et al.* 1995). Based on additional findings that a truncated version of the H1 domain can be recombinantly expressed whilst retaining its binding capacity for terminal galactose (Meier *et al.* 2000), it was decided to engineer a fusion enzyme comprising human α-galactosidase A (GAL) linked to a truncated version of the H1 domain of the ASGPR, namely CRDH1 (Figure 24b). The intention here was to mask terminal galactose possibly present at the surface of the "companion enzyme" GAL, with the fused CRDH1 moiety (Figure 24c).

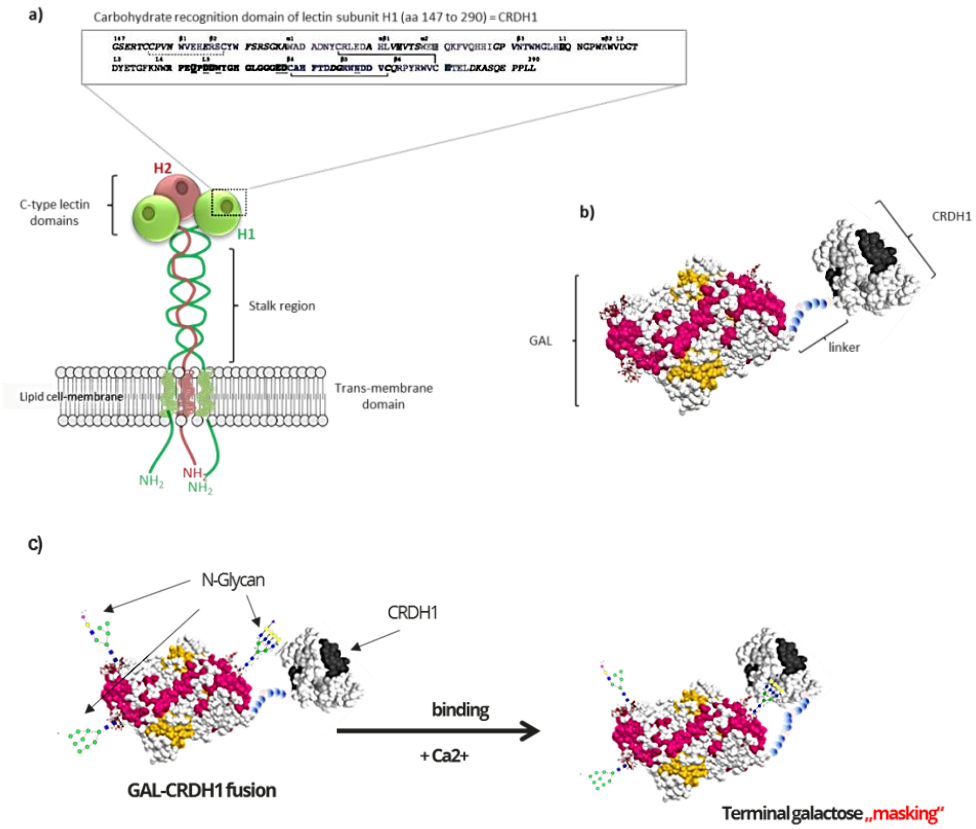

Figure 24 The asialoglycoprotein receptor a) Structure, including C-type lectin subunits H1 and H2 b) Schematic representation of GAL-CRDH1 fusion enzyme c) Possible "masking" mechanism of terminal galactose carbohydrates present on recombinant GAL enzyme.

To this end, recombinant genes encoding the following fusion proteins were constructed:

- human GAL linked to CRDH1 domain by a flexible GS linker (GAL-CRDH1)
- human GAL, where asparagine 108 (N108) was replaced by glutamine (Q), linked to CRDH1 domain by a flexible GS linker (GALn108q-CRDH1)

The latter construct was an additional "precaution", whereby reduction of complex-type carbohydrates was intended by elimination of α-Galactosidase's first N-glycosylation site (Asn108). Once generated, the recombinant genes were integrated into the GEX expression vector as described in Materials and Methods, upon which the fusion enzymes could be expressed in the host cell line H9D8.

3.2.2 Expression, purification and characterization of GAL-CRDH1 and GALn108q-CRDH1 fusion enzymes

Expression of both fusion enzymes was performed by stably transfecting H9D8 host cell line with the relevant expression vector. The transfection pools were amplified up to 200 nM MTX, ensuring enzyme levels of around 1 µg/mL. Analysis of the culture supernatants by 4MU-Gal activity assay (see 2.7) was performed at regular intervals during this amplification stage in order to ensure enzymatic activity and successful recombinant expression. For GAL-CRDH1 the 200 nM pool was used to set up single clone selection by the limited dilution technique. This led to the generation of three expression clones, each yielding recombinant enzyme levels of around 2 µg/mL. In order to produce larger amounts of both fusion enzymes for initial product characterization, spinner cultures were set up. The culture supernatants were then purified over a galactose-coupled sepharose column (see 2.6.3). Product yields ranged between 1 and 1.5 mg of GAL-CRDH1 and 0.8 to 1 mg of GALn108q-CRDH1 per liter of culture supernatant.

Initial characterization was performed in order to assess structural and functional integrity of the recombinant fusion enzymes. Analysis of the purified enzymes by SDS-PAGE (Figure 25a), revealed distinct differences in size compared to normal 48 kDa large GAL-His enzyme. Indeed, fusion enzymes migrated distinctly above the 50 kDa mark. A slight difference in electrophoretic mobility between GAL-CRDH1 and GALn108q-CRDH1 fusion enzymes was observed. The respective protein bands were found at apparent molecular weights of around 69 kDa and 65 kDa, the 4 kDa discrepancy likely resulting from the deglycosylation at Asn108. Finally, gel electrophoresis in non-reducing conditions revealed migration of protein bands to higher molecular weights, with GAL-CRDH1 found around 100 kDa mark and GALn108q-CRDH1 around the 80 kDa mark. This shows that the GAL enzyme homodimerization ability was preserved.

Next, product stability of the new constructs was assessed. To this end, the purified enzymes were added to mouse serum at a final concentration of 100 µg/ml and incubated at 37°C for a period of 4 hours. Samples were taken at various time points and assayed for residual activity. The values obtained this way were normalized to the initial activity measured at t = 0 min in order to express the percentage of remaining activity (% activity). Relative residual activity was plotted against time and the resulting profiles are presented in Figure 25b. For all enzymes, similar curves are observed with a steady decline of enzyme activity to a base level of around 15 to 20 %. This decline was slightly faster for GALn108q-CRDH1 fusion.

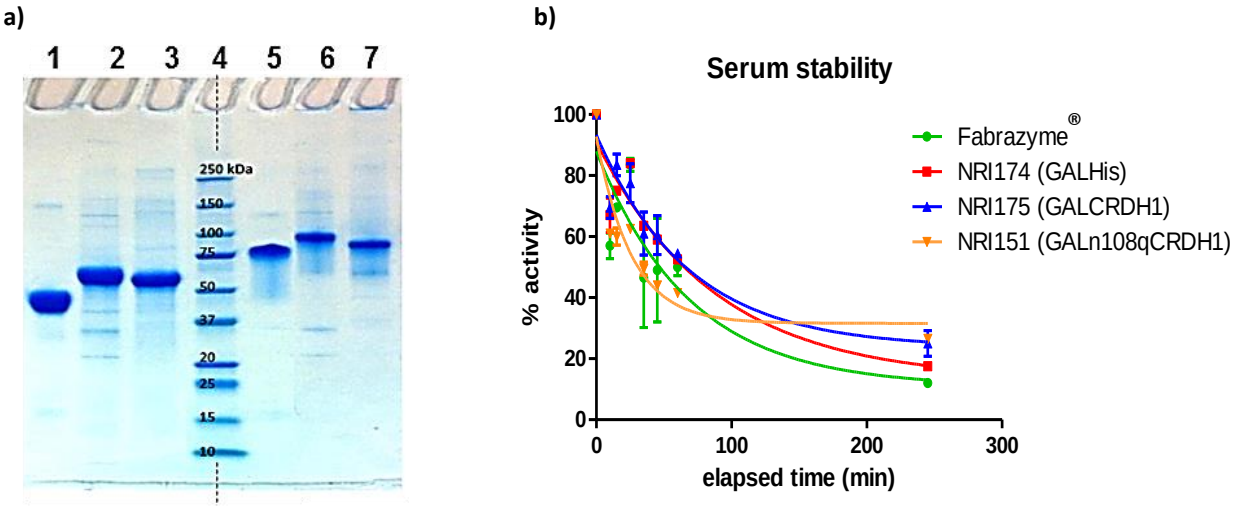

Figure 25 Characterization of recombinant fusion enzymes GAL-CRDH1 and GALn108q-CRDH1, a) SDS-PAGE (10 % gel, lanes 1-3 reducing conditions (R), lanes 4-7 non-reducing (NR) conditions, Coomassie blue staining) of fusion enzymes after affinity chromatography step – Lane 1: GAL (R), Lane 2: GAL-CRDH1 (R), Lane 3: GALn108q-CRDH1 (R); Lane 4: Protein marker; Lane 5: GAL (NR), Lane 6: GAL-CRDH1 (NR); Lane 7: GALn108q-CRDH1 (NR), b) Enzyme stability following incubation in mouse serum (37°C, enzyme concentration = 1 mg/mL). For each time point duplicate measurements were made (±SEM, n=2).

Catalytic characteristics of fusion enzymes were determined using the 4MU-Gal substrate assay as described in material and methods. The enzymes were compared in a kinetic setup. Following the incubation of 12 ng recombinant enzyme with different substrate concentrations (0 mM to 2.5 mM 4MU-Gal) for 60 min at 37°C, enzymatic reaction was stopped by addition of a 0.1M Glycin/NaOH solution. Substrate hydrolysis was then measured in an Enspire® multi-well plate reader. The resulting activities were expressed as the micro molar amount of 4MU substrate released per minute (µM 4MU released.min^{-1}) and plotted against the corresponding substrate concentration. The profiles generated in this manner and the corresponding kinetic parameters are presented in Figure 26. Overall, the kinetic profiles demonstrated that both fusion enzymes were comparable to reference product GAL-His with regards to activity. Even though specific activities were found to be slightly lower for GAL-CRDH1 (2.82 mmol 4MU released.min^{-1}.mg enzyme^{-1}) and GALn108qCRDH1 (2.70 mmol 4MU released.min^{-1}.mg enzyme^{-1}), when compared to GAL-His (3.35 mmol 4MU released.min^{-1}.mg enzyme^{-1}), the maximum velocities (V_{max}) reached were nearly identical. In fact, the 12 to 15 % decrease observed in specific activity was to be expected, considering the fact that each fusion enzyme bears an additional 19 kDa molecule at its C-terminus, which may result in an altered enzyme conformation.

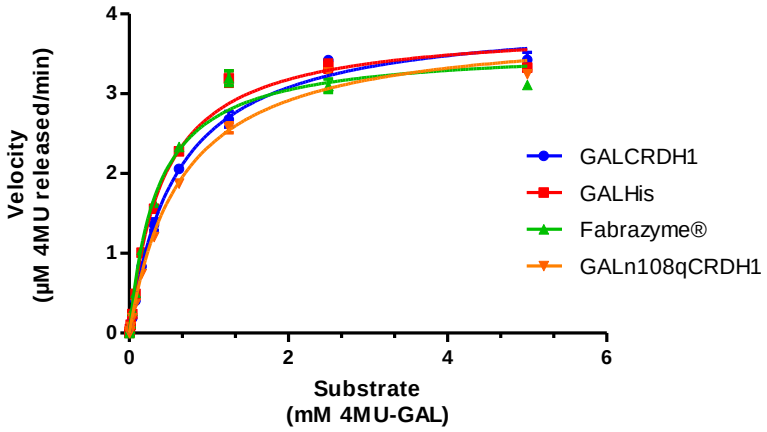

Sample	V_{max} (µM 4MU released /min)	K_M (mM)	Specific activity (mmol 4MU released.min^{-1}.mg enzyme^{-1})
GALCRDH1	3.42	0.58	2.82
GALn108q-CRDH1	3.24	0.80	2.70
GAL-His	3.33	0.45	3.35
Fabrazyme®	3.11	0.37	3.35

Figure 26 Kinetic profiles for fusion enzymes GAL-CRDH1 and GALn108q-CRDH1; duplicate enzyme samples (12 ng/well, n=2) were incubated with varying 4MU-GAL substrate concentrations (0 to 5 mM/well) and left for 60 min at 37°C. Reaction was then stopped and substrate hydrolysis measured. The curves were fitted in GraphPrism based on the Michaelis-Menten kinetic model. Resulting catalytic parameters are listed in the table below (V_{max}-maximal velocity; K_M-Michealis constant).

The purified fusion enzymes were also analyzed for their relative mannose-6-phosphate (M6P) content by CE-LIF as well as their N-glycan profiles by UltraPerformance Liquid Chromatography (UPLC®). The resulting oligosaccharide composition and relative M6P levels are presented in Table 7.

Table 7 Oligosaccharide analysis of 2-AB labelled N-glycan by UltraPerformance Liquid Chromatography (UPLC®), n=1) as well as APTS-labelled N-glycan by CE-LIF (n=1).

Oligosaccharide type	% glycoform			
	Fabrazyme®	GAL-His	GAL-CRDH1	GALn108q-CRDH1
Terminal Galactose	26	36	31	41
Hybrid	8	12	10	14
High-mannose	29	7	5	6
"M6P eligible" structures (hybrid + high-mannose)	37 (8+29)	19 (12+7)	15 (10+5)	20 (14+6)
Containing M6P (CE-LIF data)	76 ± 2% (±SEM, n=3)	48 ± 3% (± SEM, n=3)	65	60

It was interesting to see that both fusion enzymes had a higher degree of phosphorylation than GAL-His and this although all products were produced using the same cell line H9D8. The relative levels of M6P were 65 % and 60 % for GAL-CRDH1 and GALn108q-CRDH1, respectively. The levels of high-mannose and hybrid-type glycoforms remained similar for both fusion enzymes compared to GAL-His. Terminal galactose, one of the structures responsible for liver uptake, were comparable for GAL-His (36 %) and GAL-CRDH1 (31 %) but slightly increased for GALn108q-CRDH1 (41 %).

Finally, the fusion enzymes were analyzed for their functionality in order to ensure that they retained their ability to be internalized in target-like cells via receptor-mediated endocytosis. To this end, the cellular uptake assay using 3T3 mouse fibroblast cells was performed as described in material and methods (see 2.9). The resulting internalization profiles are shown in Figure 27. Good internalization was observed for fusion enzyme GAL-CRDH1 with a maximal internalization level of 14 µmol 4MU released.mg lysate^{-1}.h^{-1}, a value twice as high as GAL-His. By contrast, the second fusion enzyme, GALn108q-CRDH1, showed no such improvement in cellular internalization; levels reached were around 5 µmol 4MU released.mg lysate^{-1}.h^{-1} which is comparable to GAL-His.

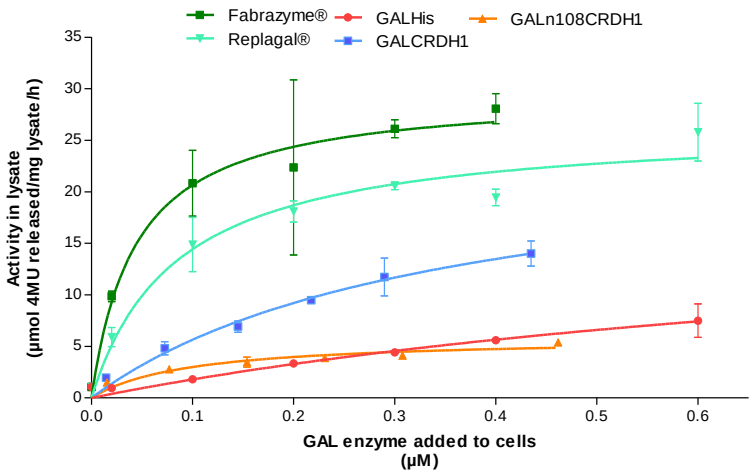

Figure 27 Internalization profiles of fusion enzymes. The 3T3 mouse fibroblasts seeded in a 24-well plate were co-incubated with concentration series (0 to 0.6 µM) of the various enzymes, for a period of 24 hours (±SEM, n=2). Following this, cells were collected, washed and lysed. The lysates were analyzed for α-Galactosidase activity levels (4MU assay) and for protein content (BCA).

In summary, human α-Galactosidase A (GAL) enzyme was modified by addition of a 19 kDa protein subunit (CRDH1) normally belonging to the asialoglycoprotein receptor (ASGPR). The

resulting fusion enzymes (GAL-CRDH1) retained activity and stability comparable to that of reference protein GAL. Carbohydrate profiles of the fusion enzymes were also similar to the reference, with the exception of a notable increase in the relative phosphorylation degree from 45 to 65 %. Finally, a 2-fold increase in mouse fibroblasts internalization was also observed for at least one of the fusion enzymes. The next step was to assess whether the fusion to the truncated receptor would have the intended effect with regards to ASGPR binding and liver uptake.

3.2.3 *In vitro* evaluation of the enzyme's binding behavior towards the asialoglycoprotein receptor

Evaluation of the re-engineered enzymes, with regards to binding behavior towards the liver receptor ASGPR was initially performed *in vitro*. To this end, two receptor binding assays were established in-house; a receptor ELISA and an assay based on surface plasmon resonance (SPR) using a BIAcore instrument. In both cases, CRDH1 molecule was used in place of full length ASGPR. One reason for this was to avoid possible interferences resulting from the presence of the N-glycosylated stalk region normally found on the full length ASGPR.

- Receptor ELISA:

The receptor ELISA was performed as described in material and methods (2.10). Briefly, serial dilutions of the different enzyme samples (0 to 280 nM) were incubated in 96-well plates coated with CRDH1. Following this, a horseradish peroxidase-coupled secondary antibody, directed against α-galactosidase A (GAL) enzyme, enabled detection of the bound recombinant hydrolases. The resulting absorption values (OD 450 nm) were plotted against the corresponding enzyme concentration in order to generate binding profiles (Figure 28). Using a one-site binding model (GraphPad Prism), the profiles were fitted and the binding constants (K_d) as well as the maximal binding sites (B_{max}) were calculated. Significant differences were observed for the respective binding profiles, in particular the initial slopes and the maximal absorbance values achieved. Whereas first binding signals were detected around 2-3 nM enzyme for GAL-His, for both GAL-CRDH1 and GALn108q-CRDH1 binding occurred later, at concentrations ranging between 10 and 50 nM. Distribution of the binding curves was as follows: highest signals were achieved by GAL-His followed by GAL-CRDH1 and then GALn108q-CRDH1. The resulting affinity constants K_d were 2.59 nM for GAL-His, 61.17 nM for GAL-CRDH1 and 1297 nM for GALn108q-CRDH1. The lower K_d value achieved by GAL-His is an indication that this enzyme has the highest binding ability to CRDH1. This was also reflected by the calculated binding potential (BP): $BP_{GAL\text{-}His} > BP_{GAL\text{-}CRDH1} > BP_{GALn108q\text{-}CRDH1}$. Altogether, these results show that

both fusion enzymes have an altered binding behavior towards CRDH1 in comparison to reference molecule GAL-His.

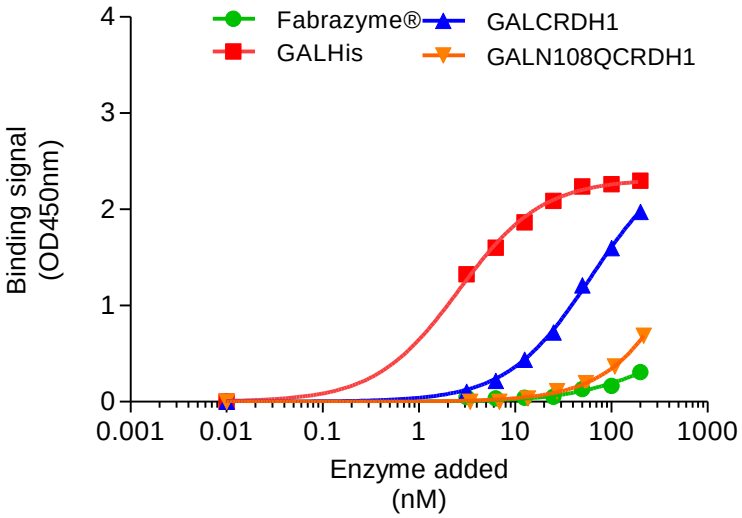

Sample	B_{max} (OD 450 nm)	K_d (nM)	Binding Potential (B_{max}/K_d)
GAL-CRDH1	2.588	61.17	0.424
GALn108q-CRDH1	4.807	1297	0.0037
GAL-His	2.317	2.59	0.846
Fabrazyme®	0.657	240.8	0.0027

Figure 28 Receptor ELISA using CRDH1. Serial dilutions of the different enzyme samples (0 to 280 nM, n=2) were incubated in 96 well plates pre-coated with CRDH1. The resulting binding profiles were fitted in GraphPad Prism based on a one-site binding model and the resulting parameters are listed in the table below (B_{max}-maximal binding; k_d-binding constant; BP-binding potential).

- Surface plasmon resonance (SPR):

In addition to the receptor ELISA, the various enzymes were also analyzed by SPR using a Biacore instrument. For each enzyme, serial dilutions (26 to 6250 nM) were prepared in binding buffer and sample preparations were then successively injected onto the CRDH1-coated CM5 sensor chip. The resulting sensorgrams for the individual enzymes and the corresponding binding constants are presented in Figure 29.

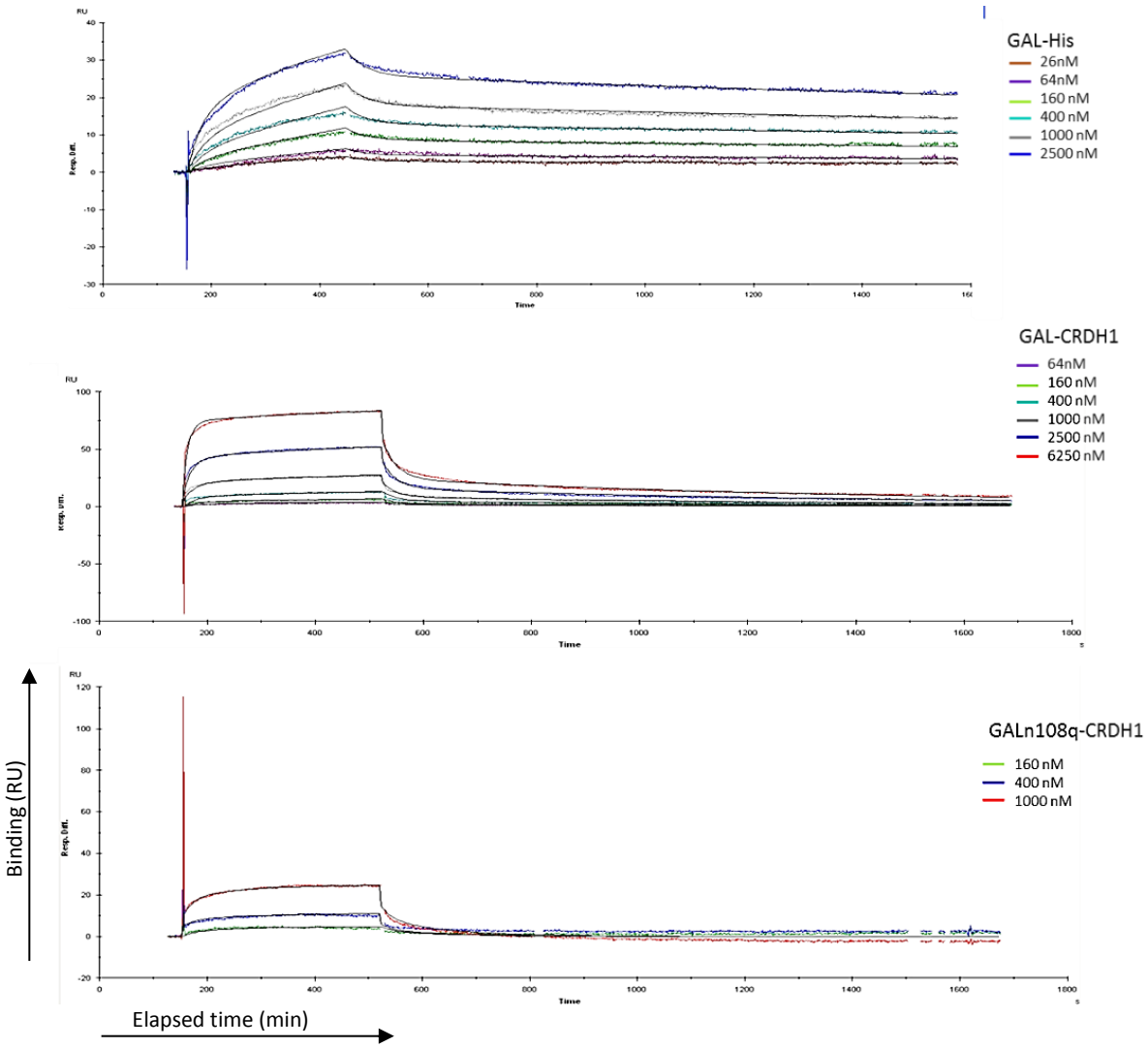

Sample (n=1)	k_{a1} ($M^{-1}s^{-1}$)	k_{d1} (s^{-1})	k_{a2} ($RU^{-1}s^{-1}$)	k_{d2} (s^{-1})	K_D (M)
GALCRDH1	9.28×10^{3}	0.038	1.72×10^{-3}	1.02×10^{-3}	2.4×10^{-6}
GALn108q-CRDH1*	1.09×10^{4}*	0.04*	6.29×10^{-3}*	9.58×10^{-3}*	5.57×10^{-6}*
GAL-His	6.68×10^{3}	0.02	6.96×10^{-3}	2.67×10^{-4}	0.11×10^{-6}

* Data based on only three concentrations

Figure 29 Receptor binding analysis using surface plasmon resonance (BIAcore) of GAL-His, GAL-CRDH1 and GALn108q-CRDH1 on a CM5 chip coated with ASGPR. Curves were fitted using the "bivalent analyte" binding model provided with BIAevaluation software.

Differences were observed for the different curves when comparing GAL-His derived sensorgrams to fusion enzyme derived sensorgrams. First of all, when looking at the association phase situated between 200 to 500 min, the slopes of the individual GAL-His sensorgrams are far less steep than

those of the fusion enzymes. This indicates a faster binding rate for the fusion enzymes, when compared to GAL-His, which is also reflected by the association constant $k_{a1.}$ Indeed, for GAL-CRDH1, a k_{a1} of 9.28 x 10^{-3} $M^{-1}s^{-1}$ was obtained as opposed to 6.68 x 10^{-3} $M^{-1}s^{-1}$ for GAL-His. Nevertheless, it is to be noted that both fusion enzymes rapidly reach a plateau whereas GAL-His binding signals continue to increase, as illustrated by association constants k_{a2}. However, when looking at the dissociation phase (>500 min), a significantly stronger drop in sensorgram intensities was observed for the fusion enzymes in comparison to GAL-His. Indeed, whereas only a 20 % reduction in GAL-His signals occurred, the fusion enzymes, on average, exhibited a 75 % drop in sensorgram intensity. Such findings indicate a quicker dissociation of the fusion enzymes from the sensor chip, which in turn reflects an overall weaker bond to CRDH1. This was confirmed by the respective dissociation constants k_{d1} and k_{d2}. Finally, the resulting affinity constants K_D better indicate how affine the various enzymes were for CRDH1. Whereas GAL-CRDH1 and GALn108q-CRDH1 fusion enzymes exhibited K_D values of 2.4 µM and 5.57 µM respectively, GAL-His K_D was found to be 0.11 µM. A low K_D indicates a high affinity of the given molecule; less ligand is required to reach equilibrium. In this case, fusion enzymes have a 20-fold lower binding affinity for the CRDH1 than GAL-His.

In summary, both *in vitro* models made it possible to show that for each fusion enzyme, there was a significant change in binding affinity and binding behavior towards CRDH1, with a strong tendency towards a reduced affinity for the asialoglycoprotein receptor. To further confirm this, an animal study was performed whereby the recombinant enzyme pharmacokinetics and dynamics were analyzed in healthy mice.

3.2.4 *In vivo* evaluation of the recombinant fusion enzymes

A mouse study was conducted in order to assess serum half-life of recombinant fusion enzymes GAL-His, GAL-CRDH1 and GALn108q-CRDH1. In addition, the subsequent tissue uptake/distribution within three main organs, namely the heart, liver and kidney, was also looked at.

Mice were injected by the tail vein at a dose of 5 mg recombinant enzyme per kg body weight. Following this, blood samples were taken at various time points and blood serum analyzed for recombinant enzyme levels. The residual enzyme activity (% activity) was plotted against the elapsed time; the resulting pharmacokinetic profiles are presented in Figure 30. Analysis of the liver, heart and kidney lysates is presented in Figure 31.

Each lysate was assayed for α-Galactosidase A amounts, which were then normalized to the total protein content of the samples (µg/g). Looking at the serum depletion profiles for the various recombinant enzymes, a biphasic curve is observed, including an early phase of rapid decline until around 150 min, followed by a second, much slower phase. The distribution pattern of the three curves was as follows: the GAL-CRDH1 residual activity was highest (0.05 %), followed by GAL-His and GALn108q-CRDH1 with respective values of 0.05 % and 0.005 % residual activity. The apparent initial half-lives ($t_{1/2}$), corresponding to the first phase, were 10 min, 20 min and 12 min for GAL-His, GAL-CRDH1 and GALn108q-CRDH1 respectively, showing a 2-fold increase in $t_{1/2}$ for the fusion. In the second phase, the respective terminal half-lives were 294 min for GAL-His, 464 min for GAL-CRDH1 and 513 min for GALn108q-CRDH1, showing a distinct separation of the fusion enzymes from GAL-His.

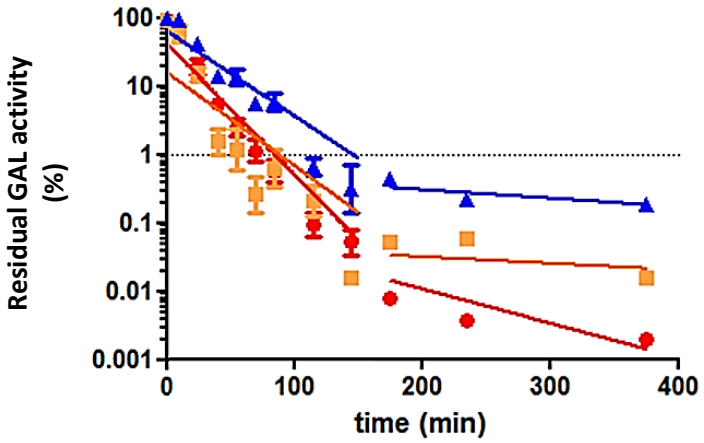

Sample	Initial $t_{1/2}$ (min)	Terminal $t_{1/2}$ (min)
GAL-His	10	294
GALn108q-CRDH1	12	513
GAL-CRDH1	20	464

Figure 30 Serum depletion profiles of three recombinant enzymes. Following a single injection with 5 mg/kg of recombinant enzyme, blood samples were taken from the tail vein of the mice (±SEM, n=3). Serum was analyzed for enzyme activity using 4MU-Gal assay. Results are shown as the percentage of GAL activity remaining in the serum sample. The curves were fitted using the linear regression model in GraphPad Prism. GAL-His (red), GAL-CRDH1(blue), GALn108q-CRDH1 (orange).

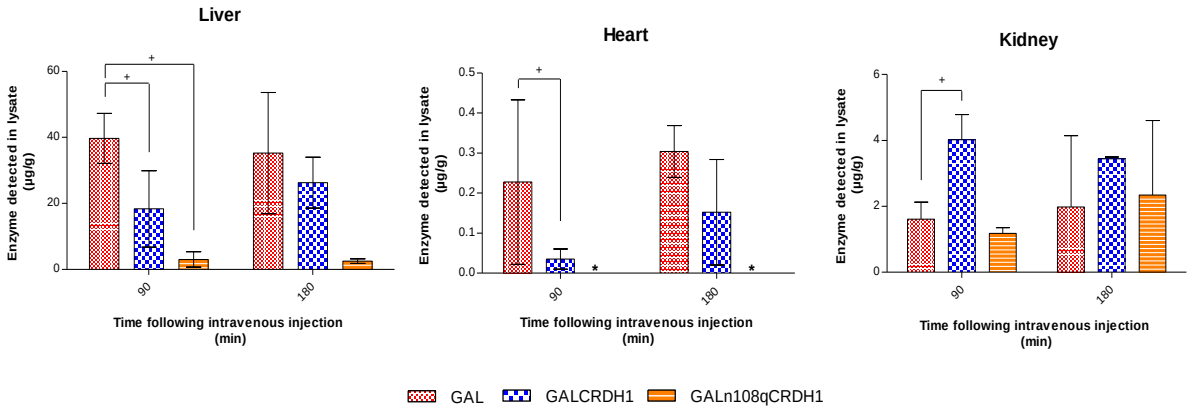

	%ID		
	liver	**heart**	**kidney**
GAL-His	46	0.04	0.46
GAL-CRDH1	28	0.03	0.75
GALn108-CRDH1	4	0	0.38

Figure 31 Organ distribution of recombinant enzymes. Following a single injection with 5 mg/kg of recombinant enzyme, mice were euthanized (90 min (±SEM, n=3) and 180 min (±SEM, n=2) following injection) and the liver, heart and kidneys isolated. Homogenates were analyzed for enzyme activity using 4MU-Gal assay. Total protein concentration of lysates was determined by BCA. Results were plotted using GraphPad Prism and shown in µg enzyme detected per mg lysate protein (µg/g). An asterisk (*) indicates a value under the lower limit of detection, + indicates a significant difference following a one-way ANOVA analysis ($p < 0.05$).

The graphs reveal distinct differences of recombinant enzyme uptake in the various organs. First of all, looking at the liver, the detected activity levels for both fusion enzymes GAL-CRDH1 and GALn108q-CRDH1 were found to be significantly lower than the activity levels detected for GAL-His. Recombinant enzyme quantification in the liver lysate indicated that only 28 % of the injected GAL-CRDH1 dose (28 %ID) was found in the liver and for GALn108-CDRH1 this value was even lower, with only 4 %ID found in the liver. By contrast, 46 %ID was found in the liver of GAL-His treated mice. When looking at the recombinant enzyme uptake in the heart, the highest activity levels were found in the GAL-His treated mice (0.04%ID), closely followed by the GAL-CRDH1 treated mice (0.03 %ID). For GALn108q-CRDH1 treated mice, no enzyme activity could be detected in the heart lysate. Finally, looking at the kidney, uptake was increased for GAL-CRDH1 (0.75 %ID) in comparison to GAL-His (0.45 %ID). The second fusion enzyme, GALn108q-CRDH1, exhibited comparable kidney internalization (0.38 %ID) as GAL-His.

Overall, these results show slight differences with regards to serum depletion for both fusion enzymes, with a tendency towards a prolonged circulation (~2-fold). In addition, distribution

profiles in the liver, heart and kidney also revealed differences, the more notable one being reduced liver uptake of the fusion enzymes.

3.3 Re-engineering lysosomal enzymes to overcome the blood-brain barrier

In order to start addressing one of the greatest limitations of enzyme replacement therapy (ERT), reengineering of recombinant lysosomal enzymes α-galactosidase A (GAL) and β-glucosidase (GBA) was undertaken so to enable binding to the transferrin receptor (TFR). Indeed, transferrin receptor is highly expressed at the apical surface of brain endothelial cells (Jefferies *et al.* 1984) and previous work has demonstrated that TFR can be used as a transportation route to harbor larger molecules beyond the blood-brain barrier (Friden *et al.* 1991). The molecular reengineering was performed using published peptide sequences (Lee *et al.* 2001, Kawamoto *et al.* 2011). These small molecules (~1 kDa) are less likely to disturb enzyme conformation and activity.

3.3.1 Molecular re-engineering of enzyme encoding DNA

Four recombinant fusion enzymes were designed based either on α-Galactosidase A (GAL), namely GAL-Ptf1 and GAL-Ptf2 or based on β-glucocerebrosidase (GBA), namely Strep-Ptf1-GBA and Strep-Ptf2-GBA. The latter constructs were added to this experiment because Morbus Gaucher more acutely requires a central nervous system (CNS) treatment than Morbus Fabry does. However, overall handling of recombinant GBA had proven difficult in the past, which is why GAL variants were run in parallel to ensure proof of concept. Four recombinant genes encoding the following proteins were generated:

- TFR binding peptide 1 (HAIYPRH) linked to C-terminus of human GAL by a flexible GS linker = GAL-Ptf1
- TFR binding peptide 2 (THRPPMWSPVWP) linked to C-terminus of human GAL by a flexible GS linker = GAL-Ptf1
- TFR binding peptide 1 (HAIYPRH) linked to N-terminus of human GBA by a flexible GS linker preceded by a streptavidin Tag = Strep-Ptf1-GBA = SPtf1-GBA
- TFR binding peptide 2 (THRPPMWSPVWP) linked to N-terminus of human GBA by a flexible GS linker preceded by a streptavidin Tag = Strep-Ptf2-GBA = SPtf2-GBA

The recombinant genes were integrated into the GT expression vectors as described previously in materials and methods (2.2) before stable transfection and expression in H9D8 host cell line took place.

3.3.2 Expression, purification and characterization of blood-brain barrier targeted enzymes

The fusion enzymes were successfully expressed in host cell line H9D8 following stable transfection of the cells with the respective recombinant expression vectors. The resulting transfectant pools were amplified up to 200 nM MTX, ensuring production rates ranging between 1 and 3 µg recombinant enzyme per milliliter of culture supernatant (1 to 3 µg/mL). In addition, for Strep-Ptf1-GBA and Strep-Ptf2-GBA pools, single cell cloning was performed using semi-solid matrix technique (Witzcak 2013). This procedure resulted in the isolation of three clones per construct, yielding between 3 and 4.5 µg/mL for Strep-Ptf1-GBA and 0.4 and 0.6 µg/mL for Strep-Ptf2-GBA. In order to produce larger amounts of the different fusion enzymes for initial product characterization, spinner cultures were set up (4 to 5 days' cultivation). The culture supernatants were purified either by galactose-coupled sepharose affinity chromatography (GAL fusions) or by streptavidin affinity chromatography (GBA fusions). Product yields ranged between 1 and 1.5 mg of GAL-Ptf1 (or GAL-Ptf2) per liter of culture supernatant and 0.8 to 1 mg Strep-Ptf1-GBA (or Strep-Ptf2-GBA) per liter of culture supernatant.

Initial characterization was performed in order to assess the integrity of the various fusion enzymes. Analysis by SDS-PAGE (Figure 32a and b) revealed distinct protein bands. The apparent molecular weights for GAL-Ptf1 and GAL-Ptf2 were around 45 kDa and 50 kDa respectively, which was comparable to reference molecule GAL-His (see 3.1.2). In addition, a 0.5 kDa variation in electrophoretic mobility was observed between the two GAL-derived fusions. In contrast, no difference was observed in the migration of Strep-Ptf1-GBA and Strep-Ptf2-GBA fusion enzymes. The resulting apparent molecular weights were found to be around 65 kDa for both GBA fusion enzymes, which is slightly higher than reference molecule GBA (58 kDa). In addition, western blotting of a gel electrophoresis in non-reducing conditions was also performed for GBA fusions in order to better assess whether aggregation occurred. (Figure 32c). Here, it becomes apparent that both GBA derived fusions have a strong tendency to aggregate. Indeed, in non-reducing conditions (lanes 1 and 3), a clear shift of electrophoretic mobility was observed towards higher molecular weights (>171 kDa). For Strep-Ptf2-GBA, a "protein smear" was observed spreading from the loading pocket all the way down to around 65kDa. In the case of Strep-Ptf1-GBA, no

band is left to be seen in non-reducing conditions, indicating that the sample probably remained "trapped" in the loading pocket. Further purification of GBA fusions (i.e. size exclusion chromatography step) did not enable generation of an aggregate free-product. Nevertheless, the GBA fusion samples were used in this state. For GAL derived fusions, no aggregation was observed (data not shown).

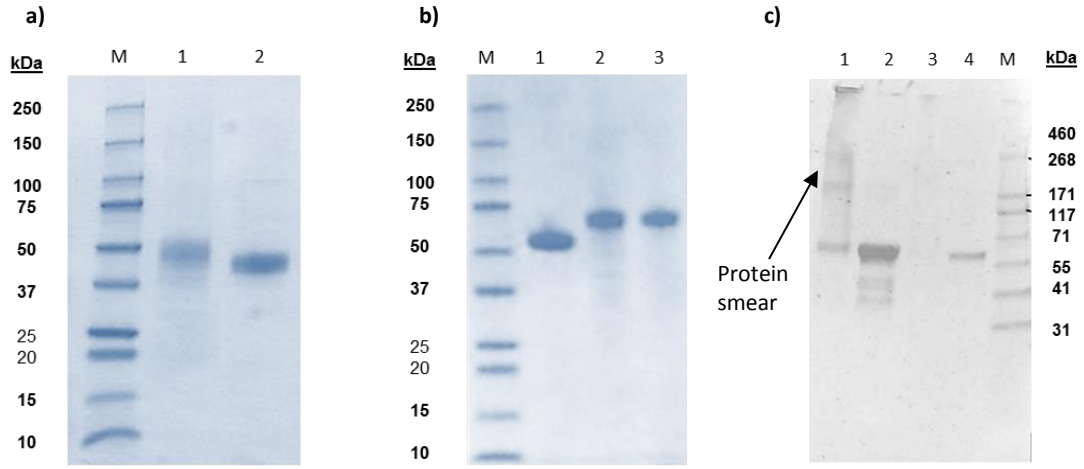

Figure 32 SDS-PAGE (4-20 % gradient gel, Coomassie blue staining) of fusion enzymes after affinity chromatography step a) M: protein marker, Lane 1: GAL-Ptf2, Lane 2: GAL Ptf1 b) M: Protein marker, Lane 1: Cerezyme®, Lane 2: Strep-Ptf2-GBA, Lane 3: Strep-Ptf1-GBA c) Western Blot analysis of GBA derived fusion enzymes (4-15% gradient gel) M: protein marker, Lane 1: Strep-Ptf2-GBA (non-reducing), Lane 2: Strep-Ptf2-GBA (reducing), Lane 3: Strep-Ptf1-GBA (non-reducing), Lane 4: Strep-Ptf1-GBA (reducing).

Following structural characterization, analysis of enzyme activity was performed (2.7) using respective substrates: pNP-β-D-glucopyranoside (pNP-Gluc) for GBA fusions and 4MU-α-D-galactopyranoside (4MU-Gal) for GAL fusions. The resulting kinetic profiles are presented in Figure 33. In the case of the GAL derived fusions, no significant differences were observed with regards to catalytic activity in comparison to reference molecules GAL-His and Farbazyme®. For the GBA variants however, a drastic loss in enzymatic activity (around 4-fold) was observed for both Strep-Ptf1-GBA and Strep-Ptf2-GBA, when compared to reference molecule Cerezyme®.

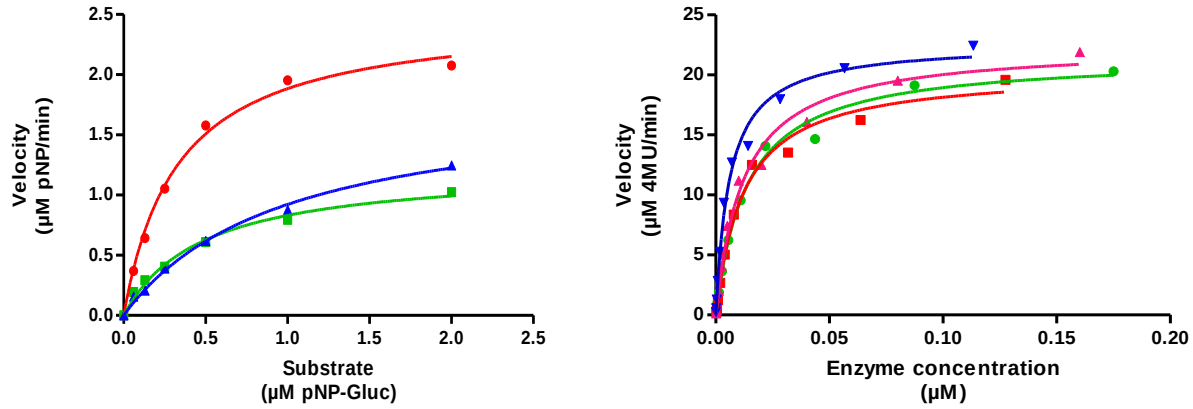

Figure 33 Kinetic profiles of transferrin peptide fusion enzymes (n=1). Left graph shows Cerezyme® (red dots), SPtf1-GBA (blue triangle) and SPtf2-GBA (green squares) in a standard kinetic plot of the enzyme velocities (µM pNP.min^{-1}) against substrate concentration (µM pNP-Gluc). Right graph shows Fabrazyme® (green dots), GAL-His (red squares), GAL-Ptf1 (pink triangles) and GAL-Ptf2 (blue triangles) in a kinetic plot of enzyme velocities (µM 4MU.min^{-1}) against enzyme concentration (µM).

3.3.3 Bi-functional characterization: is transferrin receptor binding enabled?

Fusion enzymes were assessed for their transferrin receptor (TFR) binding ability. To this end, a cell-binding assay using T47D cells was developed (2.12). Indeed, being myeloma derived cells, T47D cells express high levels of TFR receptor to allow for their rapid proliferation (Kawamoto *et al.* 2011). Following co-incubation of T47D cells with the different enzymes, cell surface binding was measured by flow cytometry using fluorescein-coupled secondary antibodies. The resulting histograms are presented in Figure 34. The series of histograms clearly revealed that the GAL fusion enzymes did not bind to T47D cell surface. Indeed, no shift in alexa-fluor-488 signal intensity was observed, regardless of the amount of fusion enzyme incubated. The profiles were comparable with those of negative control GAL-His (Figure 34a, b and c). For the GBA fusion enzymes on the other hand, results were more promising. Indeed, when Strep-Ptf2-GBA construct was co-incubated with T47D cells, a dose-dependent increase in alexa-fluor-488 signal occurred (shift to the right). The percentage of positive cells (cells that bound Strep-Ptf2-GBA) was found to be around 15, 18 and 35 % following co-incubation with 10, 20, 30 µg of GBA fusion enzyme respectively (Figure 34e). In comparison, negative control Cerezyme® showed no changes in alexa-fluor-488 signal intensity (Figure 34d).

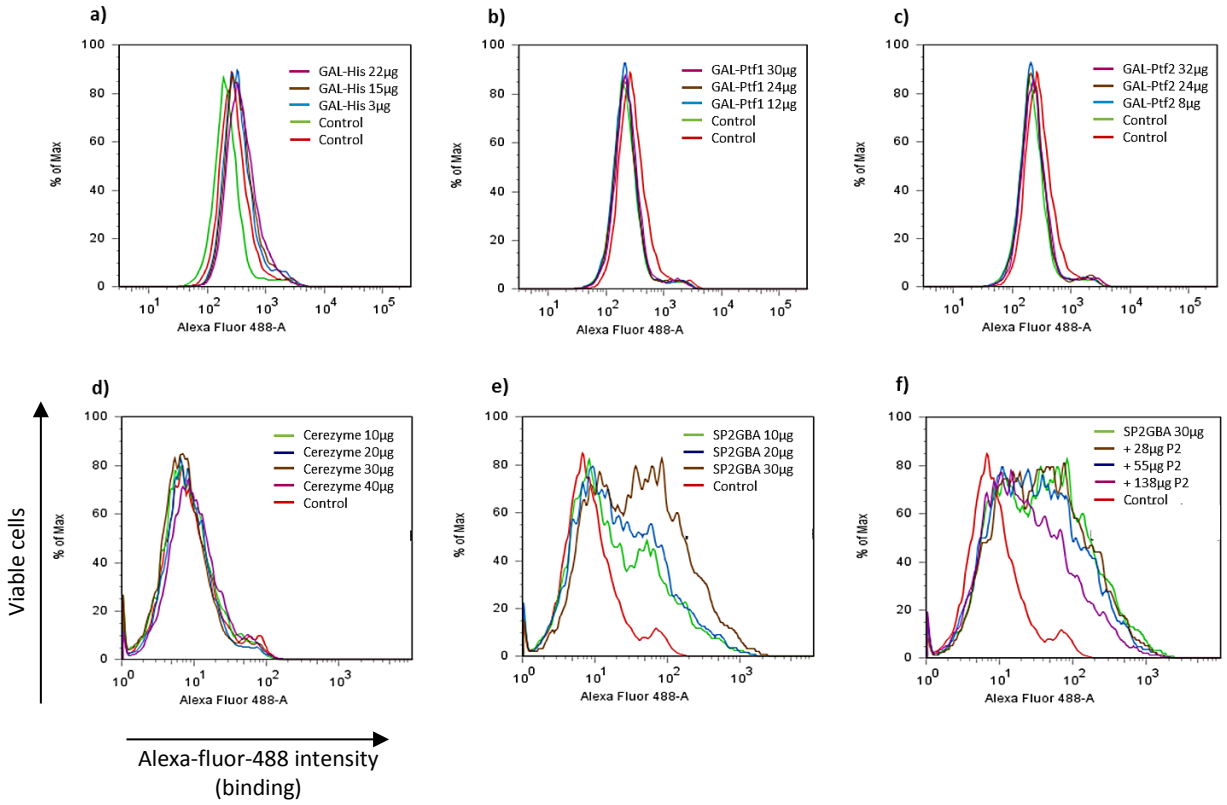

Figure 34 TFR cell-binding assay and FACS analysis. TFR positive T47D cells were incubated with various recombinant enzyme samples (n=2) at 4°C (binding only) and detected using a mouse monoclonal anti-GAL antibody followed by Alexa-Fluor labelled secondary antibody a) GAL-His b) GAL-Ptf1 c) GAL-Ptf2 d) Cerezyme® e) Strep-Ptf2-GBA (SP2GBA) f) Strep-Ptf2-GBA (SP2GBA) in the presence of free Ptf2 (P2).

In order to ensure that this signal shift was truly the result of Strep-Ptf2-GBA-specific binding to the TFR receptor, an additional experiment was performed in the presence of a competitor substance. To this end, 30 µg of Strep-Ptf2-GBA fusion enzyme was co-incubated with T47D, as described previously, however, in presence of "free" peptide Ptf2 (0 to 138 µg). The resulting histogram (Figure 34f) revealed a reduction in alexa-fluor-488 signal intensity (shift to the left) when the fusion enzyme was co-incubated with the free peptide. Indeed, following the addition of 28, 55 and138 µg of Pft2 peptide, the level of Strep-Ptf2-GBA bound cells (positive cells) was 35, 30 and 20 % respectively. This is a strong indication that the cell surface interaction between Strep-Ptf2-GBA and T47D is TFR related.

In summary, an active recombinant GBA fusion enzyme with the ability to bind to cell surface transferrin receptor (TFR) was produced. However, because receptor binding alone is not sufficient for the actual goal of passing the BBB, further assessment including TFR-mediated endocytosis or even transcytosis should be performed. This was unfortunately not possible in this study.

4 Discussion

The aim of this study was to address selected aspects often reported as being critical for enzyme replacement therapy (ERT) and the treatment of lysosomal storage diseases (LSDs). One element to consider is the phosphorylation of recombinant lysosomal enzyme, generating an important recognition marker (M6P moieties) involved in the correct delivery of these enzymes to the target cells. However, this particular feature can prove to be problematic when producing recombinant proteins due to the fact that glycosylation is a complex process to define and control, which very much depends on the expression host cell and/or the recombinant product in question (see 1.1.2). An example of this is CHO derived recombinant acid α-glucosidase (rhGAA) used to treat Pompe disease. Indeed, carbohydrate analysis of the rhGAA preparations indicated a relatively low content of mannose-6-phosphate (M6P) residues of around 0.9 mole M6P/mole rhGAA (Zhu *et al.* 2004). This is almost 4-fold lower than M6P levels of CHO derived recombinant α-galactosidase A (GAL) for example (Sakuraba *et al.* 2005), illustrating the variation which can arise within a production host cell system. Furthermore the low M6P levels of rhGAA mean that high doses (10 to 40 $mg.kg^{-1}.week^{-1}$) are required to partially reduce glycogen storage, thus involving high therapy costs. This shows the importance of having a good production host cell line able to generate highly phosphorylated recombinant enzymes. Therefore, the first aspect chosen for this study was the engineering of Glycotope's production host cell line H9D8, in order to ensure robust and reproducible delivery of highly phosphorylated molecules. The focus here was upon modifying the cellular vesicle trafficking route of M6P bearing lysosomal enzymes (generation of endosomal acidification mutants).

Another critical aspect to consider when making ERTs is the rapid and significant loss of therapeutic enzyme to the liver following intravenous administration. Product loss has repeatedly been reported as being over half of the injected dose, leaving little enzyme for the organs really requiring it (Bijsterbosch *et al.* 1996). Because of this high uptake, enzymes also generally have a short circulating time (≤10 min) and intracellular half-lives, i.e., the therapy requires regular, often biweekly, administrations of relatively large amounts of the relevant enzyme (Cheng and Smith 2003). This not only increases the likelihood of an immune response but also inherently increases the overall cost of the therapy. Liver uptake is in part driven by the asialoglycoprotein receptor (ASGPR), which recognizes and binds terminal galactose (tGAL) and terminal galactosamine (tGal*NA*c) present in protein glycans (Iobst and Drickamer 1996). Therefore, the

second focus of this study was upon decreasing the ASGPR affinity for the recombinant proteins produced. In particular, a fusion molecule was engineered where masking of potential terminal galactose structures would be attempted.

Finally, the most critical aspect related to ERT to date is the inability of the therapeutic molecules to cross the blood-brain barrier (BBB) and enter the brain parenchyma. Unfortunately, because storage in brain parenchyma is common to almost all of the lysosomal diseases (Cheng and Smith 2003), this is a problem which desperately needs to be addressed. To date, several groups have reported the great potential of a technique referred to as "molecular Trojan Horse technology" (Pardridge 2006, Karkan *et al.* 2008, Farrington *et al.* 2014). In this case, large molecules such as recombinant acid hydrolases are "disguised" and pass for entities normally able to cross the BBB, such as transferrin (Jefferies *et al.* 1984) or insulin (Duffy and Pardridge 1987). The modified recombinant molecules are thereby able to cross over to the brain parenchyma, using the mechanism of receptor mediated transcytosis (RMT). In light of this, the last aspect which was looked at in this study was the tackling of BBB transport for recombinant enzymes. To this end, triggering of RMT was attempted by making use of peptides known to bind and internalize via the transferrin receptor (Lee *et al.* 2001, Kawamoto *et al.* 2011). Several fusion molecules were designed, expressed and assessed for their ability to interact with cell-surface transferrin receptor (TFR).

4.1 Improving mannose-6-phosphate mediated transport of recombinant lysosomal enzymes

In the late 1980s, the wish to fully understand vesicular trafficking in cells led to the generation of mutants with vacuole defects and in particular a CHO cell line named G.7.1 (Marnell *et al.* 1984). Follow-up characterization revealed that G.7.1 most probably had an altered proton pump activity, leading to a deficiency in endosomal acidification (Colbaugh *et al.* 1988). More importantly though, trafficking of newly synthesized lysosomal enzymes within these cells was also altered, revealing an increase in phosphorylated product (Park *et al.* 1991). Therefore, generation of a similar mutant was undertaken, however using Glycotope's human host cell line H9D8. The required alteration, a modified acidic vesicular trafficking, would be beneficial for the production of recombinant lysosomal enzymes. The goal here was to obtain a host cell capable of producing fully human glycosylated acid hydrolases with an appropriate level of phosphorylated carbohydrates.

4.1.1 A mutation induces a change in acidic vesicle content

Using EMS, random mutations were introduced into Glycotope's production host cell line H9D8. Selection of "appropriately mutated" cells was enabled by follow-up treatment consisting of a combination of Diphtheria Toxin (DT) and Exotoxin A (ExA) toxins. Indeed, both toxins are known to become lethal to an organism only when internalized and trafficked to their target via acidic vesicles. The low pH of the late endosomes enables cleavage and activation of toxin subunit A, later responsible for protein synthesis inhibition and cell death (see Figure 35). Therefore, following treatment with these two toxins, sensitive cells die, whilst cells with an altered acidic vesicle content or trafficking remain alive.

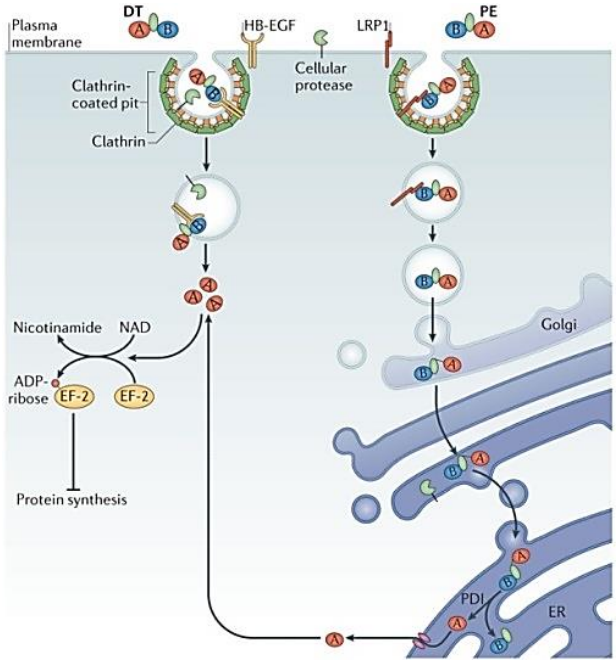

Figure 35 Mechanism of action of Diphtheria toxin (DT) and *Pseudomonas* exotoxin A (ExA or PE) toxins. DT binds to host membrane-bound receptor HB-EGF and enter cells via receptor-mediated endocytosis. Following endosomal acidification, the A domain of DT is translocated into the cytosol. Conversely, PE undergoes LRP1 mediated endocytosis, however, following endosomal acidification, retrograde trafficking to the ER occurs. Once in the cytosol, the A domains of the toxins prevent activation of ADP-ribosylated elongation factor 2 (EF2), which in turn inhibits protein synthesis and kills the cell (from Simon *et al.* 2014).

The surviving cells were analyzed by flow cytometry in order to determine their relative acidic vesicle contents in relation to originating cell line H9D8. As a positive control, H9D8 cells were treated with Bafilomycin, a substance known to inhibit proton pumps and thereby mimicking endosomal acidification deficiency. The results clearly showed that several of the surviving clones

repeatedly exhibited a reduced relative acidity ranging between 60 and 80 % of that found in H9D8 cells. Furthermore, these lower values were comparable to that found for the positive control (Bafilomycin treated cells). These cell clones were thought to bear the required modification and were retained for further testing. Indeed, the translation of this reduced acidity phenotype into an increased M6P content of recombinant product was yet to be confirmed (see 4.1.2).

A few questions remain open however, as to the nature of the mutant cell clones generated. Selection by simultaneous use of two toxins ensures that cells survive by developing a lesion affecting a common event in the mode of action of the toxins as opposed to just acquiring a random resistance. At the time Marnell used modeccin as the second toxin due to the subtle differences in its mode of action compared to DT (Marnell *et al.* 1984). Indeed, modeccin is internalized by a different receptor than DT and induces cell death by inhibiting the ribosome (Simon *et al.* 2014). Thus, the only common events during the mode of action of DT and moddeccin are endocytosis and vesicular trafficking. In this study however, ExA differs in its receptor binding, but unfortunately not quite in the mechanism of cell death, i.e., that potentially, some of the surviving cells may have developed a resistance to both toxins only at protein synthesis level. This could in part explain the presence of mutant cells exhibiting little to no differences with regards to their acidic vesicle content when assessed in the flow cytometry assay. Nevertheless, acidic vesicle trafficking of ExA also remains a common event to the DT mode of action leaving room for a mutation to occur at that level. This would correlate with the mutant clones which did exhibit significantly reduced acidity in the flow cytometry assay. In addition, ExA is similar to modeccin with regards to its trafficking mode which is retrograde trafficking to the Golgi (Yoshida *et al.* 1991), thus increasing the likelihood of having generated the desired cell phenotype. However, the question of whether the mutant cells can be classified as an endosomal acidification mutant remains open. Indeed, further characterization would need to be performed, including resistance tests, growth properties and complementation analysis, as described by Colbaugh (Colbaugh *et al.* 1988). Such studies would shed more light upon the nature of the mutation and the induced change, for example if an altered proton pump function was involved. Alternatively, mutant cell genome sequencing could be performed and compared to original host cell H9D8. This would additionally help to determine whether the three isolated mutants have the same mutation or not.

4.1.2 GAL-His derived from the new mutant expression host exhibits an increase in mannose-6-phosphate and an altered N-glycan processing

Following the mutant cell generation and selection, alteration of the "phosphorylation capacity" was assessed on a protein level. Indeed stable transfection using GAL-His DNA and subsequent overexpression of recombinant GAL-His was performed. The purified enzymes revealed no changes on a structural and functional level (SDS-PAGE analysis and 4MU activity assay) when compared to reference molecule GAL derived from H9D8. The mutant derived GAL enzymes were further characterized with regards to relative mannose-6-phosphate (M6P) content and N-glycan profiles were generated. The capillary electrophoresis analysis (CE-LIF) of phosphorylated molecules revealed that in all cases, the relative phosphorylation had increased by 5 to 30 % compared to the H9D8 derived GAL-His (H9D8-GAL). It was interesting to observe that the relative increases in M6P correlated somewhat with the acidic vesicle quantification data generated previously; the highest M6P levels were achieved when the lowest "% acidity" was measured. Indeed, acidic levels for B3G7-GAL (50 % ± 4% M6P), A3G2-GAL (59 % ± 2% M6P) and A3F12-GAL (79 % ± 4% M6P) were 74, 70 and 60 % respectively. This strongly suggests that the mutation affects intracellular pH regulation. In addition, the N-glycan profiling using UltraPerformance Liquid Chromatography (UPLC®) revealed differences with regards to oligosaccharide composition between H9D8 derived product and mutant derived product. This was particularly true for oligomannose structures. Indeed, whereas H9D8-GAL had relative levels of around 7% high-mannose, mutant cell line derived enzymes exhibited a 2-fold increase in high-mannose levels, achieving up to 15 % of the glycoform. These findings clearly demonstrate a difference in N-glycan maturation within the mutant host cells compared to H9D8 cell; the mutation and resulting increased acidity levels may have directly impacted Golgi processing of high-mannose glycan (i.e. high-mannose is not processed into hybrid or complex type glycan – see 1.1.1, Figure 2). Indeed, an increased level of mannose structures often correlates with a reduced retention time in the Golgi (Varki *et al.* 2009), which may in turn have resulted from the altered acidic vesicle trafficking. This change in N-glycan composition was also observed for the hybrid-type glycan structures present in the samples, in particular for A3F12-GAL. Indeed, whereas the product derived from A3G2, B3G7 and H9D8 showed relatively comparable hybrid-type glycan levels, ranging between 12 and 17 %, A3F12-GAL only showed a level of 6 % hybrid glycoform (~ 2-fold less). This again illustrates a change in N-glycan processing, which can in turn be positive when considering M6P generation (see 4.1.3).

To conclude, the overall increase of oligomannose-type structures (UPLC® data) observed for the three mutants in combination with the increased phosphorylation degree (CE-LIF data) made it possible to conclude on a more quantitative basis this time (as opposed to relative), that GAL-His produced in either of the three mutant cells bears a higher molar amount of M6P. This should be beneficial for cellular targeting and internalization. In addition, it is very likely that the induced mutation(s) led to an altered acidic vesicular trafficking (reduced percent acidity). This may in turn have affected the N-glycan processing of recombinant enzymes in the Golgi, in particular by increasing the levels of high-mannose whilst reducing the levels of hybrid and/or complex type glycan. This change could be beneficial due to the increased chance of obtaining phosphorylated high-mannose structures (high binding affinity) rather than the phosphorylated hybrid structures.

4.1.3 Mutant-derived GAL-His has an improved mannose-6-phosphate receptor-mediated cellular uptake

The last step of the evaluation process was the functional characterization of the mutant derived enzymes in order to confirm that the increased phosphorylation degree translates into an improved interaction with the cation-independent mannos-6-phosphate receptor (CI-MPR). Therefore, cellular uptake analysis of the various GAL-His enzymes was undertaken using 3T3 mouse fibroblasts. These cells have a high level expression of CI-MPR at their surface, making them an appropriate model for evaluating target-cell-like uptake.

The resulting data confirmed that all three mutant cell-derived GAL-His enzymes were internalized significantly better than the reference molecule, GAL-His produced in H9D8 (H9D8-GAL). Indeed, the maximum uptake levels achieved by the mutant derived product were up to 4-fold higher than those achieved by H9D8-GAL. Surprisingly, the relative mannose-6-phosphate (M6P) quantification data did not quite correlate with the uptake data. Indeed, the highest uptake was achieved by A3G2-GAL (28 µmol 4MU released.mg lysate^{-1}.h^{-1}), although it had only shown relative M6P levels of 59 %. In contrast, A3F12- GAL bearing 79 % relative M6P levels was internalized 2-fold less (14 µmol 4MU released.mg lysate^{-1}.h^{-1}) than A3G2-GAL. Finally B3G7-GAL, which had shown the lowest relative M6P levels of all mutants with 50 % M6P, was internalized to a lesser extent (21 µmol 4MU released.mg lysate^{-1}.h^{-1}) when compared to A3G2-GAL, yet to a 1.5-fold higher extent than A3F12-GAL. These observations illustrate the difficulty of predicting enzyme uptake based solely on a relative M6P quantification. Indeed, the relative value given by the capillary electrophoresis analysis (CE-LIF) does not take into account possible differences in oligosaccharide composition and in particular the level of

"M6P eligible" structures. Consequently, if for example "enzyme A" exhibits a relative M6P level of 79 % but only bears 1 mole of hybrid/oligomannose-type glycan, then the absolute amount of M6P present will be 0.79 mole M6P per mole "Enzyme A". On the other hand, if "enzyme B" exhibits a relative M6P level of only 56 % but bears 2 moles of hybrid/oligomannose-type glycans, then the absolute amount of M6P would be 1.12 mole of M6P per mole "enzyme B". Thus, relatively speaking, enzyme B is less phosphorylated however, absolutely speaking, it bears the largest amount of M6P. Therefore, "enzyme B" will most probably be internalized to a higher extent than "enzyme A", just like it was observed for the mutant enzymes. An absolute quantification of the M6P molecules per molecule enzyme therefore seems indispensable to adequately understand and predict the uptake of a given enzyme.

Lacking such a quantification method during the study, UPLC® N-glycan profiling data was used in order to come closer to an absolute quantification and better define the glycoforms involved. As mentioned earlier, these results showed that all the mutant cell lines produced GAL-His enzymes which overall exhibited at least twice the amount of oligomannose structures compared to the H9D8-GAL (13-15 % versus 7 %). Thus, it is understandable that these three molecules were internalized to a higher extent by the mouse fibroblasts. The evaluation of the high-mannose structures is however not sufficient to fully explain the internalization data. Indeed, whereas high-mannose levels were comparable for the three mutant cell-derived GAL-His molecules (~14 %), their internalization profiles still differed from one another. Indeed, as mentioned above, maximal internalization was achieved by A3G2-GAL followed by B3G7-GAL and finally by A3F12-GAL. The binding affinity however was highest for A3F12-GAL with 143 nM versus 430 nM for A3G2-GAL and 1867 nM for B3G7-GAL. To explain this data, the hybrid structures must also be taken into account. Indeed these can also bear M6P molecules but exhibit a lower binding affinity/capacity for the M6P-receptor (Sly and Fischer 1982, Varki and Kornfeld 2009). The UPLC® data indicated that the levels of hybrid-type glycan were almost 3-fold higher for A3G2 and B3G7 product (16 and 17% respectively) than they were for A3F12 derived product (6 %). Thus the differences in internalization could be explained by a higher amount of phosphorylated hybrid-type glycan present in A3G2- and B3G7-derived molecules, in turn leading to a less affine and slower uptake. For A3F12 derived molecules on the other hand, phosphorylation was more "focused" on high-mannose structures, thereby leading to higher binding affinity, as was observed in the internalization assay. However, because the overall percentage of "M6P-eligble" glycoforms (i.e. hybrid + high-mannose) was higher in A3G2 and B3G7 (29 and 32 %), these enzymes are

still able to achieve an overall higher cell penetration than A3F12-GAL which only has 18 % "M6P-eligible" molecules.

Even though the combination of CE-LIF and UPLC® data made it possible to explain some of the cell penetrating behavior, it does not give full insight into a major parameter, namely the structural identity of the phosphorylated oligosaccharide. Indeed, as mentioned before, the cation-independent mannos-6-phosphate receptor (CI-MPR) has preferences with regards to different phosphorylated structures (see 1.1.2). A phosphorylated hybrid carbohydrate will bind less to the receptor than a phosphorylated oligomannose would. In addition, if a glycan "tree" bears two phosphates (so-called bis-M6P) then the affinity for the CI-MPR can be 100- to 1000-fold higher (Tong and Kornfeld 1989). These structural differences in glycans cannot be identified by the methodology used in the present study, but could explain the discrepancies observed for the internalization assay. Indeed, it is possible that A3G2 derived GAL-His internalized so well compared to the other mutants because it bares more di-phosphorylated oligomannose structures. Furthermore, it has previously been reported that two appropriately spaced monophosphorylated glycans can act in unison as a high affinity MPR ligand (Roberts *et al.* 1998). Such structures may also be involved in the higher uptake.

In summary all of the recombinant hydrolases produced in mutant cell lines A3G2, A3F12 or B3G7 exhibited an increased level of high-mannose glycoforms as well as increased relative phosphorylation levels. These changes most probably enabled an improved MPR mediated endocytosis in mouse fibroblasts. Despite these promising results however some improvements could still be made. On the analytical side, an absolute quantification of M6P would be more appropriate for determining whether a molecule or a cell line is preferable for the production platform. Indeed, the combined CE-LIF/UPLC® method is time-consuming and unable to deliver a mole per mole M6P quantification. Therefore, it would be advantageous to look into quantification methods such as the ones described by Lee (Lee *et al.* 2003) or Sakuraba (Sakuraba *et al.* 2005). In addition, determination of the exact nature of the phosphorylated glycan, (i.e. mono or bis-M6P, high-mannose or hybrid) would also be of great value (Bones *et al.* 2011). On the cellular level, glycan analysis revealed that despite the fact that the oligomannose levels were 2-fold higher than in H9D8 derived product, there is still room for improvement. Indeed the commercial drug Fabrazyme®, for example, shows high-mannose levels of 29% which is still 2-fold higher than the mutant cell-derived GAL enzymes. A molecular engineering of the production clone could be envisaged in order to promote the generation of oligomannose structures. This could, for example, be done via genetic knock-out of the enzyme α-mannosidase

(see 1.1.1). Such an alteration could increase the levels of high-mannose and therefore the number of potential phosphorylation sites. Finally, at the downstream level, a purification process of the recombinant enzyme could be developed in order to preferably enrich phosphorylated molecules (i.e. using M6P-receptor column).

4.2 Reducing the loss of therapeutic enzyme to the liver asialoglycoprotein receptor

In parallel to the development of a new host cell line for improved expression of recombinant lysosomal enzymes, the focus was on improving the recombinant enzymes themselves. In this part of the project, the objective was to address the high uptake of the administered recombinant lysosomal enzymes by the liver and in particular by the asialoglycoprotein receptor (ASGPR) of the hepatocytes.

4.2.1 Effect of fusing CRDH1 domain to α-Galactosidase A enzyme

A recombinant gene encoding human α-Galactosidase A (GAL) linked to the H1 subunit of the human asialoglycoprotein receptor (CRDH1) via a flexible GS linker was generated (Figure 36a). The enzyme-receptor fusion was expressed in the H9D8 host cell and purified using a D-galactose affinity column. First analysis of the protein by gel electrophoresis (reducing SDS-PAGE) revealed a slight increase in molecular weight of around 20 kDa compared to reference molecule GAL-His. This was to be expected and correlates with the additional CRDH1 domain. In non-reducing conditions and size exclusion chromatography (SEC), dimerization of the recombinant fusion was apparent with a band found around 100 kDa. This is in accordance with literature findings supporting that GAL is known to form homodimers (Figure 36b) (Garman 2007).

Furthermore, functional characterization (activity assay and cellular uptake assay) showed that the additional 20 kDa did not significantly impair the fusion enzyme, neither in its activity nor in its cellular uptake capacity. In fact GAL-CRDH1 fusion enzyme even exhibited an improved cellular uptake (2-fold) compared to GAL-His. This can be explained by the increased relative phosphorylation which was found to be around 65 % for GAL-CRDH1 compared to 45 % for GAL-His. The N-glycan profiling additionally revealed no differences with regards to high-mannose-type or hybrid-type glycans (“M6P eligible glycans”). Therefore in this, case the increase

in relative phosphorylation is also an absolute increase: GAL-CRDH1 carries more M6P overall and is internalized better via MPR mediated endocytosis.

The reasoning behind the fusion enzyme was to acquire the possibility of masking terminal galactose moieties present in the own N-glycan structures of the fusion enzyme. Indeed a simple receptor-ligand interaction between the potential terminal galactose moieties present on the recombinant enzyme and the CRDH1 unit fused at the C-terminus is conceivable if these are sterically close. Furthermore, because the linker GS is long and relatively flexible (~80Å), it is possible that it allows for receptor interaction with GAL surface, where terminal galactose are potentially found (Figure 36d and e). Indeed, a similar strategy was used for increasing circulation half-life of hormones, whereby the recombinant hormone was fused to its natural receptor (Wilkinson *et al.* 2007). However, the nature of the fusion protein generated during this project opens more than one conformational possibility which are presented in Figure 36. Indeed, just like GAL, CRDH1 is also known to form homodimers, thus giving an additional dimerization potential and/or possibly increasing the strength of existing GAL-GAL homodimers (Figure 36c). Furthermore, the nature of the fusion protein could also allow for reciprocal "head-to-tail" dimerization, as described by Wilkinson for his receptor-ligand fusions (Wilkinson *et al.* 2007). Indeed intermolecular binding of the receptor unit in each fusion molecule to terminal galactose of the other GAL moiety is conceivable (Figure 36f). In fact such a conformation would even be beneficial, as it would enable the masking of potential ASGPR binding structures. Finally, it is also conceivable that multimerization could also occur via the homodimerization of GAL moieties within the fusion and in addition reciprocal head-to-tail dimerization of CRDH1 and terminal galactose (Figure 36g). Such interactions would be less beneficial, as the molecules could start aggregating and lose functionality.

The examples above are all suppositions based on the knowledge of the individual elements found in the fusion enzyme (GAL, the linker and CRDH1). Unfortunately, the analytical methods used are insufficient to confirm the existence of the various conformations described above. Indeed any form of interaction between CRDH1 and terminal galactose requires the presence of calcium ions and these are absent in both the SDS-PAGE and SEC running buffers. Validation and accurate representation of these various conformations would have to be done by X-ray crystallography for example. Nevertheless, an attempt to answer some of the conformational questions mentioned above was made, in particular with regards to the possibility of masking terminal galactose.

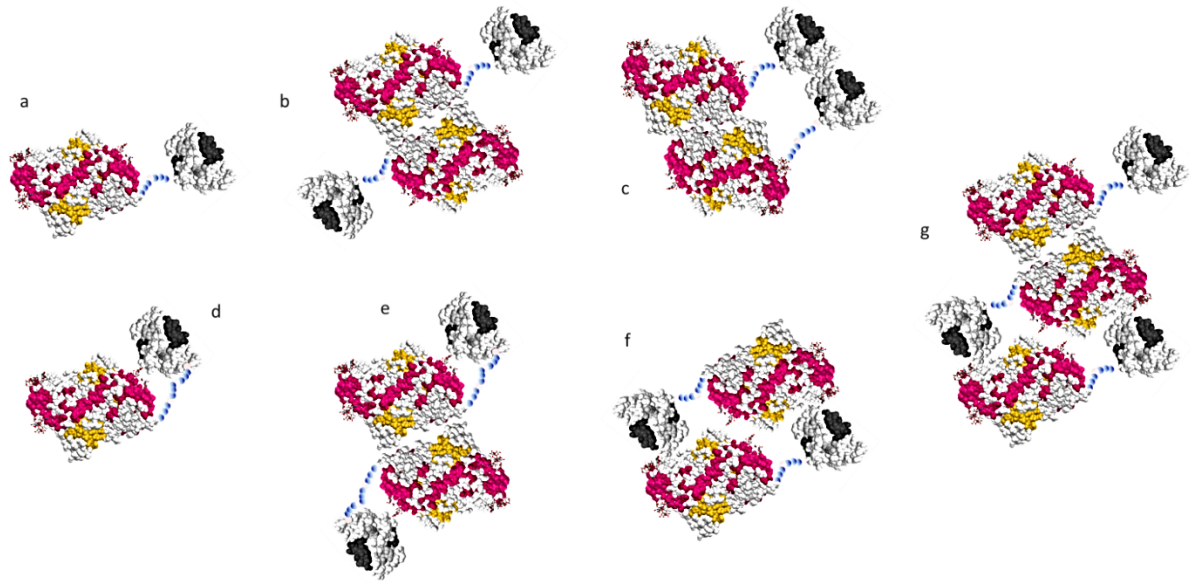

Figure 36 Possible conformations/assembly of GAL-CRDH1 fusion enzyme. a) GAL-CRDH1 monomer b) GAL-CRDH1 dimerization based on GAL-GAL dimerization c) GAL-CRDH1 dimerization based on CRDH1-CRDH1 dimerization and/or GAL-GAL dimerization d) CRDH1 interaction with molecule surface presenting terminal galactose e) CRDH1 interaction with molecule surface presenting terminal galactose within GAL-GAL based homodimer f) reciprocal head-to-tail recognition of terminal galactose by CRDH1 units g) example of "multimer" resulting of GAL-GAL homodimerization and reciprocal head-to-tail recognition of terminal galactose by CRDH1 unit.

Receptor binding assays were developed. Indeed, by looking at the binding behavior of GAL-CRDH1 in direct comparison to GAL-His, it was expected that differences in ASGPR binding affinity resulting from conformational masking would be identified. Both surface plasmon resonance assay (SPR) and receptor ELISA resulted in similar data. Indeed, both assays showed a significant decrease (20-fold in SPR and 8-fold in ELISA) in binding affinity t the ASGPR for GAL-CRDH1 when compared to GAL-His.

This reduction in ASGPR binding affinity could be the result of several factors:

Hypothesis 1 : A difference in glycan composition between GAL-CRDH1 and GAL-His, in particular the ratio of sialic acid to terminal galactose

Hypothesis 2 : Differences in glycan conformation, in particular antennarity. Indeed mono-, bi-, and tri-antennary terminal galactose glycans not only exhibit different affinities for the receptor, but would also affect the number of binding sites occupied and thereby the affinity or binding potential calculated.

Hypothesis 3 : Conformational "hindrance" as a result of either masked galactose by binding of the fused CRDH1 to free galactose structures at the fusion enzyme surface or steric hindrance due to mere presence of CRDH1

The first hypothesis can be refuted when looking at the N-glycan profiling data presented earlier (see 3.2.2). Indeed, the data clearly revealed that all the molecules have comparable levels of sialic acid and terminal galactose. As to the second hypothesis and the question whether the glycan conformation differs from one molecule to another with regards to antennarity of terminal galactose, remains open. A more in depth glycan analysis would need to be performed. Finally, with regards to the third hypothesis, it is conceivable that a conformational change occurs as a result of the additional CRDH1 at the C-terminus of GAL. This structural change could affect the nature of the glycans present on Asn108 for example (reduced antennarity of the terminal galactose) due to a different accessibility of the glycosylation enzymes. Furthermore, binding of the fused CRDH1 to terminal galactose structure present at the surface of the fusion enzyme is also possible. In both cases, a reduced affinity towards the ASGPR would occur.

4.2.2 Effect of knocking-out Asn108 glycosylation site

Alpha-Galactosidase A (GAL) is known to possess four possible N-glycosylation sites, of which only three are occupied, namely asparagines (Asn) at positions 108, 161 and 174. These three sites play a major role in the enzyme's functionality. Indeed, literature findings reported that Asn161 and Asn174 are necessary for activity, stability and correct secretion of the enzyme. Furthermore, these 2 sites (Asn161 and 174) are occupied predominantly by oligomannose structures or hybrid-type structures (Ioannou *et al.* 1998). For Asn108 however, carbohydrate population is almost exclusively of the complex-type, i.e. these would be the source of asialoglycoprotein receptor (ASGPR) binding. Lacking the knowledge whether Asn108 is structurally located close to the C-terminus once the protein is folded and therefore whether Asn108 is "in range" of the fused CRDH1 domain, an additional measure was taken. Indeed, suppression of Asn108 glycosylation site was performed in order to reduce complex-type glycosylation. The resulting fusion enzyme GALn108q-CRDH1, showed an even stronger reduction of its binding affinity in both assays (50-fold in SPR and 10-fold in ELISA), confirming the importance of Asn108 glycans for ASGPR recognition and binding. In addition, it was interesting to see that the functionality of GALn108-CRDH1 was not significantly impaired by the absence of Asn108. Indeed specific activity was only slightly reduced (4 % loss) compared to GAL-CRDH1. This differs from other publications reporting a more significant drop in activity (10-15 %) when removing Asn108 from

GAL (Ioannou *et al.* 1998). One explanation could be the presence of CRDH1, playing a stabilizing role for the enzyme. Indeed, the loss of activity observed by Ioannou and colleagues was caused by a change in conformation affecting the catalytic site, as a result of the missing glycan. It is conceivable that the additional GS linker and CRDH1 in the fusion molecule compensate for this steric change by inducing an additional stabilizing conformation change. Deletion of Asn108 had no significant impact on N-glycan composition or relative phosphorylation, with 60 % M6P detected for GALn108q-CRDH1 compared to 65 % for GAL-CRDH1. However, it must be kept in mind that this is only a relative figure as opposed to absolute. Indeed, GALn08qCRDH1 bares fewer glycans on an absolute basis due to the missing glycosylation site. Therefore the 60 % value most probably represents lower absolute M6P levels. This is confirmed by the internalization of GALn108q-CRDH1 in NIH-3T3 mouse fibroblast cells which was 2-fold lower than for GAL-CRDH1, but comparable to GAL-His.

4.2.3 Translation of *in vitro* data to *in vivo*

The *in vitro* data generated for the new fusion enzymes was very positive, with results showing a definite change in asialoglycoprotein receptor (ASGPR) affinity and binding with regards to both GAL-CRDH1 and GALn108-CRDH1. However, because *in vitro* studies can lead to results which do not always correspond to reality (i.e. living organism), it was important to confirm the results in an animal study.

Monitoring of the serum half-life in mice revealed biphasic serum depletion profiles for all three enzymes. The initial phase, which in this case was of rapid decline, corresponds to tissue distribution of the drug. It is monitored by the initial half-life. The second phase, occurring once equilibrium in circulation is reached, corresponds to the drug elimination form the system by the liver and kidney and is monitored by terminal half-life. In the initial phase, GAL-CRDH1 fusion revealed a 2-fold increase in initial $t_{1/2}$ compared to GAL-His. For GALn108q-CRDH1 however, clearance from the blood by surrounding tissues occurred at a faster rate than GAL-His. These observations were rather surprising, as *in vitro* data, and in particular cellular uptake assays, had shown that GAL-CRDH1 was best internalized in comparison to both GALn108q-CRDH1 and GAL-His. One would therefore have expected GAL-CRDH1 to be cleared faster as a result of increased target cell uptake. It is possible however that the difference observed was a direct result of liver uptake. Indeed, if GAL-CRDH1 was internalized to a lesser extent by the liver, which is in agreement with the *in vitro* binding assays, then initial circulation could be prolonged. In this case however, differences should also have been observed for GALn108q-CRDH1. The more

likely explanation is that the differences observed are not significant but rather fall within the assay's variation range. Indeed, with literature reports of 13 to 15 min half-life (Furbish *et al.* 1981, Kizhner *et al.* 2014) for recombinant α-Galactosidase A (GAL) preparations, the values measured at 10 min for GAL-His, 20 min for GAL-CRDH1 and 12 min for GALn108q-CRDH1 fall within that range and would therefore be deemed as being comparable to one another.

When looking at the elimination phase, profiles and terminal half-life values correlate somewhat better with *in vitro* data and expectations. Indeed, once equilibrium is reached between 120 and 140 min, a slower decrease in serum concentration can be observed (smaller slope values). At this point, respective terminal half-lives of 464 min and 513 min for GAL-CRDH1 and GALn108q-CRDH1 were estimated compared to 294 min for GAL-His. This correlates better with the *in vitro* data which had shown a reduced affinity for the ASGPR for both fusion enzymes. This could in turn have translated into a reduced liver elimination. These findings are also in line with the organ lysate analysis which revealed that both GAL-CRDH1 and GALn108q-CRDH1 were internalized far less by the liver than GAL-His. Nevertheless, it is to be noted that the values making up the terminal half-life calculation are all significantly lower than 1 % residual enzyme. It is therefore questionable whether actual differences would be detectable in this assay range.

If the serum clearance data was somewhat questionable, the organ distribution data on the other hand was more reliable in confirming the *in vitro* observations. Indeed, resulting data clearly showed reduced liver uptake levels for the fusion enzymes, with %ID values of 25 % for GAL-CRDH1 and 4 % for GALn108q-CRDH1 compared to 46 % for GAL-His control. When comparing that last value to literature findings, control substance GAL-His was comparable to the value, on average of 50 %ID described for other recombinant α-Galactosidase A (GAL) preparations (Lee *et al.* 2003). Unfortunately, if the data was positive with regards to liver uptake, the levels of recombinant enzyme in the other two organs was not necessarily improved, as one could have hoped. Indeed, similar levels of GAL-His (0.04 %ID) and GAL-CRDH1 (0.03 %ID) were found in the heart, and GALn108q-CRDH1 could not be detected. Furthermore, recombinant enzyme levels in the kidney were also comparable (0.4 %ID on average), with the exception of GAL-CRDH1, whose level was found to be slightly higher (0.75 %ID). In light of these results, it may be advantageous in the future to focus on increasing the circulation time of the fusion enzyme. Indeed, recent work with a PEGylated α-Galactosidase (Kizhner *et al.* 2014), resulting in turn in a 10-fold increase in serum half-life, revealed significantly increased internalization in the heart (1.4 %ID) and kidneys (1.5 %ID). This was the case even though liver uptake was not significantly

reduced (46 %ID). Combining such strategies with the reduced liver uptake achieved in this study could possibly help increase therapeutic benefit even more.

To conclude, a fusion enzyme was generated, retaining all the characteristics of the natural α-Galactosidase A (GAL) enzyme (i.e. catalytic activity and receptor mediated endocytosis). In addition, and as intended, *in vitro* evaluation proved that this fusion enzyme exhibited a significantly reduced binding affinity for the liver asialoglycoprotein receptor. Even though this did not translate into an increased circulation half-life, a significantly reduced accumulation of the recombinant fusion enzyme within the liver of healthy mice was nevertheless observed. Unfortunately, the proportion in which this observed effect benefited the therapeutics' distribution is arguable. Indeed, even though a 2-fold increase in the kidney internalization was observed for GAL-CRDH1, this was not the case for the heart. Still, it is important to mention that too few organs were looked at to properly draw conclusions as to how the organ distribution was changed or not. Therefore, this mouse study should be repeated not only to look at more organs but also to confirm the first data set. Furthermore, it might be advisable to work with radio-labelled enzymes in order to improve the sensitivity of detection, especially for the determination of half-lives during the elimination phase. Finally, to fully assess the therapeutic benefit of the fusion molecule, the study should be performed using Fabry mice models and globotriaosylsphingosine (Gb3) degradation in the various organs should be monitored. Indeed, in the end it is not alone the amount of enzyme (percent activity) reaching certain organs which factors success of an ERT but rather how well the accumulated substrate can be hydrolyzed.

4.3 Recombinant lysosomal enzymes and passing the blood-brain barrier

The ability to overcome the blood-brain barrier (BBB) is one greatly required for recombinant lysosomal enzymes. To date, molecular Trojan horse technology seems to be the most promising strategy. Indeed, since initiation of the concept in the late 1980s early 90s. (Pardridge 1987), many have followed and started to develop antibodies or peptides with the purpose of enabling a receptor mediated passage across the BBB (Lajoie and Shusta 2015). In this study, a similar achievement was attempted using two peptides previously identified and described by Lee et al. as being able to bind to the transferrin receptor (Lee *et al.* 2001). The objective was to generate a fusion between a lysosomal enzyme and either one of these peptides and assess whether double functionality was achieved: intact catalytic activity and transferrin receptor (TFR) binding ability enabling transcytosis.

Initially, work was performed with the lysosomal enzyme β-glucosidase (GBA) as central nervous system (CNS) disorder is more likely to occur in M. Gaucher than in M. Fabry. However, due to great difficulties in the handling of recombinant GBA, it was decided to additionally work with GAL in order to fully assess the usefulness of the peptides (proof of concept). In total, four recombinant fusion enzymes were designed and expressed using host cell H9D8, namely Strep-Ptf1-GBA, Strep-Ptf2-GBA, GAL-Ptf1 and GAL-Ptf2.

4.3.1 Modified β-glucosidase is prone to aggregation and loss of activity

Structural and functional characterization of GBA derived fusions revealed complications early on. Indeed, both Strep-Ptf1-GBA and Strep-Ptf2-GBA were prone to aggregation and catalytic activity of both fusions was significantly altered (4-fold less active) in comparison to commercial reference Cerezyme®. The reduced catalytic activity could be a direct result of the additional strep-tag linker and peptide present at the N-terminus of the enzyme. Indeed it has been reported that changes in amino acids of the polypeptide backbone on either N- or C-terminus can alter enzyme activity (Meghdari *et al.* 2015). It is therefore conceivable that the additional 20 to 25 amino acids induced conformational changes leading to the reduced activity. It is also possible however, that the aggregation itself is the cause of the reduced catalytic activity. Indeed, aggregates often lead to a false determination of recombinant enzyme monomer concentration which itself influences activity assay setup and catalytic activity determination: enzyme "trapped" in an aggregated formation are less likely to be accessible to substrate.

With regards to aggregate formation, the amino acid modifications to the enzyme may also be a cause. Indeed protein aggregation can be the result of a conformational change or partial unfolding of the protein monomer rendering it more prone to oligomerisation (Philo *et al.* 2009). Such modifications could be induced by additional amino acids. Furthermore, it is very likely that GBA also undergoes modifications such as oxidation or deamidation at any stage in the production process. An optimization of the purification process for example and use of a carefully formulated storage buffer are therefore advisable for optimal working conditions. In light of these results, isolation of the GBA monomers was attempted by SEC unfortunately without success.

Considering this, the GAL derived fusions were prepared, fortunately showing neither aggregation nor loss of catalytic activity. It seems that overall, GAL enzyme is more stable and easier to handle than GBA.

4.3.2 Transferrin-like peptides retain transferrin receptor binding ability when fused to acid hydrolases

Following production of the recombinant molecules, the next step consisted in assessing preservation of the bifunctionality. Indeed, the fusion enzymes not only need to be active but also have to have the ability to be recognized and bound by the transferrin receptor (TFR). This was assessed in a flow cytometry assay by looking at cell surface binding to T47D cells known to have increased levels of TFR.

In this case, the fusions derived from α-Galactosidase A (GAL) proved more challenging. Indeed, no cell surface binding to T47D cells could be detected, neither for GAL-Ptf1 nor GAL-Ptf2. This strongly suggests that the peptides are not accessible to bind to the TFR. It is conceivable that the GS linker is too short, thus leading to "burial" of the peptides within the enzyme units. This is however somewhat surprising because in the case of GAL-His for example, the c-terminal His-tag remained accessible in native conditions. Another possible explanation could be that the peptides, even if accessible, can no longer be bound by TFR receptor due to the presence of the GAL enzyme. Yet, in their publication Lee et al. explicitly showed TFR mediated internalization of a green-fluorescent-protein (GFP)-Ptf2 fusion protein. However, GFP is only 27kDa large as opposed to 50kDa for GAL and the nature of the linkage is unknown.

In the case of Strep-Ptf2-GBA fusion enzyme, cell surface binding could be detected. Because of the nature of the protein sample, in particular the presence of aggregates, additional binding experiments were performed to ensure that the binding was not just an artefact. Indeed aggregates can influence protein-protein interactions and in particular antibody recognition. This is why an additional flow cytometry experiment was performed with co-incubation of the fusion enzyme with "naked" peptides (binding competition). The results clearly showed differences in the cell surface binding, with a concentration dependent inhibition of Strep-Ptf2-GBA binding to T47D cells. This strongly indicates that the binding of Strep-Ptf2-GBA is not an artefact but more the result of a specific interaction with TFR receptor.

4.3.3 The necessity of a human transcytosis assay

So far, the experimental work performed during the study showed the feasibility of producing a bifunctional recombinant GBA fusion enzyme. Indeed, the product retained catalytic activity, though diminished and more importantly it acquired the ability to bind to a key BBB receptor, namely TFR. Although these features are indispensable when trying to achieve receptor mediated

transport across the BBB, they are not sufficient. Indeed, the key functionality is the triggering of an internalization followed by a transfer to the "other side" of the cell. This was why the project next focused on the development of an internalization assay in order to monitor TFR mediated endocytosis. However this approach is too simplistic. Indeed, endocytosis does not directly imply transcytosis, the mechanism required to cross the BBB. Therefore it was decided to move directly towards observing actual transcytosis and establishing an *in vitro* BBB-model. Indeed, in the last years, several models have been described and deemed appropriate for an *in vitro* assessment of a drugs' BBB permeability (Sade *et al.* 2014). The work is currently in progress, leaving the question of whether the fusion enzymes could mediate a TFR transcytosis unanswered for now.

In the future however, several improvements could be made. First, it would be advisable to attempt working with a different target than TFR receptor. Indeed, because TFR was one of the first RMT systems studied with the intention of developing BBB delivery applications, it is by now a well-studied and established target. Another more important reason however, is the possible limitations related to TFR mediated delivery. Indeed, tissue mistargeting is a drawback due to the fact that TFR expression is not confined to the brain endothelium (Lajoie and Shusta 2015). Furthermore, full transcytosis of modified molecules via TFR may actually be limited (Roberts *et al.* 1992) and recent findings have shown that a large amount of TFR-directed antibodies stay trapped in the endothelium (Moos *et al.* 2001). Although this can be somewhat overcome by modifying the targeting molecule with regards to binding affinity (Yu *et al.* 2011), it still raises the question of finding more appropriate BBB targets. Such research has already been started, resulting in the identification of new potential receptors (Stutz *et al.* 2014). This includes TMEM30A receptor, for example, which not only showed promising results with regards to the trafficking of an antibody across the BBB (Abulrob *et al.* 2005) but which also exhibits specific tissue expression at the brain endothelium. In addition, a different type of targeting molecule should be looked at, namely an antibody rather than a peptide. Indeed, even though the use of peptides has some advantages (i.e. small molecule leading to low steric hindrance), the binding affinity of peptides may be too low to ensure good drug transport. In comparison, an antibody not only helps increase the molecule's half-life due to the size, but also has a higher affinity for the target. Furthermore, if required, this affinity can be more easily modulated by single amino acid modifications in order to accommodate for better transcytosis (Bien-Ly *et al.* 2014). Finally, when using an antibody, one should consider whether the entire molecule or just a part of it should be used. Furthermore, the valence may also play a role depending on the nature of the target (Niewoehner *et al.* 2014). Finally, a possible drawback related to the use of an antibody as the

targeting molecule should be kept in mind, in particular looking at ERT. Indeed fusing a larger molecule may affect enzymatic activity and functionality. Although little is shown with regard to activity in the case of the already existing lysosomal enzymes fused to an entire anti-human insulin receptor antibody (HIRMAb) (Boado *et al.* 2013), it is more than conceivable that the additional 90kDa will affect enzyme conformation and possibly its activity.

As an overall conclusion, the present study shows that by A) mutating Glycotope's host cell lines H9D8, a new cell line was generated with the ability to better phosphorylate recombinant lysosomal enzymes. Indeed, relative mannose-6-phosphate (M6P) levels for recombinantly produced human α-Galactosidase A (GAL) were increased from 40% to 80%. This relative M6P increase translated *in vitro* into an improved penetration of target-like cells; B) Reengineering of recombinant GAL was possible, resulting in a fusion enzyme (GAL-CRDH1) with a reduced affinity towards the liver receptor asialoglycoprotein receptor (ASGPR) but retaining lysosomal catalytic activity. These findings directly translated *in vivo* where a reduced liver uptake was observed for modified recombinant GAL following intravenous injection of healthy mice; C) Lysosomal enzyme β-glucosidase (GBA) can be reengineered into a fusion enzyme, thereby acquiring the ability to bind to cell surface transferrin receptor and retaining lysosomal catalytic activity. Further assessment in a transcytosis model is necessary, however, these findings are nonetheless promising with regard to transporting a recombinant GBA across the blood-brain barrier.

List of abbreviations

2-AB	2-Aminobenzamide
ADA	Anti-Drug Antibody
APTS	8-Aminopyrene-1,3,6-Trisulfonic Acid, Trisodium Salt
ASGPR	Asialoglycoprotein Receptor
Asn	Asparagine
ATP	Adenosine Triphosphate
AV	Acidic Vesicle
BBB	Blood-Brain Barrier
BCA	Bicinchoninic Acid
BCIP	5-Bromo-4-Chloro-3'-Indolyphosphate P-toluidine salt
bp	base pair
BP	Binding Potential
CD-MRP	Cation Dependent Mannose-6-phosphate Receptor
cDNA	“coding” Deoxyribonucleic Acid
CE	Capillary Electrophoresis
CHO	Chinese Hamster Ovary
CI-MPR	Cation Independent Mannose-6-phosphate Receptor
CNS	Central Nervous System
CRDH1	Carbohydrate Recognition Domain H1
CSF	Cerebral Spinal Fluid
DHFR	Dihydrofolate Reductase
DNA	Deoxyribonucleic Acid
DT	Diphtheria Toxin
ELISA	Enzyme-Linked Immunosorbent Assay
EMS	Ethylmethansulfonate
em	emission
ER	Endoplasmic Reticulum
ERT	Enzyme Replacement Therapy
ex	excitation
ExA	Exotoxin A
FBS	Fetal Bovine Serum
FDA	Food and Drug Administration
GAL	alpha-galactosidase A

Gb3	Globotriaosylceramide
GBA	acid beta-glucosidase or glucocerebrosidase or glucosylceramidase
GalNAc	Galactosamine
GlcNAc	N-Acetylglucosamine
GlcNAc-1-P	N-Acetylglucosamine-1-phosphate
GM2	Monosialic Ganglioside 2
GS	Glycine-Serine
GT	Glycotope
His	Histidine
HRP	Horseradish Peroxidase
HSCT	Hematopoietic Stem-Cell Transplantation
ID	Injected Dose
IgG	Immunoglobulin G
ka	association constant
kd	dissociation constant
kDa	kilo Dalton
K_M	Michaelis Menten constant
LIF	Laser Induced Fluorescence
LIMP-2	Lysosomal Integral Membrane Protein 2
LSD	Lysosomal Storage Disease
M6P	Mannose-6-phosphate
MPR	Mannose-6-phosphate Receptor
MR	Mannose Receptor
MTX	Methotrexate
4MU	4-Methylumbelliferyl
4MU-G	4-Methylumbelliferyl-beta-(D)-glucopyranoside
4MU-GAL	4-Methylumbelliferyl-alpha-(D)-galactopyranoside
NBT	Nitro-Blue Tetrazolium
Neu5GC	N-Glycolylneuraminic acid
PBS	Phosphate Buffer Saline
Ptf	transferrin-binding peptide
pNP	para-nitrophenyl
pNP-G	para-nitrophenyl-beta-(D)-glucopyranoside
pNP-GAL	para-nitrophenyl-alpha-(D)-galactopyranoside
RAP	Receptor-Associated Protein
RFU	Relative Fluorescence Units

rhGAA	recombinant human acid alpha-glucosidase
RMT	Receptor-Mediated Transcytosis
RNA	Ribonucleic Acid
mRNA	messenger Ribonucleic Acid
SDS-PAGE	sodium dodecyl sulfate polyacrylamide gel electrophoresis
SEC	Size Exclusion Chromatography
SEM	Standard Error of the Mean
SPR	Surface Plasmon Resonance
Strep	Streptavidine
SRT	Substrate Reduction Therapy
tGAL	terminal Galactose
tGalNAc	terminal Galactosamine
TFR	Transferrin Receptor
TBS	Tris Buffer Saline
UPLC®	UltraPerformance Liquid Chromatography

List of References

Abbott, J., Patabendige, A., Dolman, D., Yusof, S., Begley, D., 2010. Structure and function of the blood–brain barrier. Neurobiology of Disease 37, 13–25.

Abulrob, A., Sprong, H., Van Bergen en Henegouwen, P., Stanimirovic, D., 2005. The blood-brain barrier transmigrating single domain antibody: mechanisms of transport and antigenic epitopes in human brain endothelial cells. J. Neurochem. 95, 1201–14.

Aird, R.B., 1984. A study of intrathecal, cerebrospinal fluid-to-brain exchange. Exp. Neurol. 86, 342–58.

Ashwell, G. and Morell, A. G., 1974. The Role of Surface Carbohydrates in the Hepatic Recognition and Transport of Circulating Glycoproteins, Advances in Enzymology and Related Areas of Molecular Biology 41, 99–128.

Barton, N.W., Brady, R.O., Dambrosia, J.M., Di Bisceglie, A.M., Doppelt, S.H., Hill, S.C., Mankin, H.J., Murray, G.J., Parker, R.I., Argoff, C.E., 1991. Replacement therapy for inherited enzyme deficiency--macrophage-targeted glucocerebrosidase for Gaucher's disease. N. Engl. J. Med. 324, 1464-70.

Berg-Fussman, Grace, Ioannou, Grabowski, 1993. Human acid beta-glucosidase. N-glycosylation site occupancy and the effect of glycosylation on enzymatic activity. The Journal of biological chemistry 268, 14861–6.

Bider, M.D., Cescato, R., Jenö, P., Spiess, M., 1995. High-affinity ligand binding to subunit H1 of the asialoglycoprotein receptor in the absence of subunit H2. Eur. J. Biochem. 230, 207–12.

Bien-Ly, N., Yu, Y.J., Bumbaca, D., Elstrott, J., Boswell, C.A., Zhang, Y., Luk, W., Lu, Y., Dennis, M.S., Weimer, R.M., Chung, I., Watts, R.J., 2014. Transferrin receptor (TfR) trafficking determines brain uptake of TfR antibody affinity variants. J. Exp. Med. 211, 233–44.

Bishop, D. F., Kovac, C. R., Desnick, R. J., 1981. Enzyme therapy. XX. Further evidence for the differential in vivo fate of human splenic and plasma forms of α galactosidase A in Fabry disease: recovery of exogenous activity from hepatic tissue. In: Callahan JW, Lowden JA (eds) Lysosomes and lysosomal storage diseases. Raven Press, New York, 381–394.

Bijsterbosch, M.K., Donker, W., van de Bilt, H., van Weely, S., van Berkel, T.J., Aerts, J.M., 1996. Quantitative analysis of the targeting of mannose-terminal glucocerebrosidase. Predominant uptake by liver endothelial cells. Eur. J. Biochem. 237, 344–9.

Boado, R.J., Hui, E.K., Lu, J.Z., Pardridge, W.M., 2013. IgG-enzyme fusion protein: pharmacokinetics and anti-drug antibody response in rhesus monkeys. Bioconjug. Chem. 24, 97–104.

Bohnsack, R.N., Song, X., Olson, L.J., Kudo, M., Gotschall, R.R., Canfield, W.M., Cummings, R.D., Smith, D.F., Dahms, N.M., 2009. Cation-independent mannose 6-phosphate receptor: a composite of distinct phosphomannosyl binding sites. J. Biol. Chem. 284, 35215–26.

Bones, J., Mittermayr, S., McLoughlin, N., Hilliard, M., Wynne, K., Johnson, G.R., Grubb, J.H., Sly, W.S., Rudd, P.M., 2011. Identification of N-glycans displaying mannose-6-phosphate and their site of attachment on therapeutic enzymes for lysosomal storage disorder treatment. Anal. Chem. 83, 5344–52.

Boven, P., Meurs, M., Boot, P., Mehta, M., Boon, P., Aerts, P., Laman, P., 2004. Gaucher Cells Demonstrate a Distinct Macrophage Phenotype and Resemble Alternatively Activated Macrophages. American Journal of Clinical Pathology 122, 359369.

Brady, R.O., Kanfer, J.N., Bradley, R.M., Shapiro, D., 1966. Demonstration of a deficiency of glucocerebroside-cleaving enzyme in Gaucher's disease. J. Clin. Invest. 45, 1112–5.

Brady, R.O., Gal, A.E., Bradley, R.M., Martensson, E., Warshaw, A.L., Laster, L., 1967. Enzymatic defect in Fabry's disease. Ceramidetrihexosidase deficiency. N. Engl. J. Med. 276, 1163–7.

Brady, R.O., Pentchev, P.G., Gal, A.E., Hibbert, S.R., Dekaban, A.S., 1974. Replacement therapy for inherited enzyme deficiency. Use of purified glucocerebrosidase in Gaucher's disease. N. Engl. J. Med. 291, 989–93.

Barton, N.W., Brady, R.O., Dambrosia, J.M., Di Bisceglie, A.M., Doppelt, S.H., Hill, S.C., Mankin, H.J., Murray, G.J., Parker, R.I., Argoff, C.E., 1991. Replacement therapy for inherited enzyme deficiency--macrophage-targeted glucocerebrosidase for Gaucher's disease. N. Engl. J. Med. 324, 1464-70.

Braulke, T., Raas-Rothschild, A., Kornfeld, S., 2013. I-Cell Disease and Pseudo-Hurler Polydystrophy: Disorders of Lysosomal Enzyme Phosphorylation and Localization. In The Online Metabolic and Molecular Bases of Inherited Disease. D. Valle, A.L. Beaudet, B. Vogelstein, K.W. Kinzler, S.E. Antonarakis, A. Ballabio, C. Scriver, B. Childs, W. Sly, F. Bunz, K.M. Gibson, G. Mitchell, editors. McGraw Hill, New York. Chapter 138.

Bruni, S., Loschi, L., Incerti, C., Gabrielli, O., Coppa, G.V., 2007. Update on treatment of lysosomal storage diseases. Acta Myol 26, 87–92.

Calias, P., Banks, W.A., Begley, D., Scarpa, M., Dickson, P., 2014. Intrathecal delivery of protein therapeutics to the brain: a critical reassessment. Pharmacol. Ther. 144, 114–22.

Chao, H.H., Waheed, A., Pohlmann, R., Hille, A., von Figura, K., 1990. Mannose 6-phosphate receptor dependent secretion of lysosomal enzymes. EMBO J. 9, 3507–13.

Cheng, S.H., Smith, A.E., 2003. Gene therapy progress and prospects: gene therapy of lysosomal storage disorders. Gene Ther. 10, 1275–81.

Colbaugh, P.A., Kao, C.Y., Shia, S.P., Stookey, M., Draper, R.K., 1988. Three new complementation groups of temperature-sensitive Chinese hamster ovary cell mutants defective in the endocytic pathway. Somat. Cell Mol. Genet. 14, 499–507.

Cooper, G.M., 2000. The Cell: A Molecular Approach. 2nd edition. Chapter 9, Sunderland (MA): Sinauer Associates.

Coutinho M., Prata M.J, Alves S., 2012. A shortcut to the lysosome: the mannose-6-phosphate-independent pathway, Mol Genet Metab. 107,257-66.

Dawson G., Matalon R. and Li Y.T., 1973. Correction of the Enzymatic Defect in Cultured Fibroblasts from Patients with Fabry's Disease: Treatment with Purified α-Galactosidase from Ficin, Pediatric Research. 7, 684–690.

De Duve, C., 1964. From cytosis to lysosome. Fed Proc. 23:1045-9.

De Duve, C., Wattiaux, R., 1966. Functions of lysosomes. Annu. Rev. Physiol. 28, 435–92.

De Duve, C., 2005. The lysosome turns fifty. Nat. Cell Biol. 7, 847–9.

De Groot, A.S., Scott, D.W., 2007. Immunogenicity of protein therapeutics. Trends Immunol. 28, 482-90.

Desnick, R.J., Dean, K.J., Grabowski, G., Bishop, D.F., Sweeley, C.C., 1979. Enzyme therapy in Fabry disease: differential in vivo plasma clearance and metabolic effectiveness of plasma and splenic alpha-galactosidase A isozymes. Proc. Natl. Acad. Sci. U.S.A. 76, 5326–30.

Desnick, RJ, Ioannou, YA, Eng, CM, 1995. Alpha galactosidase A deficiency: Fabry Disease. In: Scriver C.R., Beaudet A.L., Sly W.S., Valle D., (eds) The metabolic and molecular basis of inherited diseases, 7th ed. McGraw-Hill, New York, 2741–2784.

Duffy, K.R., Pardridge, W.M., 1987. Blood-brain barrier transcytosis of insulin in developing rabbits. Brain Res. 420, 32–8.

Farrington, G., Caram-Salas, N., Haqqani, A., Brunette, E., Eldredge, J., Pepinsky, B., Antognetti, G., Baumann, E., Ding, W., Garber, E., Jiang, S., Delaney, C., Boileau, E., Sisk, W., Stanimirovic, D., 2014. A novel platform for engineering blood-brain barrier-crossing bispecific biologics. The FASEB Journal 28, fj.14–253369.

Fratantoni, J.C., Hall, C.W., Neufeld, E.F., 1968. Hurler and Hunter syndromes: mutual correction of the defect in cultured fibroblasts. Science 162, 570–2.

Friden, P.M., Walus, L.R., Musso, G.F., Taylor, M.A., Malfroy, B., Starzyk, R.M., 1991. Anti-transferrin receptor antibody and antibody-drug conjugates cross the blood-brain barrier. Proc. Natl. Acad. Sci. U.S.A. 88, 4771–5.

Friedman, B., Vaddi, K., Preston, C., Mahon, E., Cataldo, J.R., McPherson, J.M., 1999. A comparison of the pharmacological properties of carbohydrate remodeled recombinant and placental-derived beta-glucocerebrosidase: implications for clinical efficacy in treatment of Gaucher disease. Blood 93, 2807-16.

Funk, B., Kessler, U., Eisenmenger, W., Hansmann, A., Kolb, H.J., Kiess, W., 1992. Expression of the insulin-like growth factor-II/mannose-6-phosphate receptor in multiple human tissues during fetal life and early infancy. J. Clin. Endocrinol. Metab. 75, 424–31.

Furbish, Steer, Krett, Barranger, 1981. Uptake and distribution of placental glucocerebrosidase in rat hepatic cells and effects of sequential deglycosylation. Biochimica et biophysica acta 673, 425–34.

Garman, S.C., 2007. Structure-function relationships in alpha-galactosidase A. Acta Paediatr. 96, 6–16.

Gaillard, P.J., Visser, C.C., de Boer, A.G., 2005. Targeted delivery across the blood-brain barrier. Expert Opin Drug Deliv 2, 299–309.

Germain, D.P., 2010. Fabry disease. Orphanet J Rare Dis 5, 30.

Goletz S., Danielczyk A., Baumeister H., Stahn R., Löffler A., Stöckl L., 2008, Use of human cells of myeloid leukaemia origin for expression of antibodies. Patent N° **WO2008028686 A2**, Glycotope GmbH.

Grabowski GA, Barton NW, Pastores G, Dambrosia JM, Banerjee TK, McKee MA, et al., 1995. Enzyme Therapy in Type 1 Gaucher Disease: Comparative Efficacy of Mannose-Terminated Glucocerebrosidase from Natural and Recombinant Sources. Ann Intern Med. 122, 33-39.

Hers, H.G., 1963. Alpha-Glucosidase deficiency in generalized glycogenstorage disease (Pompe's disease). Biochem. J. 86, 11–6.

Hickman, S., Shapiro, L.J., Neufeld, E.F., 1974. A recognition marker required for uptake of a lysosomal enzyme by cultured fibroblasts. Biochem. Biophys. Res. Commun. 57, 55–61.

Hossler, P., Khattak, S.F., Li, Z.J., 2009. Optimal and consistent protein glycosylation in mammalian cell culture. Glycobiology 19, 936–49.

Ioannou, Y.A., Bishop, D.F., Desnick, R.J., 1992. Overexpression of human alpha-galactosidase A results in its intracellular aggregation, crystallization in lysosomes, and selective secretion. J. Cell Biol. 119, 1137–50.

Ioannou, Zeidner, Grace, Desnick, 1998. Human alpha-galactosidase A: glycosylation site 3 is essential for enzyme solubility. The Biochemical journal 332 (Pt 3), 789–97.

Iobst, S.T., Drickamer, K., 1996. Selective sugar binding to the carbohydrate recognition domains of the rat hepatic and macrophage asialoglycoprotein receptors. J. Biol. Chem. 271, 6686–93.

Imperiali, B., O'Connor, S.E., 1999. Effect of N-linked glycosylation on glycopeptide and glycoprotein structure. Curr Opin Chem Biol 3, 643–9.

Jefferies, W.A., Brandon, M.R., Hunt, S.V., Williams, A.F., Gatter, K.C., Mason, D.Y., 1984. Transferrin receptor on endothelium of brain capillaries. Nature 312, 162–3.

Kaplan, A., Achord, D.T., Sly, W.S., 1977. Phosphohexosyl components of a lysosomal enzyme are recognized by pinocytosis receptors on human fibroblasts. Proc. Natl. Acad. Sci. U.S.A. 74, 2026–30.

Karkan, D., Pfeifer, C., Vitalis, T.Z., Arthur, G., Ujiie, M., Chen, Q., Tsai, S., Koliatis, G., Gabathuler, R., Jefferies, W.A., 2008. A unique carrier for delivery of therapeutic compounds beyond the blood-brain barrier. PLoS ONE 3, e2469.

Kawamoto, M., Horibe, T., Kohno, M., Kawakami, K., 2011. A novel transferrin receptor-targeted hybrid peptide disintegrates cancer cell membrane to induce rapid killing of cancer cells. BMC Cancer 11, 359.

Kizhner, T., Azulay, Y., Hainrichson, M., Tekoah, Y., Arvatz, G., Shulman, A., Ruderfer, I., Aviezer, D., Shaaltiel, Y., 2014. Characterization of a chemically modified plant cell culture expressed human α-Galactosidase-A enzyme for treatment of Fabry disease. Molecular Genetics and Metabolism 114, 259-267.

Kontermann, R.E., 2011. Strategies for extended serum half-life of protein therapeutics. Curr. Opin. Biotechnol. 22, 868–76.

Kornfeld, R., Kornfeld, S., 1985. Assembly of asparagine-linked oligosaccharides. Annu. Rev. Biochem. 54, 631–64.

Kornfeld, S., 1987. Trafficking of lysosomal enzymes. FASEB J. 1, 462–8.

Lajoie, J.M., Shusta, E.V., 2015. Targeting receptor-mediated transport for delivery of biologics across the blood-brain barrier. Annu. Rev. Pharmacol. Toxicol. 55, 613–31.

Lee, J., Engler, J., Collawn, J., Moore, B., 2001. Receptor mediated uptake of peptides that bind the human transferrin receptor. European Journal of Biochemistry 268, 2004–2012.

Lee, K., Jin, X., Zhang, K., Copertino, L., Andrews, L., Baker-Malcolm, J., Geagan, L., Qiu, H., Seiger, K., Barngrover, D., McPherson, J., Edmunds, T., 2003. A biochemical and pharmacological comparison of enzyme replacement therapies for the glycolipid storage disorder Fabry disease. Glycobiology 13, 305-313.

Leinekugel, P., Michel, S., Conzelmann, E., Sandhoff, K., 1992. Quantitative correlation between the residual activity of beta-hexosaminidase A and arylsulfatase A and the severity of the resulting lysosomal storage disease. Hum. Genet. 88, 513–23.

Linthorst, G.E., Hollak, C.E., Donker-Koopman, W.E., Strijland, A., Aerts, J.M., 2004. Enzyme therapy for Fabry disease: neutralizing antibodies toward agalsidase alpha and beta. Kidney Int. 66, 1589–95.

Lis, H., Sharon, N., 1993. Protein glycosylation. Structural and functional aspects. Eur. J. Biochem. 218, 1–27.

Lodish, H., Berk, A., Zipursky, S.L., et al., 2000. Protein Glycosylation in the ER and Golgi Complex (Section 17.7), Molecular Cell Biology. 4th edition New York: W. H. Freeman; 2000.

Marnell, M.H., Mathis, L.S., Stookey, M., Shia, S.P., Stone, D.K., Draper, R.K., 1984. A Chinese hamster ovary cell mutant with a heat-sensitive, conditional-lethal defect in vacuolar function. J. Cell Biol. 99, 1907–16.

McIvor R. S. and Simonsen C., 1990. Isolation and characterization of a variant dihydrofolate reductase cDNA from methotrexate-resistant murine L5178Y cells. Nucleic Acids Research, Vol. 18, No. 23 7025

Meghdari, M., Gao, N., Abdullahi, A., Stokes, E., Calhoun, D.H., 2015. Carboxyl-terminal truncations alter the activity of the human α-galactosidase A. PLoS ONE 10, e0118341.

Mehta, A., West, M.L., Pintos-Morell, G., Reisin, R., Nicholls, K., Figuera, L.E., Parini, R., Carvalho, L.R., Kampmann, C., Pastores, G.M., Lidove, O., 2010. Therapeutic goals in the treatment of Fabry disease. Genet. Med. 12, 713–20.

Meier, M., Bider, M.D., Malashkevich, V.N., Spiess, M., Burkhard, P., 2000. Crystal structure of the carbohydrate recognition domain of the H1 subunit of the asialoglycoprotein receptor. J. Mol. Biol. 300, 857–65.

Moos, T., Morgan, E.H., 2001. Restricted transport of anti-transferrin receptor antibody (OX26) through the blood-brain barrier in the rat. J. Neurochem. 79, 119–29.

Munier-Lehmann, H., Mauxion, F., Hoflack, B., 1996. Function of the two mannose 6-phosphate receptors in lysosomal enzyme transport. Biochem Soc T 24, 133–6.

Nakayama, Y., Nakamura, N., Tsuji, D., Itoh, K., Kurosak, A., 2013. Genetic Diseases Associated with Protein Glycosylation Disorders in Mammals.

Niewoehner, J., Bohrmann, B., Collin, L., Urich, E., Sade, H., Maier, P., Rueger, P., Stracke, J.O., Lau, W., Tissot, A.C., Loetscher, H., Ghosh, A., Freskgård, P.-O.O., 2014. Increased brain penetration and potency of a therapeutic antibody using a monovalent molecular shuttle. Neuron 81, 49–60.

Pardridge, W., Eisenberg, J., Yang, J., 1987. Human blood-brain barrier transferrin receptor. Metabolis 36, 892–895.

Pardridge, W.M., Kumagai, A.K., Eisenberg, J.B., 1987. Chimeric peptides as a vehicle for peptide pharmaceutical delivery through the blood-brain barrier. Biochem. Biophys. Res. Commun. 146, 307–13.

Pardridge, W.M., 2006. Molecular Trojan horses for blood-brain barrier drug delivery, Discov Med 6, 139-43.

Pardridge, W.M., Boado, R.J., 2012. Reengineering biopharmaceuticals for targeted delivery across the blood-brain barrier. Meth. Enzymol. 503, 269–92.

Park, J., Draper, R., Brown, W., 1991. Biosynthesis of lysosomal enzymes in cells of the End3 complementation group conditionally defective in endosomal acidification. Somat Cell Molec Gen 17, 137–50.

Park, E.I., Baenziger, J.U., 2004. Closely related mammals have distinct asialoglycoprotein receptor carbohydrate specificities. J. Biol. Chem. 279, 40954–9.

Philo, J., Arakawa, T., 2009. Mechanisms of protein aggregation. Curr Pharm Biotechno 10, 348–51.

Reitman, M.L., Kornfeld, S., 1981. Lysosomal enzyme targeting. N-Acetylglucosaminyl-phosphotransferase selectively phosphorylates native lysosomal enzymes. J. Biol Chem. 256, 11977–80.

Reuser, A.J., Kroos, M.A., Visser, W.J., Willemsen, R., 1994. Lysosomal storage diseases: cellular pathology, clinical and genetic heterogeneity, therapy, Ann Biol Clin 52(10), 721-8.

Roberts, R., Sandra, A., Siek, G.C., Lucas, J.J., Fine, R.E., 1992. Studies of the mechanism of iron transport across the blood-brain barrier. Ann. Neurol. 32 Suppl, S43–50.

Roberts, D.L., Weix, D.J., Dahms, N.M., Kim, J.J., 1998. Molecular basis of lysosomal enzyme recognition: three-dimensional structure of the cation-dependent mannose 6-phosphate receptor. Cell 93, 639–48.

Sade, H., Baumgartner, C., Hugenmatter, A., Moessner, E., Freskgård, P.-O., Niewoehner, J., 2014. A Human Blood-Brain Barrier Transcytosis Assay Reveals Antibody Transcytosis Influenced by pH-Dependent Receptor Binding. PLoS ONE 9.

Sakuraba, H., Murata-Ohsawa, M., Kawashima, I., Tajima, Y., Kotani, M., Ohshima, T., Chiba, Y., Takashiba, M., Jigami, Y., Fukushige, T., Kanzaki, T., Itoh, K., 2006. Comparison of the effects of agalsidase alfa and agalsidase beta on cultured human Fabry fibroblasts and Fabry mice. J. Hum. Genet. 51, 180–8.

Scriver, C.R., Beaudet A.L., Sly W.S., Valle, D., (eds), 2001. The metabolic and molecular bases of inherited disease. 8th edn (Part 16), McGraw-Hill; New York.

Shargel, L., Wu-Pong, S., Yu, A., 2005. Applied Biopharmaceutics & Pharmacokinetics. New York: Appleton & Lange Reviews/McGraw-Hill, Medical Pub.

Simon, N.C., Aktories, K., Barbieri, J.T., 2014. Novel bacterial ADP-ribosylating toxins: structure and function. Nat. Rev. Microbiol. 12, 599–611.

Sly, W.S., Kaplan, A., Achord, D.T., Brot, F.E., Bell, C.E., 1978. Receptor mediated uptake of lysosomal enzymes. Prog. Clin. Biol. Res. 23, 547-51.

Sly, W., Fischer, D., 1982. The Phosphomannosyl Recognition System for Intracellular and Intercellular Transport of Lysosomal Enzymes. Journal of Cellular Biochemistry 18, 67–85.

Song, X., Lasanajak, Y., Olson, L., Boonen, M., Dahms, N., Kornfeld, S., Cummings, R., Smith, D., 2009. Glycan Microarray Analysis of P-type Lectins Reveals Distinct Phosphomannose Glycan Recognition. J. Biol. Chem. 284, 35201–35214.

Stahl, P., Six, H., Rodman, J.S., Schlesinger, P., Tulsiani, D.R., Touster, O., 1976. Evidence for specific recognition sites mediating clearance of lysosomal enzymes *in vivo*. Proc. Natl. Acad. Sci. U.S.A. 73, 4045–9.

Stahl, P.D., Rodman, J.S., Miller, M.J., Schlesinger, P.H., 1978. Evidence for receptor-mediated binding of glycoproteins, glycoconjugates, and lysosomal glycosidases by alveolar macrophages. Proc. Natl. Acad. Sci. U.S.A. 75, 1399–403.

Stutz, C.C., Zhang, X., Shusta, E.V., 2014. Combinatorial approaches for the identification of brain drug delivery targets. Curr. Pharm. Des. 20(10), 1564-76.

Sweeley, C.C., Klionsky, B., 1963. Fabry's disease: classification as a sphingolipidosis and partial characterization of a novel glycolipid. J. Biol. Chem. 238, 3148–50.

Tong, P.Y., Kornfeld, S., 1989. Ligand interactions of the cation-dependent mannose 6-phosphate receptor. Comparison with the cation-independent mannose 6-phosphate receptor. J. Biol. Chem. 264, 7970–5.

Van Beers, M.M., Bardor, M., 2012. Minimizing immunogenicity of biopharmaceuticals by controlling critical quality attributes of proteins. Biotechnol J 7, 1473–84.

Varki, A., Kornfeld, S., 1980. Structural Studies of Phosphorylated High Mannose-type Oligosaccharides. J. Biol. Chem., 255, 10847-10858.

Varki, A., Kornfeld, S., 2009. P-type Lectins. In: Varki, A., Cummings, R.D., Esko, J.D., (eds). Essentials of Glycobiology. (2nd edn). Cold Spring Harbor (NY) Chapter 30.

Vellodi, A., 2005. Lysosomal storage disorders. Brit J Haematol 128, 413–431.

Walsh, G., Jefferis, R., 2006. Post-translational modifications in the context of therapeutic proteins. Nat. Biotechnol. 24, 1241–52.

Wang, F., Song, W., Brancati, G., Segatori, L., 2011. Inhibition of endoplasmic reticulum-associated degradation rescues native folding in loss of function protein misfolding diseases. J. Biol. Chem. 286, 43454–64.

Wilcox, W., 2004. Lysosomal storage disorders: the need for better pediatric recognition and comprehensive care. J Pediatrics 144, S3–S14.

Wilkinson, I.R., Ferrandis, E., Artymiuk, P.J., Teillot, M., Soulard, C., Touvay, C., Pradhananga, S.L., Justice, S., Wu, Z., Leung, K.C., Strasburger, C.J., Sayers, J.R., Ross, R.J., 2007. A ligand-receptor fusion of growth hormone forms a dimer and is a potent long-acting agonist. Nat. Med. 13, 1108–13.

Witzack, W., 2013. Expression, Reinigung sowie Charakterisierung des lysosomalen Enzyms Glukozerebrosidase. Bachelor Thesis, Fakultät für Pharmazeutische Biotechnologie der Hochschule Biberach.

Wraith, J.E., 2006. Limitations of enzyme replacement therapy: current and future. J. Inherit. Metab. Dis. 29, 442–7.

Yasuda, K., Chang, H.-H., Wu, H.-L., Ishii, S., Fan, J.-Q., 2004. Efficient and rapid purification of recombinant human α-galactosidase A by affinity column chromatography. Protein Expres Purif 37, 499-506.

Yoshida, T., Chen, C.C., Zhang, M.S., Wu, H.C., 1991. Disruption of the Golgi apparatus by brefeldin A inhibits the cytotoxicity of ricin, modeccin, and Pseudomonas toxin. Exp. Cell Res. 192, 389–95.

Yu, Y.J., Zhang, Y., Kenrick, M., Hoyte, K., Luk, W., Lu, Y., Atwal, J., Elliott, J.M., Prabhu, S., Watts, R.J., Dennis, M.S., 2011. Boosting brain uptake of a therapeutic antibody by reducing its affinity for a transcytosis target. Sci Transl Med 3, 84ra44.

Zarate, Y.A., Hopkin, R.J., 2008. Fabry's disease. Lancet 372, 1427–35.

Zhang, X.S., Brondyk, W., Lydon, J.T., Thurberg, B.L., Piepenhagen, P.A., 2011. Biotherapeutic target or sink: analysis of the macrophage mannose receptor tissue distribution in murine models of lysosomal storage diseases. J. Inherit. Metab. Dis. 34, 795–809.

Zhu, Y., Li, X., Kyazike, J., Zhou, Q., Thurberg, B., Raben, N., Mattaliano, R., Cheng, S., 2004. Conjugation of Mannose 6-Phosphate-containing Oligosaccharides to Acid α-Glucosidase Improves the Clearance of Glycogen in Pompe Mice. Journal of Biological Chemistry 279, 50336–50341.

Zhu, Y., Li, X., Mcvie-Wylie, A., Jiang, C., Thurberg, B., Raben, N., Mattaliano, R., Cheng, S., 2005. Carbohydrate-remodelled acid α-glucosidase with higher affinity for the cation-independent mannose 6-phosphate receptor demonstrates improved delivery to muscles of Pompe mice. Biochem J. 389, 619-628.

Eidesstattliche Versicherung

„Ich, Nathalie Rigal, versichere an Eides statt durch meine eigenhändige Unterschrift, dass ich die vorgelegte Dissertation mit dem Thema: „Improving Enzyme Replacement Therapy for Lysosomal Storage Diseases“ selbstständig und ohne nicht offengelegte Hilfe Dritter verfasst und keine anderen als die angegebenen Quellen und Hilfsmittel genutzt habe.

Alle Stellen, die wörtlich oder dem Sinne nach auf Publikationen oder Vorträgen anderer Autoren beruhen, sind als solche in korrekter Zitierung (siehe „Uniform Requirements for Manuscripts (URM)“ des ICMJE -www.icmje.org) kenntlich gemacht. Die Abschnitte zu Methodik (insbesondere praktische Arbeiten, Laborbestimmungen, statistische Aufarbeitung) und Resultaten (insbesondere Abbildungen, Graphiken und Tabellen) entsprechen den URM (s.o) und werden von mir verantwortet.

Die Bedeutung dieser eidesstattlichen Versicherung und die strafrechtlichen Folgen einer unwahren eidesstattlichen Versicherung (§156,161 des Strafgesetzbuches) sind mir bekannt und bewusst.“

Lebenslauf

Mein Lebenslauf wird aus datenschutzrechtlichen Gründen in der elektronischen Version meiner Arbeit nicht veröffentlicht.

Danksagung

I would like to thank Dr. Steffen Goletz, founder and CSO of the Glycotope GmbH, for the opportunity to pursue my PhD within the company. At the same time, I would also like to thank Prof. Dr. Ursula Plöckinger, Head of the Centre of Excellence for Rare Metabolic Diseases at the Interdisciplinary Centre of Metabolism Charité Berlin, for accepting to mentor my ambitious project and for always lending a helping hand whenever required.

Special thanks also go to Dr. Lars Stöckl, Dr. Sven Bahrke and Dr. Doreen Weigelt for their mentoring, help and support during the project.

A big thank you goes to all the colleagues at the Glycotope GmbH for the lovely working environment and the excellent technical assistance. In particular I would like to thank the DSP Glycoprotein team who in essence became my adoptive "lab family", the Lead Discovery team for their support in molecular biology and cell culture, Dr. Marion Schlangstedt and her Clone Development team for helping make some good clones and the Immunology department for their valuable advice with regards to cell-based assays and *in vivo* studies.

Finally I would like to thank my family and friends, foremost my parents for supporting me morally and financially through all these years: you guys made sure that my only worries concerned the Lab! Thank you very much.